

Univerza v Ljubljani
Fakulteta za elektrotehniko

Timotej Kodek

**DOLOČANJE BIOMEHANSKIH PARAMETROV
ZGORNJE EKSTREMITETE Z UPORABO
ROBOTA**

Doktorska disertacija

Ljubljana, september 2004

Univerza v Ljubljani
Fakulteta za elektrotehniko

Timotej Kodek

**DOLOČANJE BIOMEHANSKIH PARAMETROV
ZGORNJE EKSTREMITETE Z UPORABO
ROBOTA**

Doktorska disertacija

Mentor: prof. dr. Marko Munih

Ljubljana, september 2004

University of Ljubljana
Faculty of Electrical Engineering

Timotej Kodek

**ESTIMATION OF UPPER EXTREMITY
BIOMECHANICAL PARAMETERS USING A
ROBOT MANIPULATOR**

Ph. D. Thesis

Supervisor: prof. Marko Munih

Ljubljana, September 2004

Zahvala

Zahvaljujem se svojemu mentorju prof. dr. Marku Munihu, ki je s svojimi koristnimi strokovnimi nasveti in bogatimi izkušnjami pripomogel k nastanku tega dela. Poleg tega se zahvaljujem tudi akad. prof. Tadeju Bajdu za njegove koristne strokovne nasvete in vzpodbude.

Pri reševanju, včasih tudi zelo zapletenih tehničnih problemov so mi bistveno pomagali tudi člani Laboratorija za robotiko. Še posebej pa bi rad izpostavil Uroša Malija, Romana Kamnika, Matjaža Mihlja, Tomaža Karčnika, Aleša Bardorferja in Gregorija Kurilla katerih pomoč je bila neprecenljiva.

Posebno zahvalo dolgujem dr. Leonu Žlajpahu iz Inštituta Jožef Stefan, ki me je med nastajanjem dela vzpodbujal s svojimi koristnimi nasveti in drznimi znanstvenimi idejami. Njegova pomoč je v marsičem korenito vplivala na končno obliko tega dela.

Zahvala gre tudi prof. Garthu Johnsonu iz Univerze v Newcastlu, ki mi je pomagal z marsikaterim koristnim strokovnim nasvetom, ter bil pripravljen recenzirati moje članke.

Zahvaljujem se Ministrstvu za šolstvo, znanost in šport za finančno podporo.

Rad bi se zahvalil tudi svoji ženi Sabini, ki je ves čas nastajanja dela verjela vame in moralno podpirala prenekatero dodatno uro, ki sem jo prebil v laboratoriju ali za računalnikom. Nenazadnje pa sem dolžan tudi zahvalo svojim staršem, ki sta mi ves čas stala ob strani in me vzpodbujala. Očetu bi se rad zahvalil tudi za nekatere pametne in koristne strokovne nasvete.

Contents

Razširjeni povzetek	1
Pregled področja	2
Biomehanika gornje ekstremitete	4
Zastavljeni cilji	6
Izvorni prispevki disertacije	7
Abstract	11
1 Introduction	13
1.1 An overview of upper extremity biomechanics	15
1.2 Thesis objectives	19
1.3 Thesis original contributions	20
2 Upper extremity dynamic modelling and identification	23
2.1 Upper extremity as a dynamic system	24
2.2 Upper extremity joint properties	25
2.3 Body segment parameters in the upper extremity	27
3 Methods	31
3.1 Mathematical modelling	32
3.2 General assumptions made in the experiments	39
3.3 An overview of the experimental setup	42
3.4 Shoulder and elbow joint passive moments	44
3.4.1 A simplification of the biomechanical model	44
3.4.2 Implementation of the experiment	46
3.5 A technique for determining upper extremity joint and body segment parameters	47
3.5.1 Model linearization	48
3.5.2 Verification of the algorithm with a 2DOF mechanical model	50
3.5.3 Implementation of the experiment	52
3.6 Simulation for calculating the required robot joint trajectory	53

4	Results	57
4.1	Determining shoulder and elbow joint passive moments	57
4.1.1	Passive moment results for one subject	57
4.1.2	Passive moment result comparison for six subjects	60
4.1.3	Discussion of obtained results	61
4.2	Upper extremity joint and body segment parameter identification .	71
4.2.1	Results obtained in the mechanical arm experiment	71
4.2.2	Results obtained in the upper extremity experiment	80
4.2.3	Discussion of obtained results	91
4.3	Simulation	93
4.3.1	Discussion of obtained results	94
5	Conclusion	99
5.1	Ideas for future work	100
	List of symbols and abbreviations	102
	Bibliography	105
	Appendix A: Error analysis in parameter identification	113
	Appendix B: "Quantification of shoulder and elbow passive moments in the sagittal plane as a function of adjacent angle fixations", <i>Journal of Technology and Health Care</i>, vol. 11, pp. 89-103, 2003.	119
	Appendix C: "An identification technique for evaluating static body segment parameters in the upper extremity", <i>Proceedings of the 2004 IEEE International Conference on Robotics & Automation - New Orleans, LA, April 2004</i>	137
	Appendix D: "An analysis of static and dynamic joint torques in elbow flexion-extension movements", <i>Simulation modelling practice and theory</i>, vol. 11, pp. 297-311, 2003.	145
	Izjava	161

Razširjeni povzetek

Pričujoče delo obravnava študij notranjih biomehanskih lastnosti človeške roke. V preteklosti je marsikateri raziskovalec prišel do spoznanja o izjemni zapletenosti tega področja. V disertaciji smo se problema določanja nekaterih biomehanskih parametrov gornje ekstremitete lotili s pomočjo uporabe industrijskih robotov, ki so primarno sicer namenjeni delu v povsem drugačnih okoliščinah. Dejstvo, da *lahko robotske gibe z veliko natančnostjo velikokrat ponavljamo* in tega da *lahko v eksperimentalno okolje na dokaj enostaven način vključimo veliko senzorjev*, nam je omogočilo zelo širok razpon možnosti.

Poudariti je potrebno, da večina pri študiju gornje ekstremitete uporablja precej drugačen pristop, kot je bil naš, saj ponavadi izhajajo iz bolj medicinsko orientiranih okolij. Po drugi strani pa obstaja tudi kar nekaj inženirsko orientiranih del, ki ponavadi uporabljajo posebne, za namen raziskave razvite robotske mehanizme.

V naših eksperimentih smo za natančno gibanje roke uporabljali dva različna tipa industrijskih robotskih manipulatorjev (Yaskawa[©] - Motoman sk6 in Motomation[©] Stäubli - RX90). Pri tem smo gornjo ekstremiteto modelirali kot preprosti planarni mehanizem s tremi prostostnimi stopnjami, vse eksperimente pa smo izvajali v sagitalni ravnini osebe. Dlan merjene osebe smo pred eksperimentom na rahlo privezali na ročaj robota pri čemer oseba ni smela izvajati nobenih hotenih mišičnih aktivnosti. Robotski mehanizem je potem roko vodil po neki vnaprej predpisani trajektoriji v prostoru. Med gibom so se preko optičnega sistema za 3D zajemanje merile značilne anatomske točke na roki, iz česar smo določili kote v sklepih, s pomočjo senzorja sile pa smo merili sile v kontaktu med roko in robotom.

V prvem eksperimentalnem delu smo poskušali ugotoviti naravo *pasivnih momentov* v sklepih gornje ekstremitete, pri čemer smo predpostavljali vrednosti ostalih biomehanskih parametrov kot so težišča in mase iz literature. Pod izrazom pasivni momenti avtorji v literaturi označujejo viskoelastične lastnosti sklepov do katerih pride takrat, ko ni nobenih aktivnosti v mišicah roke. Vrednosti teh momentov so torej notranja lastnost posameznega sklepa, odvisna le od notranjih struktur, ki sestavljajo določen sklep. Parametre smo ugotavljali medtem, ko je

bil eden od kotov rame ali komolca v smeri fleksije-ekstenzije fiksiran pri desetih različnih kotih, nefiksiran sklep pa se je med gibom lahko premikal skozi precej široko kotno območje. Metodo za določanje pasivnih momentov smo izpeljali iz inverznega dinamičnega opisa trosegmentnega planarnega manipulatorja. Rezultati te študije potrjujejo tiste, do katerih so prišli nekateri drugi avtorji in kažejo na izjemno zapletenost biomehanskega modeliranja gornje ekstremitete.

V drugem eksperimentalnem delu se študija osredotoča na identifikacijo vseh biomehanskih parametrov, ki opisujejo gibanje gornje ekstremitete pri nizkih hitrostih. Gornjo ekstremiteto smo pri tem postopku zopet vodili po neki vnaprej predpisani počasni trajektoriji, pri čemer smo zajemali podatke o kotih in silah v kontaktu med roko in robotom. Pri trajektoriji smo upoštevali precej majhne kotne spremembe, znotraj katerih pasivni momenti v roki še niso izkazovali nelinearnih lastnosti in smo zato lahko predpostavili linearni model roke. Rezultati identifikacije so vrednosti mas in težišč za dlan in podlaket, njun produkt za nadlaket in pasivni momenti v določeni kotni delovni točki za vse tri sklepe v sagitalni ravnini. Rezultate smo nato primerjali z ocenami iz literature, ki so pridobljene na podlagi meritev določene povprečne populacije. Razvili smo identifikacijsko metodo na osnovi optimizacije, ki zopet privzema trosegmentni planarni model gornje ekstremitete. Rešitev temelji na prileganju izmerjenih navorov v sklepih roke in tistih, ki jih predvideva inverzni dinamični model. Da bi preverili kvaliteto predlagane identifikacijske metode smo celoten merilni in identifikacijski proces izvedli najprej na mehanskem modelu z dvema prostostnima stopnjama, ki je bil po dimenzijah primerljiv s pravo roko. Mehanski model smo načrtovali s pomočjo CAD programske opreme, kar nam je omogočilo celovit vpogled v vse dinamične parametre. Rezultati izvedenega identifikacijskega postopka in znanih vrednosti iz modela so se le minimalno razlikovali.

Za izvedbo celotnega eksperimenta na računalniku smo razvili simulacijo v okolju Matlab[©]-Simulink. To simulacijsko okolje nam je omogočilo vpogled v vrednosti fizikalnih veličin in precej več kontrole nad izvajanjem eksperimenta. Rezultati simulacije so nam poleg tega omogočili tudi spremljanje vseh kinematičnih veličin, kot so koti v sklepih, kotne hitrosti in kotni pospeški. Na drugi strani pa smo lahko opazovali tudi dinamične veličine kot so navori v sklepih in sile v kontaktu med obema manipulatorjema. S tem okoljem smo lahko hipotetično izvajali tudi tiste eksperimente, ki v realnosti niso bili izvedeni. Rezultati simulacije so bili primerljivi s tistimi, ki smo jih pridobili iz posameznih meritev.

Pregled področja

Raziskovalci se že od nekdaj zavedajo pomembnosti razumevanja delovanja biomehanskih sistemov v vsakdanjem življenju. Tako kot vsako mehansko telo, so

tudi vsakdanji človekovi gibi in njegova interakcija z okolico podvrženi zakonom mehanike. Z napredkom v znanosti in tehnologiji je biomehanika človekovega telesa zato relativno hitro postala tema prvih znanstvenih raziskav. Ni presenetljivo, da je bila prva celovita študija, ki je poskušala ugotoviti parametre telesnih segmentov (PTS), napravljena že v letu 1860 [1]. S pojavom industrijske revolucije je interakcija ljudi z okoljem postala veliko hitrejša kot kadarkoli poprej. Ta interakcija je vsebovala tudi večja tveganja, kar je v ljudeh spodbudilo interes za razumevanje kompleksnejših procesov. Velikokrat je vzpodbuda za tovrstne raziskave prišla s strani vojske, tako kot je to še danes primer na marsikaterem znanstvenem področju.

Začetne študije so vključevale zelo omejeno število kadavrov, na katerih so poskušale ugotavljati PTS človekovega telesa kot so naprimer mase, težišča in vztrajnostni momenti posameznih segmentov. Z nadaljnjim tehnološkim napredkom se je potreba po biomehanskem modeliranju bistveno povečala. Poleg tega je razvoj znanstvenikom omogočil, da so lahko pri študijah uporabljali nove, bolj sofisticirane metode. Namesto *in-vitro* raziskav, izvedenih na zelo omejeni množici kadavrov, so se novejšše študije lahko izvajale na večjem številu živih oseb *in-vivo*, poleg tega pa je bilo mogoče izmeriti tudi nekatere nove fizikalne veličine. Ta napredek je še posebej opazen v zadnjih desetletjih, ko so osebni računalniki in merilna oprema postali bolj razširjeni v raziskovalnih in zdravstvenih inštitucijah po vsem svetu.

Medtem ko se je večina študij osredotočala na biomehansko modeliranje celotnega telesa z namenom študija hoje ali vstajanja [2, 3], je bilo opazno manj interesa na področju modeliranja posameznih telesnih segmentov. Pozornost pri modeliranju segmentov se je najprej osredotočila na študij spodnjih ekstremitet, kar je najbrž posledica velike pomembnosti, ki jo imajo spodnje ekstremitete pri človekovem gibanju in pa bržkone tudi dejstva, da je njihovo gibanje v večji meri planarno. Razlog za manjšo znanstveno pozornost, ki je bila namenjena gornji ekstremiteti gre, najbrž predvsem iskati v njeni večji kompleksnosti in s tem tudi mobilnosti. Pomembnost gornje ekstremitete lahko razberemo iz dejstva, da je danes znanstveno uveljavljeno mnenje, da je prav okretnost človekove roke v največji meri botrovala tako uspešnemu razvoju njegovih možganov skozi evolucijski razvoj. Ni presenečenje, da je bilo to dejstvo omenjeno že v antičnih časih [4].

Pomanjkanje študij gornje ekstremitete ni presenetljivo, sploh če upoštevamo, da je kinematična struktura roke veliko bolj kompleksna od strukture spodnje ekstremitete. Razlog za to leži v dejstvu, da gornja ekstremiteta služi kot primarno orodje, s pomočjo katerega človek izvaja interakcijo z okolico. Njena pomembnost za človeka je zato povsem primerljiva ali pa celo pomembnejša od spodnje ekstremitete.

Nastanek doktorske disertacije je bil v marsičem spodbujen s pojavom novih rehabilitacijskih metod in naprav, kot so denimo *haptični roboti* [5–9]. Zaradi ve-

likega napredka pri razumevanju in uporabi robotskih manipulatorjev se je njihovo število v industrijskem okolju namreč bistveno povečalo. Pomembnost robotske tehnologije pa se močno povečuje tudi na ostalih področjih, kot so denimo medicinska robotika in rehabilitacijska terapija. Haptični roboti predstavljajo robotske manipulatorje, ki omogočajo interakcijo med robotom in uporabnikom preko sile in dotika, s čimer so ti roboti sposobni ustvarjanja navideznega fizičnega okolja. V takšnih novodobnih rehabilitacijskih napravah bi lahko ugotavljanje biomehanskih parametrov razgibavanega uda predstavljalo velik prispevek h evalvaciji samega rehabilitacijskega procesa.

Kot smo že omenili, se predvsem v zadnjem času pojavlja povečan interes za razvoj novih naprav, ki bi pomagale zdravnikom in fizioterapevtom pri terapiji njihovih pacientov z motnjami v gornji ekstremiteti. Tovrstni pacienti so v največji meri tisti z okvaro centralnega živčnega sistema (CŽS), kjer le ta ne more več normalno opravljati svojih funkcij. Pri tovrstnih pacientih je takojšnja terapija po poškodbi bistvenega pomena. Razlog za to je nedavno odkrito dejstvo, da drugi deli CŽS lahko prevzamejo določene funkcije poškodovanega dela [5, 9, 10]. Tovrstni pacienti so v največji meri pacienti po kapi ali tisti, ki trpijo za posledicami poškodbe hrbtenjače. Ker pa so tovrstne poškodbe velikokrat povezane tudi s starostjo oseb, se njihovo število v zadnjem času povečuje. Razlog tiči v postopnem staranju populacije v razvitem svetu, kar hkrati razloži tudi povečan interes družbe za tovrstne študije.

Biomehanika gornje ekstremitete

Zaradi izjemne kompleksnosti anatomske zgradbe gornje ekstremitete njeno modeliranje predstavlja zelo velik problem. Gornjo ekstremiteto sestavlja mehanizem, ki ga s skeletnega vidika lahko razdelimo na naslednje tri logične sklepne celote [11]:

- *Ramenski sklop*, ki predstavlja daleč najbolj kompleksno sklepno strukturo v človeškem telesu. Omogoča zelo visok nivo mobilnosti, saj pri njegovem gibanju sodelujejo kar štiri kosti (*nadlaktica*, *prsnica*, *lopatica* in *ključnica*). Te štiri kosti sestavljajo tri rotacijske in en translacijski sklep v okviru ramenskega sklopa:
 - *Glenohumeralni sklep*, ki ga sestavlja kontakt med lopatico in nadlaktico in vsebuje izjemno veliko mobilnost.
 - *Sternoklavikularni sklep*, ki povezuje robni del ključnice s prsnico.
 - *Akromioklavikularni sklep*, ki med seboj povezuje lopatico in ključnico.

- *Skapulotorakalni sklep* pa ustvarja translacijski sklep v kontaktu med trupom in lopatico.

Ti štiri sklepi omogočajo tri rotacijske prostostne stopnje ramenskega sklopa (*fleksija - ekstenzija, pronacija - supinacija in abdukcija - addukcija*) in eno translacijsko (*skapulotorakalna pomičnost*).

- *Komolčni sklep* z dvema rotacijskima prostostnima stopnjama, ki omogočata gibe *pronacije - supinacije* in *fleksije - ekstenzije* v komolcu.
- *Zapestni sklep*, ki prav tako omogoča dve rotacijski prostostni stopnji v obliki *fleksije - ekstenzije* in interne rotacije zapestja.

Poleg naštetih sklepnih struktur, ki vse skupaj torej omogočajo 8 prostostnih stopenj, pa prsti prav tako predstavljajo izjemno kompleksen mehanizem s preko 25 dodatnimi prostostnimi stopnjami [12], kar omogoča zelo veliko spretnost.

Skeletna struktura gornje ekstremitete pa določa le njeno kinematiko, medtem ko moramo za dinamični opis upoštevati še vsa ostala tkiva, ki sestavljajo posamezne telesne segmente. Ta tkiva morajo med seboj sodelovati na ustrezen način, kar zagotavlja dinamično stabilnost in želeno gibanje.

Očitno je torej anatomsko zgradbo gornje ekstremitete izjemno težko umetno posnemati. To velja tako za kinematično [13], še posebej pa za dinamično modeliranje [14, 15]. Prav ta kompleksnost avtorje sili h poenostavljanju svojih modelov pri raziskavah. Predstavljena doktorska disertacija pri tem ni nobena izjema, saj v celotni roki upošteva le tri prostostne stopnje, ki pri izvajanih gibih brez bistvenih napak v celoti opišejo gib.

Kadar govorimo o dinamiki gornje ekstremitete, moramo upoštevati veliko dejavnikov, ki prispevajo k njenemu dinamičnemu obnašanju. V grobem bi jih lahko združili v naslednjih dveh kategorijah [16]:

1. Najprej je potrebno omeniti *statične prispevke* h gibanju, ki so prisotni ves čas, tudi takrat ko gibanja ni. To so z gravitacijo povezani vplivi in tisti, do katerih pride zaradi specifičnih biomehanskih lastnosti, struktur kot so mišice, kite, tetive in koža, ki sestavljajo posamezen telesni segment. Te lastnosti neposredno vplivajo na viskoelastičnost sklepov oziroma na *pasivne momente* [17, 18] v primeru, ko ni nobene hotene mišične aktivnosti.
2. Na drugi strani pa lahko govorimo o *dinamičnih prispevkih* na gibanje, ki pa delujejo le takrat, ko se izvaja gibanje. Pospeški segmentov povzročajo vztrajnostne vplive, medtem ko so Coriolisovi, centrifugalni in viskozni vplivi neposredno povezani s hitrostmi. Potrebno je poudariti, da viskoznost predstavlja notranjo lastnost vseh sklepov v človekovem telesu, njihovi vplivi pa so premo sorazmerni s hitrostjo posameznih sklepov [19, 20].

Celotna dinamika gornje ekstremitete je rezultat koordinacije dinamičnih lastnosti sklepnih in segmentnih dinamičnih in statičnih lastnosti. Pri našem pristopu smo skušali ločiti in ovrednotiti obe omenjeni kategoriji.

Zastavljeni cilji

V bližnji preteklosti se je relativno majhno število študij ukvarjalo z razvojem novih tehnik za ugotavljanje parametrov gornje ekstremitete [21–24]. Zaradi tega dejstva predstavljamo metodo, ki s pomočjo uporabe robotskega manipulatorja skuša ugotoviti te parametre na podlagi vsiljevanja *trajektorije gibanja* v sklepe človeške roke. Relativno enostavno eksperimentalno okolje omogoča enostavno metodo, ki bi se lahko uporabljala v *novih robotskih rehabilitacijskih metodah*. Po drugi strani pa tovrstno eksperimentalno okolje lahko pomeni tudi novo *metodo za ugotavljanje parametrov zanimivo z vidika biomedicinske tehnike*, kjer so predmet zanimanja predvsem notranje fizične lastnosti telesnih segmentov in sklepov. Cilje disertacije bi lahko strnili v naslednjih treh točkah:

- Najprej smo skušali *ovrednotiti notranje viskoelastične lastnosti sklepov*. Te smo proučevali tako, da smo upoštevali inverzni dinamični model gornje ekstremitete, ki je bila modelirana kot planarna togosegmentna struktura s tremi prostostnimi stopnjami. Mase segmentov in težišča smo pri tem postopku privzeli iz literature, medtem ko smo merili sile na vrhu, kote v sklepih in dolžine segmentov. Naš cilj je bilo ugotavljanje teh internih sklepnih lastnosti, medtem ko smo roko gibali na različne načine. Skušali smo ugotoviti, kako se pasivne viskoelastične lastnosti spreminjajo v odvisnosti od različnih veličin, kot so na primer *različne kotne konfiguracije, mišična aktivacija in do določene mere tudi kotna hitrost*. Takšna metoda bi lahko predstavljala alternativo obstoječim metodam klinične evalvacije gornje ekstremitete na pacientih z živčnomišičnimi boleznimi, ki velikokrat nastopijo po kapi. Vzorci pasivnih viskoelastičnih lastnosti pridobljeni na tovrstnih pacientih se bodo po naših predvidevanjih bistveno razlikovali od tistih, pridobljenih na zdravih osebah [25, 26]. V disertaciji smo študijo omejili zgolj na skupino šestih zdravih ljudi in vrednosti pasivnih momentov v določenem sklepu predstavili v odvisnosti od kota v tistem sklepu in v sosednjih sklepih.
- Naš drugi cilj je bil razvoj *splošne metode za ocenjevanje parametrov gornje ekstremitete*, ki v nasprotju s prej omenjeno metodo ne privzema mas posameznih segmentov in njihovih težišč iz literature pač pa jih poskuša identificirati. Motivacija za to študijo je med drugim prišla tudi kot posledica nepredvidljivih napak, do katerih prihaja pri privzemanju biomehan-

skih parametrov iz literature. Te napake so včasih lahko precej visoke, sploh če se struktura telesa posamezne osebe v precejšnji meri razlikuje od povprečne populacije, za katero ponavadi veljajo izsledki tovrstnih študij. Skušali smo identificirati mase in težišča nadlakti, podlakti in dlani in pridobljene vrednosti primerjati z rezultati drugih študij. Hkrati pa smo v procesu identifikacije ugotavljali tudi interne pasivne viskoelastične lastnosti sklepov. Identifikacijski postopek smo izvedli v različnih kotnih konfiguracijah roke z majhnimi kotnimi spremembami, kar nam je omogočilo *predpostavljanje linearnosti internih sklepnih lastnosti roke*. Da bi ugotovili kvaliteto razvite metode smo jo najprej izvedli na mehanskem modelu narejenem iz aluminija, medenine in nerjavečega jekla. Ta model je vključeval dva planarna segmenta in mehanizem, ki je v vsakega od sklepov lahko vnašal poljubno zaviralno silo, ki je bila neposredno merjena z dvema merilnima celicama. Vsi parametri modela so bili znani iz CAD modela in so tako lahko služili kot referenčna vrednost za verifikacijo postopka identifikacije.

- Tretji cilj je bil *razvoj simulacijskega okolja*, ki bo omogočalo ponovitev in načrtovanje eksperimenta na osebem računalniku. Simulacija je morala vsebovati planarni model gornje ekstremitete s tremi prostostnimi stopnjami in robotski manipulator, ki je z roko povezan v zaprti kinematični verigi. Poleg modela gornje ekstremitete s tremi prostostnimi stopnjami je bilo mogoče vnesti tudi mehanski model z dvema prostostnima stopnjama. Simulacijsko okolje nam je moralo omogočati vpogled v vse pomembne podatke o sili, navoru, kotu, kotni hitrosti in kotnem pospešku z namenom lažjega načrtovanja eksperimenta. Neposredno uporaben rezultat simulacije je predstavljala sklepna trajektorija robotskega manipulatorja, ki je potrebna za izvedbo željenega giba roke ali mehanskega modela. Sklepi gornje ekstremitete so se morali med simulacijo gibati vzdolž predpisane kotne trajektorije. Simuliran model je moral omogočati tudi ugotavljanje vseh parametrov sklepov in segmentov, ki so bili določeni z obema izvedenima eksperimentoma.

Rezultati in izvorni prispevki disertacije

Ko govorimo o izvirnih prispevkih disertacije, je potrebno na prvem mestu poudariti, da na delo lahko gledamo iz dveh različnih zornih kotov. Na eni strani je predstavljena *biomehanska študija* zanimiva predvsem za boljše poznavanje biomehanskega modeliranja roke, medtem ko po drugi nanjo lahko gledamo kot na *rehabilitacijsko metodo*, zanimivo z vidika medicine in fizioterapije. V naslednjih

točkah bomo poskušali strniti pogloblitve prispevke disertacije:

- Predlagana metoda uporablja robotski manipulator za določanje biomehanskih parametrov gornje ekstremitete, kar že samo po sebi predstavlja *nov, robotsko orientiran pristop, ki ga je v preteklosti uparabljalo relativno malo raziskovalcev*. Trajektorije, ki smo jih vprogramirali v robota so bile dejansko dokaj preproste in počasne in bi jih lahko izvedli tudi s pomočjo precej bolj enostavnih in cenejših naprav. Kriteriji, katerim je moral zadostiti manipulator, so bili dovolj velik delovni prostor, zmožnost vsiljevanja vsaj dveh prostostnih stopenj v sagitalni ravnini osebe, ter zadostna časovna zveznost generiranih trajektorij.
- V okviru doktorske disertacije predlagamo, da lahko katerokoli od opisanih metod za ocenjevanje parametrov gornje ekstremitete uporabimo v namene *bodoče robotske rehabilitacijske terapije*. Tovrstna hitra in neboleča metoda bi bila lahko stranski produkt normalne vsakodnevne rehabilitacijske terapije pri pacientih z motnjami v gornji ekstremiteti.
- V delu predlagamo nov pristop za ugotavljanje *pasivnih momentov* v rami in komolcu merjene osebe. Pristop je zelo enostaven s stališča uporabnika, saj ne zahteva nobenih dodatnih fiksirnih mehanizmov in omogoča hiter vpogled v izračunane parametre.
- Eksperimentalno smo dokazali, da *pasivni momenti v rami in komolcu izkazujejo velike nelinearnosti v odvisnosti od fiksacije sosednjih sklepov*. V ta namen smo izmerili šest zdravih oseb, od katerih je bila vsaka izmerjena v desetih različnih kotnih konfiguracijah. Rezultati kažejo podobne trende v spreminjanju vrednosti pasivnih momentov, v odvisnosti od različnih kotnih konfiguracij.
- Razvita je bila nova metoda za ugotavljanje PTS, ki *identificira parametre mas in težišč za vse tri segmente gornje ekstremitete*. Metoda se izvaja hitro in dokazano daje primerljive rezultate s študijami iz literature [21, 27, 28]. Ker smo metodo verificirali s pomočjo mehanskega modela, lahko na podlagi teh izsledkov sklepamo na velikost napak, katerim so podvrženi rezultati identifikacijske metode. Le-ta ostaja znotraj zadovoljivih meja in dokazuje, da je razvita metoda uporabna tudi z vidika ugotavljanja PTS. Predstavljena metoda je precej *bolj predvidljiva* in enostavna, kot primerljive obstoječe metode.
- *Skonstruirali smo mehanski model za verifikacijo identifikacijskega postopka*, s pomočjo katerega smo lahko preko zavornega mehanizma poljubno nastavljali nivo Coulombovega trenja v sklepih. Nastali zaviralni momenti

so bili preko sile merjeni s pomočjo dveh uporovnih celic pritrjenih na sklepe mehanskega modela. Podoben mehanizem bi bilo moč uporabiti tudi v drugačnih aplikacijah, v katerih je potrebno direktno merjenje zaviralnih momentov. Identifikacijska metoda je bila s tem mehanskim modelom zadovoljivo verificirana, saj so bili dobljeni rezultati povsem primerljivi s tistimi iz CAD modela.

- Zaradi predpostavljanja planarnega modela s tremi prostostnimi stopnjami za gornjo ekstremiteto je bilo mogoče *vse parametre izračunati sočasno* v okviru enega samega giba roke. Zato je metoda precej prijaznejša do uporabnika, saj je do rezultatov mogoče priti skoraj takoj po izvedbi meritve.
- V disertaciji smo pokazali, da navidez *visok nivo poenostavitve*, ki smo jo napravili pri predpostaviti idealnega planarnega modela s tremi prostostnimi stopnjami, *še vedno lahko uporabljamo pri modeliranju gornje ekstremitete*. To dejstvo je razvidno iz rezultatov, ki se dokaj dobro ujemajo z izsledki iz literature.
- *Simulacijsko okolje*, ki smo ga razvili za študij in napoved eksperimentalnih rezultatov, bi prav tako lahko uporabili pri modeliranju poljubnega planarnega eksperimenta, ki vključuje dva mehanska sklopa, ki sta med seboj povezana v zaprti kinematični verigi.

*“Genius is one percent inspiration and
ninety-nine percent perspiration.”*

Thomas Alva Edison (1847-1931)

Abstract

This thesis deals with studying the internal biomechanical characteristics of the human upper extremity. This issue long ago proved to be very complex by numerous researchers. The problem of determining biomechanical properties in the upper extremity was dealt with in a laboratory environment using industrial robots which are normally used for other tasks in different environments. In the presented experiments we took advantage of the fact that *robot movements can be accurately repeated as many times as desired* and that *several other sensory devices can also be incorporated into the experimental setup* enabling us a very wide range of experimental possibilities. It needs to be emphasized that most upper extremity studies come from a more medically-oriented environment resulting in a fairly different approach researchers have towards the subject. On the other hand however, there are also many engineering oriented works which usually utilize special purpose robots developed especially for a certain experimental task.

In our experiments we used two different types of industrial robots (Yaskawa[©] - Motoman sk6 and Motomation[©] Stäubli - RX90) to impose accurately controlled robot motions into the upper extremity. The upper extremity was modelled as a simple 3 degree of freedom (3DOF) planar manipulator while all the experiments were performed in the sagittal plane of the studied subject. The subject's hand was always lightly strapped to the robot attached handle while not exerting any voluntary muscle activity. The upper extremity was then lead through a specified trajectory in space. During this process angle measurements were taken by means of an optical 3D positioning system and end-point forces were measured with a force sensor attached to the robot end-effector.

Firstly we tried to determine the nature of upper extremity joint passive moments while assuming other biomechanical parameters such as masses and centers of gravity (COG) from the literature. The parameters were determined when the shoulder and elbow flexion-extension angles were fixed at ten different angles while the unfixed joint was allowed to slowly move through a wide portion of its range, along a programmed robot trajectory. The method for determining passive moments was derived from the inverse dynamic equation of a planar 3DOF arm.

Comparing the obtained passive moments of six young male subjects unequivocally showed that there was a large non-linear adjacent angle dependency. On the other hand this non-linear nature could also be observed in relation to muscle activation and different joint velocities. The results came as a further confirmation to those obtained by other authors and showed a severe complexity with which the modelling of upper extremity biomechanical behaviour can be performed.

The second experimental phase of this thesis focused on identifying all biomechanical parameters which determine upper extremity motion at low speed. Again the upper extremity was guided through a specified trajectory while measuring angle data and contact forces. A suitable low velocity trajectory was imposed into all joints, with very small angular deviations. The arm was assumed to be linear within a small angular region, since passive properties from the first experiment showed no significant nonlinearities for such small angular ranges. The outcome of the identification was an estimate of masses and COG coordinates for the lower arm and palm segments, their products for the upper arm and the passive moments around the measured angle of all joints in the sagittal plane. These results were then compared to the literature estimates which are based on average population. An optimization based identification procedure was developed, which assumes the upper extremity model of a 3DOF rigid body planar structure in a closed kinematic chain configuration with the robot. The solution is based on fitting the joint torques calculated from contact forces to those predicted by the inverse dynamic model of the linkage. In order to verify the proposed identification procedure the experiment was first performed on a 2DOF mechanical arm with dimensions similar to those of the actual human arm. This mechanical model was designed using CAD software that provided an accurate assessment of all necessary dynamic parameters. The results showed good correlation between our identification outcome and reference values.

Thirdly a simulation of the whole experimental setup made with Matlab[®]-Simulink is presented. This gave a better insight into the experimental quantities and allowed us to gain much more control over performing the experiment. The simulation environment allowed us to observe all kinematic data such as joint angles, angular velocities and angular accelerations on one side and dynamic quantities such as joint torques and contact forces on the other. This also allowed us to hypothetically perform experiments which were not performed in reality. The results of the simulation gave comparable results to those obtained from measurement.

In the following chapters, the data from all performed experiments are shown, analyzed and put into context with current biomechanical research. It is also discussed whether the study could have useful implications to developing future application and research methods.

Chapter 1

Introduction

Researchers have long been aware of the importance for understanding biomechanical systems in everyday life. Like every mechanical body, human everyday movements and interactions with the outside world are governed by laws of mechanics. With the advances made in science and technology, human body biomechanics has soon become a topic of scientific research. Not surprisingly the first studies dealing with the determination of human *body segment parameters* (BSP) already date back to as far as 1860 [1]. With the industrial revolution humans started interacting with the environment in a previously unfamiliar way with speeds far exceeding those which were common before. This also involved greater risks making it more and more important for people to understand better the processes behind this interaction. Many times the stimulation for such research came from the military sphere which is still the case today, just like in many other scientific fields.

The beginning studies included a very limited number of cadavers and tried to quantify BSPs of the human body such as masses, centers of gravity and moments of inertia. With further technological improvements the need for biomechanical modelling increased significantly. On the other hand however, this progress also made it possible for researchers to use new more sophisticated methods which were not possible before. Instead of *in-vitro* studies performed on a very limited number of cadavers the newer studies could be performed on larger numbers of living subjects and enabled measuring of some previously unmeasurable physical quantities. This progress is especially visible in the last decades when computers and much of the measuring equipment have become widely available in research and medical institutions all over the world.

While most studies have been focused on biomechanical modelling of whole body movements such as gait or standing up [2, 3], there has been far less interest in modelling particular body segments. The lower extremity was the first to have received attention of many biomechanical researchers due to its importance in hu-

man locomotion and the fact that most of the interaction movements are planar. The greater complexity and thereby mobility may also be seen as one of the reasons why the upper extremity has not been dealt with so extensively in the past. The importance of the upper extremity on the other hand, may be understood by the fact that the dexterity of the human upper extremity is commonly considered to be the main reason for the so successful development of human brain in evolution. This has been shown by numerous modern researchers in paleanthropology [29, 30]. Not surprisingly this fact has already been mentioned by the famous ancient Greek philosopher Anaxagora [4].

The lack of studies dealing with the upper extremity comes as no surprise because the kinematic structure of the upper limb is far more complex to that of the lower extremity. The reason for this lies in the fact that the upper extremity serves as the primary tool which people use for interacting with the environment. Its importance therefore equally rivals and many times surpasses that of the lower limb.

The motivation for our study was in many ways inspired by the appearance of new rehabilitation devices such as *haptic robots* [5–9, 31]. These are robotic devices enabling the interaction between the robot and the user by means of force and touch simulating a virtual physical environment. In such new rehabilitation treatment devices estimating biomechanical parameters could enable an on-line parameter estimation technique used for evaluation purposes during the rehabilitation practice itself.

There is a growing interest in developing new interfaces which would assist the doctors and physiotherapists in treating their patients with upper extremity disorders. The patients in question are mostly those whose central nervous system (CNS) has been damaged to the extent where it cannot perform its normal functions. With such patients the immediate post-injury treatment is of vital importance. The reason lies in the recently discovered fact that other parts of the CNS can take over some of the functions which have been damaged during the injury [5, 9, 10]. The patients in question are many times after stroke patients or patients suffering from physical injuries of the spinal cord. Because such injuries are many times age related they are becoming more and more prominent due to graduate ageing of the population which also explains the growing interest for the subject in the society of the developed world.

Because of big advances made in understanding and using robotic manipulators their number has become very widespread in the industrial environment. The importance of robotic manipulators is also growing considerably in other fields such as medical robotics and rehabilitation therapy.

1.1 An overview of upper extremity biomechanics

Due to the severe complexity of the upper extremity anatomical structure only some basic facts which were important in conducting our research will be stated here. To get an anatomical insight into upper extremity kinematics we need to consider the bones in the shoulder girdle and those in the upper limb. They all contribute to the degrees of freedom in the upper extremity and can be divided into three logical joint structures [11](figure 1.1):

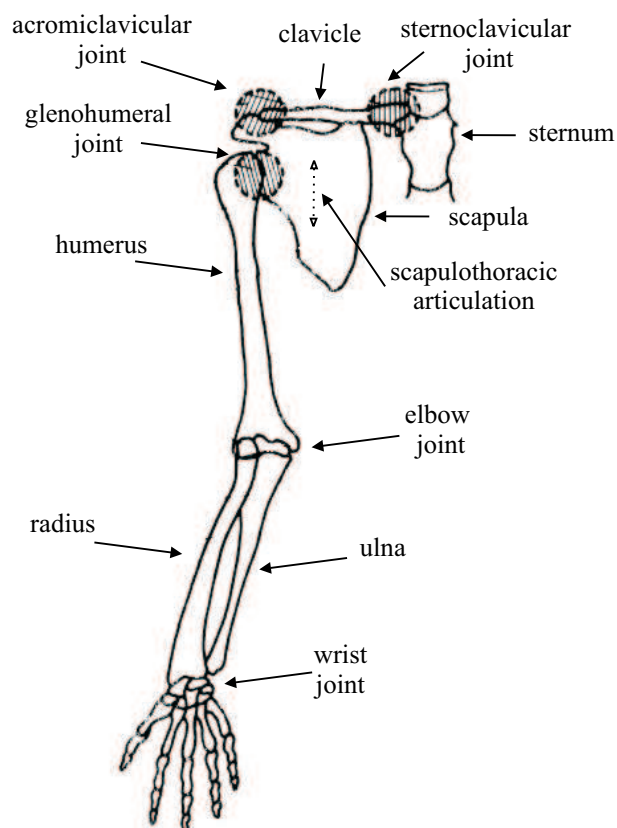


Figure 1.1: *The skeletal structure of the upper extremity with all joints contributing to mobility.*

Apart from the skeletal structure we should also observe the distribution of muscles in the upper limb. These also significantly contribute to dynamic properties of the upper extremity (figures 1.2 and 1.3):

- **Shoulder complex** which is by far the most complex joint structure in the human body enabling very big mobility. Four skeletal segments are in-

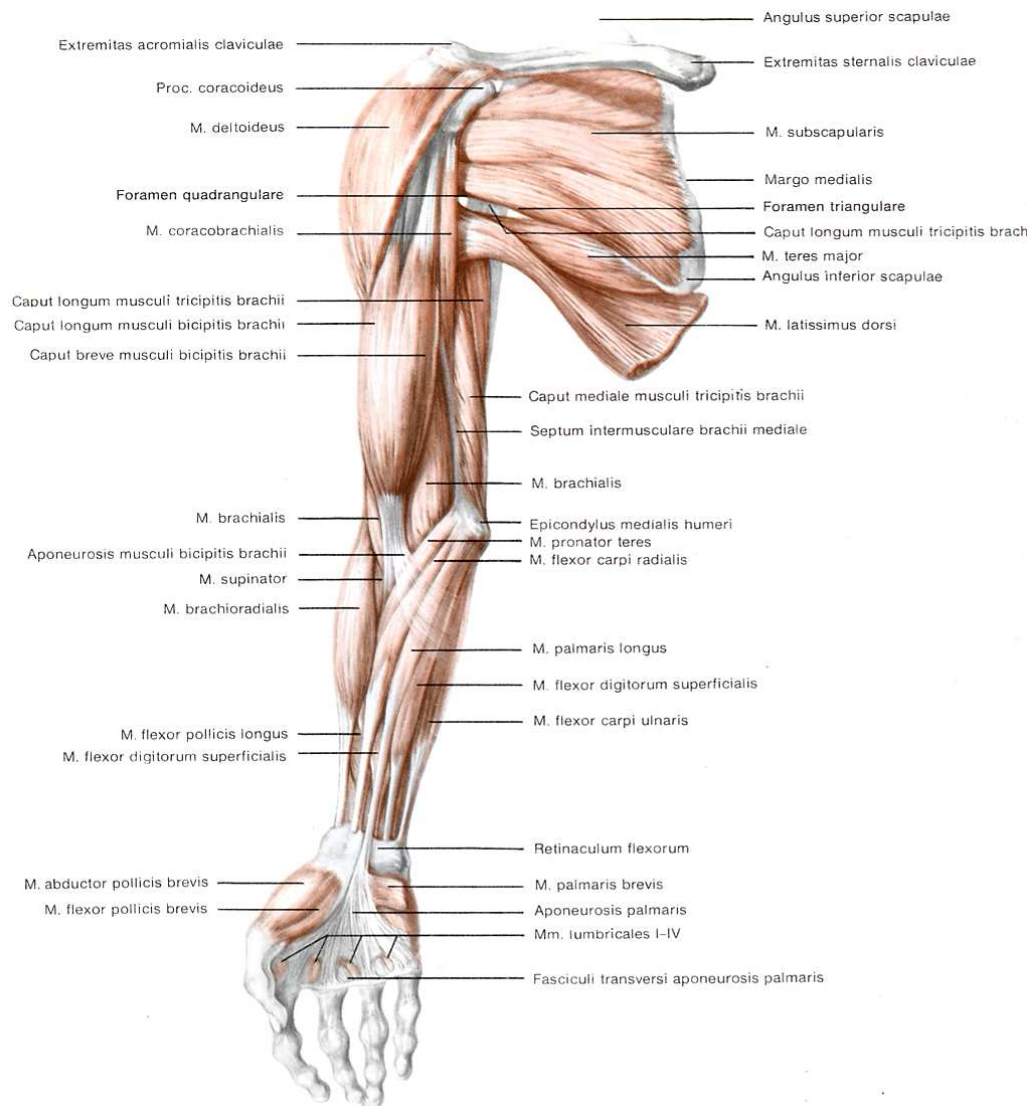


Figure 1.2: *Anterior view of the muscles in the upper extremity.* Source: R. Bertolini et al., *Anatomski atlas, I. del: Zgornji in spodnji ud, DZS 1987.*

involved, the humerus, sternum, scapula and clavicle, the latter two combined to make up the shoulder girdle. All but the sternum move simultaneously and in combination to permit the large range of motion between trunk and humerus [32]. These four bones compose three rotational and one translational joints:

- *Glenohumeral joint* which is formed by a synovial ball and socket joint

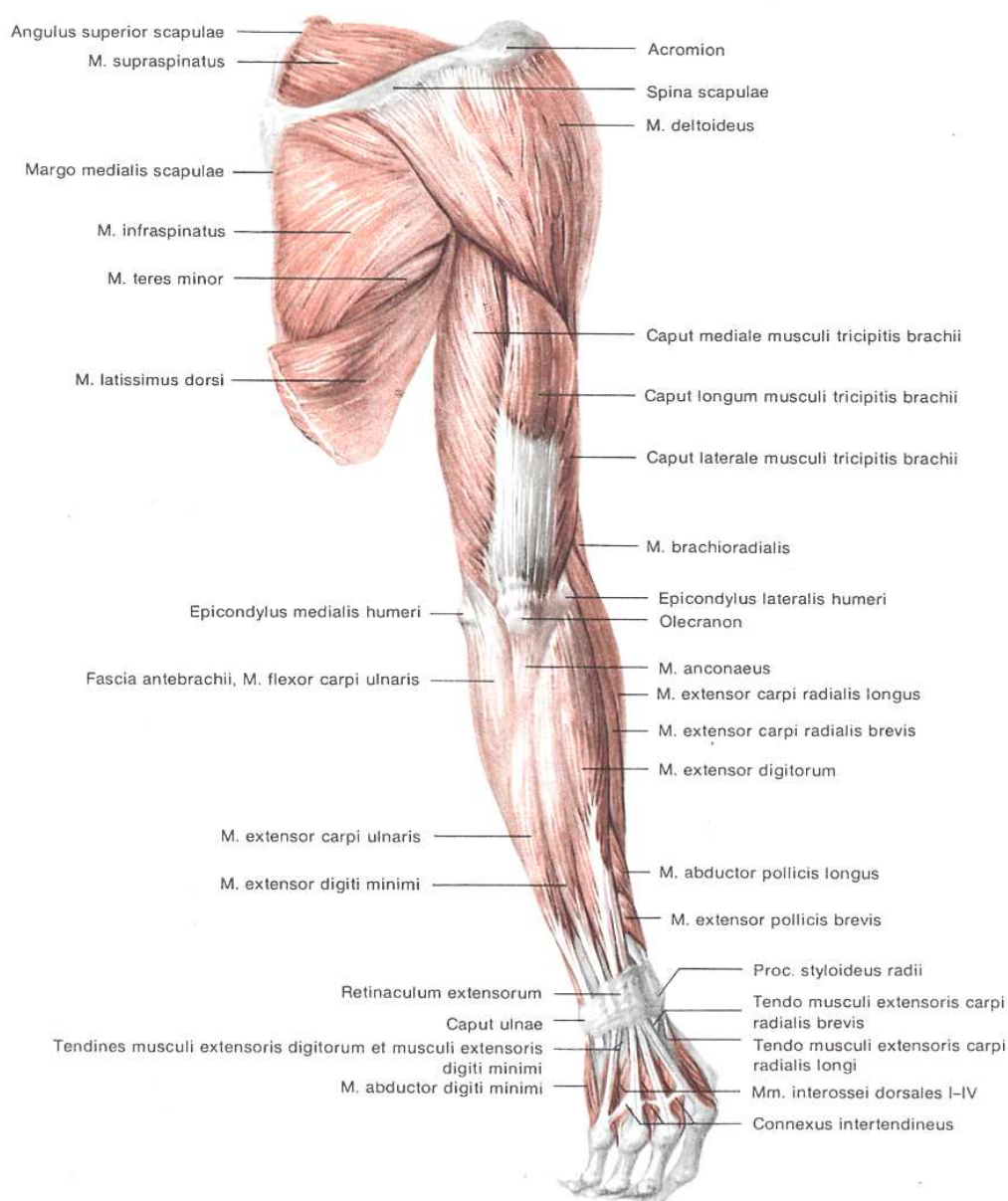


Figure 1.3: *Posterior view of the muscles in the upper extremity.* Source: R. Bertolini et al., *Anatomski atlas, I. del: Zgornji in spodnji ud, DZS 1987.*

in the contact between the humerus and the scapula with extremely large mobility.

– *Sternoclavicular joint* which links the medial end of the clavicle with

sternum. It also behaves functionally as a ball and socket joint although its form does not really suggest that.

- *Acromioclavicular joint* is a synovial passive joint linking the clavicle and scapula. It provides three additional rotational DOF to the shoulder complex after the sternoclavicular joint range of motion limits have been reached.
- *Scapulothoracic articulation* which forms a translational joint between the scapula and thorax with small range of motion. Many authors simply discard this degree of freedom [33].

Obviously, the shoulder complex does not only include three rotational DOF (*flexion-extension, pronation-supination and abduction-adduction*) but also one translational DOF in the contact between the scapula and thorax (*scapulothoracic mobility*).

- **Elbow joint** with two rotational DOF allowing the forearm to perform flexion-extension and pronation-supination movements as a linkage between the humerus radius and ulna bones. This linkage forms three separate joints (i.e. *art. humero-ulnaris, art. humero-radialis and art. radio-ulnaris*). The three bone configuration allows for a very small amount of *elbow abduction, adduction, lateral and medial rotation* although these are generally discarded in the literature. The elbow joint is a synovial joint between the arm and forearm and can for practical purposes be regarded as a pure hinge joint.
- **Wrist joint** which also gives two rotational DOF in the form of *wrist flexion-extension* and very limited wrist *internal and external rotation* movements. The contact is formed by metacarpal bones of the hand and radius and ulna bones of the lower arm.

These articulations link together the upper arm, lower arm and hand which all together already form a very complex structure. Apart from this the hand fingers contain an additional over 25DOF allowing an extremely large level of dexterity [12].

It needs to be emphasized that the explained skeletal structure is surrounded by many muscles, tendons, skin and ligaments which play a very important role in describing the upper extremity biomechanical interaction with the environment. The surrounding tissues must interact with the bone structure in order to provide dynamic stability and desired movements.

It is evident that the upper extremity anatomical structure makes it extremely difficult to artificially recreate. This is true both for kinematic [13] and especially

for dynamic modelling [14, 15]. It is this complexity which forces authors to simplify their models of the upper extremity when performing their research.

1.2 Thesis objectives

There have been relatively few studies [22–24, 34–36] dealing with developing new techniques for upper extremity parameter estimation. We therefore attempt to present a method which utilizes a robot manipulator for *imposing repeatable movement trajectories* into the joints of the human arm for parameter estimation. Relatively simple experimental setup enables a straightforward method which could be used with *new robotic rehabilitation treatment devices*. On the other hand the same experimental setup can also provide the means to develop a new *estimation technique interesting from the biomechanical point of view* where internal physical properties of body segments and joints are of interest. The thesis objectives could be summed up into the following three crucial points:

- Firstly we tried to *quantify the internal joint passive viscoelastic properties*. These were studied by accounting for an inverse dynamic model of the upper extremity which was modelled as a 3DOF planar rigid body structure. Segment masses and mass centers were taken from the literature while the end-point forces, angles and segment lengths were measured during the course of the experiment. Our aim was to investigate these internal joint properties while the arm was exposed to various conditions. We tried to determine how the passive viscoelastic properties varied in relation to various quantities such as *different angle configuration, muscle activation and to some extent also the angular joint velocity*. Such a method is meant to provide an alternative upper extremity clinical evaluation method which could be used on patients suffering from neuromuscular disorders usually following a stroke and other kinds of neuromuscular diseases. Patterns of passive viscoelastic properties obtained from such subjects are expected to show noticeable differences from the healthy ones [25, 26]. In this study, however, the research was limited to a group of healthy individuals only.
- Our second aim was to develop a *more general upper extremity parameter estimation technique* which in contrast to the previous investigation, does not presume the segment masses and mass centers from the literature but tries to identify them. The motivation for this work came as a result of unpredictable errors when taking biomechanical parameters from the literature which can sometimes be quite high especially if the subjects body structure differs from the average population taken for granted in these studies. We

attempted to identify the masses of the upper arm, lower arm and hand segments together with their centers of mass and compare these results to other studies. At the same time joint internal passive viscoelastic properties also had to be accounted for. This was done in various configurations of the arm with small angular deviations which allowed us to presume the *linearity of the model joint internal properties*.

- The third goal was *developing a simulation environment* which would allow a complete recreation and planning of the experiment on a personal computer. It had to incorporate the 3DOF planar model of the upper extremity and the robot manipulator which is coupled with it forming a closed kinematic chain. The simulation had to allow us to have an insight into all relevant force, torque, joint angle, velocity and acceleration data in order to be able to easily plan the experiment in advance. The upper extremity was allowed to move along a specified angular trajectory determined by the user. The simulated model also had to allow a determination of all joint and segment parameters which were determined experimentally.

1.3 Thesis original contributions

When speaking of the contributions which this thesis has to scientific research it needs to be pointed out that we can look at it from two different aspects. On one hand it represents a *biomechanical study* which should be interesting to those dealing with upper extremity biomechanics. On the other hand however, it can be regarded as a *rehabilitation treatment method* which could be of interest to the medical and physiotherapy communities. We will try to sum up the main thesis contributions in the following points:

- It needs to be emphasized that the proposed method for evaluating biomechanical upper extremity parameters utilizes a robot manipulator which by itself represents a *novel robotically oriented approach which has been used by relatively few researchers in the past*. The reasons for this have been explained at the beginning of this chapter. The trajectories we programmed into our robots were straightforward and slow not actually requiring robot manipulators as complicated and expensive as the ones used in our study. The only criteria the manipulator needs to meet are a large enough range of motion and at least 2DOF in the sagittal plane of the subject.
- In the work it is proposed that any of the described parameter estimation methods could be used in *future robotic rehabilitation treatment*. Such

quick and painless method could be used as a side product of normal everyday rehabilitation treatment of patients with upper extremity neuromuscular disorders.

- It has been experimentally proven that *passive moments in the shoulder and elbow express a severe nonlinear relation to the fixations of adjacent joints*. Six healthy individuals were examined for this purpose, each being tested in ten different angular configurations. The results showed a similar trend in changes of passive moments in relation to different angular configurations.
- A new BSP estimation technique has been developed for *predicting the masses and centers of gravity for all three upper extremity segments*. This method is quick and was proven to result in results comparable to those in the literature. Because the method has been verified by means of a mechanical model it is possible to estimate the amount of error which the results are subject to. The presented method involves *more predictability* and simplicity in relation to other methods.
- *A mechanical model for method verification has been constructed* with which it was possible to adjust the joint Coulomb frictions by means of a disk brake mechanism. The produced resistive moment could be measured with two attached load cells allowing a direct measurement of joint mechanical properties. A mechanism of a similar kind could also be used in different applications requiring the knowledge of resistive torques.
- Because a 3DOF planar model has been assumed for the upper extremity, *all parameters could be determined simultaneously* in only one movement. This makes the method more elegant from the point of view of the user since results can be obtained almost immediately after the measurement.
- It has been shown that a seemingly *large level of simplification* which we made by assuming an ideal 3DOF planar model *can still be used for upper extremity modelling purposes*. To see this we need to observe the results which show good correlation with the literature.
- *The simulation environment* which was designed for studying and predicting the experimental results could also be used with an arbitrary planar experiment involving two mechanical linkages connected in a closed kinematic chain.

Chapter 2

Upper extremity dynamic modelling and identification

The modelling of biomechanical systems has recently gained importance in research related to fields such as rehabilitation engineering, kinesiological studies and analyzing biomechanical systems in various situations. A dynamic relationship among different human body segments depends on the values of various body segment parameters such as *segment moments of inertia, segment masses and a distribution of mass within segments (centers of gravity - COG)* [37, 38]. On the other hand it is equally important to understand the joint dynamics which is governed by joint viscoelastic properties. These properties exert a nonlinear relationship as a function of joint angle, joint angular velocity and voluntary muscle action [26, 39–42]. By knowing the kinematic parameters such as segment geometry and angular configurations and by accounting for all relevant body segment parameters it is possible to mathematically describe the behavior of a biomechanical system in any given moment. When applying *inverse dynamics* it is possible to calculate joint moments from joint angles, angular velocities and angular accelerations. The reciprocal problem of determining joint angles, angular velocities and angular accelerations on the other hand is solved by *direct dynamics* [37, 38].

There have been many studies attempting to understand the dynamic effects in human body motion, most of which were concentrated on trajectories of the whole human body. Some studies dealt with human locomotion [43], whereas in many other studies the dynamic effects in human rising was observed [44, 45]. In the latter two studies the subject was asked to rise from a chair at various speeds at which the dynamic contributions were scrutinized, whereas the study of Pai *et al.* analyzed the dynamic effects of different body weight during the body rising action [46].

Since the biomechanical system in this study was the human upper extremity we will try to give some basic insight into its dynamics and show how the matter

was regarded by other authors. We will give an introduction to the upper extremity joint mechanical properties and to different body segment parameters (BSPs).

2.1 Upper extremity as a dynamic system

When considering movements of the upper extremity there are many factors contributing to the dynamic behavior which could be divided into the following two categories [16]:

1. Firstly there are the *static contributions* which are present at all times such as the gravity related contributions and those arising from specific biomechanical properties of the muscles, tendons, ligaments, and skin which all comprise a particular body segment. The latter directly affect joint properties are usually referred to as joint viscoelastic properties or *passive moments* [17, 18] in a case when there is no muscle activity.
2. On the other hand the *dynamic contributions* are in effect only when motion is in progress. The accelerations cause inertial contributions, while the Coriolis-centrifugal effects and viscosity contributions relate to the joint speed of motion. It needs to be noted that viscosity is an internal non-Newtonian property of all joints in the human body whose effects are non-linear in relation to the joint's angular speed of motion [19, 20]. It is determined by the synovial fluid and joint tissues surrounding joints which are all non-newtonian in nature.

The dynamic effect of motion on the upper extremity has not been studied to such an extent as with some other human body segments. Hollerbach and Flash for example studied the generation of various joint dynamic torques using the inverse dynamics Newton-Euler formulation in an experiment involving arm movements in the horizontal plane while holding a simple passive two degree of freedom manipulandum [47].

In the upper extremity dynamic studies much work has been concentrated on studying angles and angular velocities, especially in the elbow and shoulder joints. The studies of Suzuki *et al.* and Lan have concentrated on normal reaching movements [48, 49], whereas the study of Morasso dealt with a wide spectrum of everyday movements [50]. From all these measurements it is clearly evident that the arm joint angular velocity profiles are bell shaped. In fact the study of Zhang *et al.* [51] proved that the joint angle vs. time profiles, derived from point to point reaching movements can be directly scalable among different subjects independent of the motion speed. From this finding it was deduced that the same also applies for bell shaped velocity profiles. On the basis of the equilibrium point

trajectory hypothesis, Flash derived a method for determining the magnitude of force exerted in the arm during reaching movements in the horizontal plane [52]. Similar findings and experimental methods can also be observed in the later work of Guomi and Kawato [53].

Being able to determine the biomechanical parameters in joints and body segments is of very big importance in biomechanical modelling as we have explained earlier. Initially we will give an overview of the joint internal properties in the upper extremity which are referred to as *passive moments* or *passive viscoelastic properties*. The latter are in question when there is no voluntary muscle action. When a movement is performed, however muscles are not inactive but also significantly contribute to the joint viscoelastic properties. Because the effects of muscle activation is many times very unpredictable and difficult to measure authors usually focus into determining passive joint properties which we think could be used in upper extremity evaluation.

The dynamics of the upper extremity is a result of the coordination of joint and segmental properties. In our approach we tried to separate and quantify both these categories.

2.2 Upper extremity joint properties

The passive moments exerted in the human musculoskeletal system are an internal property of every joint in the upper and lower extremities. They arise mostly due to the presence and deformations of structures such as tendons, ligaments, skin, joint capsules, inactive muscles and bones composing a particular joint [17, 18]. By definition they are composed of elastic and dissipative contributions [18] where most authors have concentrated only on elastic effects [17, 54].

There have been a large number of studies dealing with these properties, out of which the majority were concentrated on lower extremities [54–56]. In addition to examining torque-angle properties for one joint, many authors have attempted to construct a model expressing the passive elastic moments as a function of the two adjacent joint angles. Most [18, 54] have used a technique proposed by Audu and Davy [57] where this function was taken to be a double exponential curve, indicating a significant torque increase at extreme angles. On the other hand, Hatze [17] proposed a model, consisting of a sum of several individual tissue exponential contributions relating to an observed joint. This relation was further simplified into a hyperbolic one, requiring an identification of a total of 53 elastic and viscous parameters for each degree of freedom in the human elbow joint (*i.e.* flexion-extension and pronation-supination). It has to be pointed out that all these studies were made without any voluntary muscle action.

There have also been some studies concentrated on the arm joint properties

in the presence of a voluntary movement, particularly in the elbow joint. These studies all had to be done by inserting perturbations of frequencies which were much higher than those which the CNS is capable of generating. Following a study on torques produced in the elbow joint with voluntary movements [58], Bennett and Hollerbach *et al.* [59] devised an ensemble parametric method for identifying the time-varying compliance of the human elbow joint, using an airjet actuator apparatus. Further studies by Xu and Hollerbach [60, 61] on the elbow joint mechanical properties concentrated on estimating elasticity, viscosity and inertial contributions during a voluntary movement, using a similar technique and a two-dimensional device capable of imposing random torque perturbations. In all these studies the inertia contribution of all joints was shown to remain constant despite the varying voluntary muscle action, whereas elasticity and viscosity, both increased and decreased proportionally with the applied muscle force. A number of other studies concentrated on the end-point stiffness of the human arm mechanism, as a result of all upper limb joint mechanical properties acting in concert [62–65].

The studies of Engin *et al.* concentrated mostly on the shoulder joint. They dealt extensively with kinematics of the human shoulder complex [33, 66, 67] and also investigated its passive resistive properties [68–70]. A study of elbow passive resistive properties limited to an area beyond the full elbow extension was also carried out [71]. A comprehensive analysis of the kinematic and dynamic behavior of the shoulder mechanism providing a good insight into mechanics of the shoulder mechanism, was presented by Van der Helm [14]. The clinical studies of Dewald and Given have studied the abnormal patterns in joint passive stiffnesses and maximum voluntary joint torques in the shoulder and elbow for spastic and hemiparetic patients as a relation to healthy subjects [25, 26]. Their work indicates obvious differences when comparing these two groups of subjects and also determines differences due to various muscular structure in the arm. The mechanism they used in their experiment was focused on only one single joint which by itself is a very different approach from the work we are presenting. It needs to be pointed out however, that most studies were carried out for the shoulder complex and that there is a lack of studies concentrating on the properties of the elbow and especially the wrist joints.

Some data on the deviations from joint axial rotations, acquired in an *in vitro* study of the upper extremity performed by Veeger *et al.* [72], were also a good lead to our study. This study was performed on five upper extremity cadaver specimens and showed that this axial deviation was within reasonable limits. On the other hand the anatomical studies also provided estimates of muscle physiological cross-sectional area (PCSA) of upper extremity muscles which are of vital importance in determining joint passive properties. A larger PCSA, hence implies more viscoelastic joint resistance.

It needs to be said, however, that estimating joint passive viscoelastic properties is very specific according to subject and could not be determined by measuring a test group of subjects. Therefore a direct measurement of these quantities is required. Unlike the work of Xu and Hollerbach [60, 61], our study separated the effects of passive and active musculoskeletal contributions to human arm dynamics. This was done by imposing slow movements into the shoulder and elbow joints and asking the subject to induce no voluntary muscle activity during the measurement.

2.3 Body segment parameters in the upper extremity

Like joint properties the body segment parameters are just as important in biomechanical modelling. The major difference between the two lies in the fact that joint viscoelastic properties vary considerably during every movement whereas body segment parameters remain relatively constant. They may vary to a small extent due to changes in tissue distribution, but since these changes are relatively small their numeric values have been investigated by a large number of authors. It needs to be mentioned, however, that their values change considerably under the influence of factors such as ageing, gender or different body structure [23, 73, 74].

Due to obvious difficulties in determining these data for a particular person directly, authors performing biomechanical modelling usually refer to studies from literature which state the desired parameters in the form of regression equations as a function of easily measurable quantities such as body masses and body heights. The oldest such studies were made *in vitro* on cadavers and only dealt with a relatively small test group of subjects. The importance of such studies is indicated by the fact that the oldest such attempt has already been made in 1680 by Borelli [75]. Surprisingly this investigation used live subjects but only determined the COGs of the entire human body and could therefore hardly be regarded as a body segment parameter estimation method. The first systematic study determining the properties of 44 particular body segments was carried out by Harless in 1860 [1] on a group of 9 cadavers. A similar *in vitro* study on 3 cadavers was performed three decades later by Braune and Fischer [76]. This study was the first to have introduced regression equations and was considered a standard for more than half a century to come. The most comprehensive study including 152 living male and female subjects was performed by Bernstein *et al.* [77] utilizing the method of reaction change where the subjects body segment COGs were measured in different configurations while lying on a balance plate. Among the still commonly cited *in vitro* studies are the pioneering works of Dempster (1955) [27] and Clauser

(1969) [28]. The former analyzed 8 older male cadavers while the latter focused on a group of 13 middle aged male cadavers. Drillis and Contini [78] performed a study on 20 living male subjects by utilizing a *segment zone method* which determines the volumes of body segments with stepwise immersion into water and their masses by observing the change in mass during the process. The last among the *in vitro* studies on cadavers were performed by Clauser in 1969 and Chandler in 1975 [28, 79]. These studies respectively included 13 and 6 frozen male cadavers on 14 different body segments. Hatze [22] developed a more complex mathematical method for body segment parameter estimation which is based on 242 simple anthropometric measurements taken from a particular subject. His model accounted for variations in mass distribution and assumed 17 different body segments. A method based on mathematical models was also developed by Contini [80].

Today most such studies are non-invasive, performed *in vivo* and include much larger test groups. Among these one we would like to point out the work made by Russian scientists Zatsiorsky and Seluyanov [21] in 1983 who used the γ ray absorption method for measuring average segment densities on a large group of 100 healthy young Caucasian male subjects. The method utilized a source of γ rays and measured their power attenuation as the radiation passed through different parts of the body. This particular study and its slight modification, performed by DeLeva [81], are often used in many present day biomechanical studies. They therefore also served us as a reference in our research. Because the study of Zatsiorsky gives regression equations for all important BSPs and because it was performed on a relatively large group it is still one of the most commonly cited works in the field. Nowadays the γ ray method would be considered too invasive meaning that new more modern methods will have to be used in future studies.

With technological progress made in the last decades some other non-invasive methods have also become available. The most significant ones are undoubtedly Computer Tomography (CT) and Magnetic Resonance Imaging (MRI), which both give detailed information concerning the distribution of internal structures such as tissues and bones in body segments. By assuming the mean tissue density values and accounting for the measured spacial distributions, it is possible to calculate the values of various body segment parameters. Several attempts in this direction have already been made [23, 24, 82–84]. Out of these only a CT study of Wei and Jensen [23] was performed on a larger group consisting of 50 individuals. The focal point of this study was the determination of different segment axial density profiles which are normally assumed constant so it did not provide a comprehensive BSP analysis. Other mentioned authors, however, do not give a comprehensive analysis on a very large test group of individuals, but it must be said that both methods offer good prospects for future researchers. These studies all tried to determine body segment moments of inertia which in the process also

Table 2.1: *Relative mass of upper extremity body segments in cadavers and living people as percentage of body mass*

Segment	Harless 1860 [1]	Braune & Fischer 1889 [76]	Dempster 1955 [27]	Clouser <i>et</i> <i>al.</i> 1969 [28]	Bernstein 1931 [77]	Zatsiorsky 1983 [21]
Upper arm	3.2	3.3	2.7	2.6	2.65	2.70±0.24
Lower arm	1.7	2.1	1.6	1.6	1.82	1.63±0.14
Hand	0.9	0.8	0.6	0.7	0.7	0.61±0.08

requires the knowledge of segment masses and COGs.

Considering all these studies a question of estimated regression equation accuracies arises since body segment properties among various people may differ quite significantly. For example the average age of subjects involved in the study made by Zatsiorsky [21] was approximately 24 years, whereas many of today's studies requiring body segment parameters focus on older individuals who have in the past suffered from certain neuromuscular disorders. It is therefore not surprising that Hinrichs [85] stated: "The use of indirect estimates of body segment masses, centers of mass and moments of inertia is arguably one of the biggest sources of error in biomechanics research." For indication of data variability we will present a table of upper extremity segment masses which were obtained by various authors in the past:

Because of the addressed problem this study proposes an alternative *in vivo* technique for determining values of BSPs in the upper extremity by utilizing an optimization curve fitting technique. In the experiment parameters were first estimated on a mechanical arm for which we knew all dynamic parameters. Comparing the results of our identification technique allowed us to obtain the accuracy level of the procedure. The same procedure was afterwards tested on three healthy individuals and the results compared to our reference literature study.

The motivation for the presented study also comes as a result of new rehabilitation devices such as haptic robots [5, 9], where this method could enable an on-line parameter estimation technique used for subsequent evaluations during rehabilitation practice. It is expected that such rehabilitation devices will significantly gain importance in the future making new evaluation methods such as the one presented in this thesis a necessity.

Chapter 3

Methods

All conducted experiments are based on moving the upper extremity along a specified planar trajectory with an industrial robot. Throughout the work two different types of robot manipulators were used. The robots both had to be capable of generating a continuous trajectory and had to have a sufficient range of motion. In the first stage the *Yaskawa*[©] *MOTOMAN sk6* robot was used which allowed us to program point to point movement trajectories provided by the manufacturer. To improve the quality (smoothness) of the movement trajectories, we later on performed experiments on a more sophisticated *Unimation Stäubli RX90* robot running in real time on a RT Linux platform. The control loop frequency was 4 kHz allowing a generation of almost continuous trajectories practically identical to the desired ideal trajectories. The latter robot was not used in the passive moment determination experiments because it only became available to us later. The experimental methods were the same with both robots and will therefore be explained generally.

The outline of the experimental setup can be seen in figure 3.1. During the movement process joint angle data was collected by means of an IR marker based motion tracking system (*Northern Digital - Optotrak*[©]) as well as forces and moments in the contact point which were obtained with the *JR³*[©] strain gauge force sensor. Sampling frequencies in both cases were 50 Hz, which was enough for the slow movements observed throughout all experiments. The reason for using this experimental equipment was its availability and proven reliability.

A *JR³* 4 dimensional strain gauge force sensor was mounted to the manipulator end-effector and used for force data collection. The maximum force for the specified output was ± 110 N, with an A/D acquisition resolution of 12 bits. A bicycle-like circular rubber coated handle was mounted on top of the sensor in such a way, that rotation around the x axis was freely allowed. The next element in the system was a bus passenger seat, equipped with additional straps as evident from the photo in Figure 3.2.

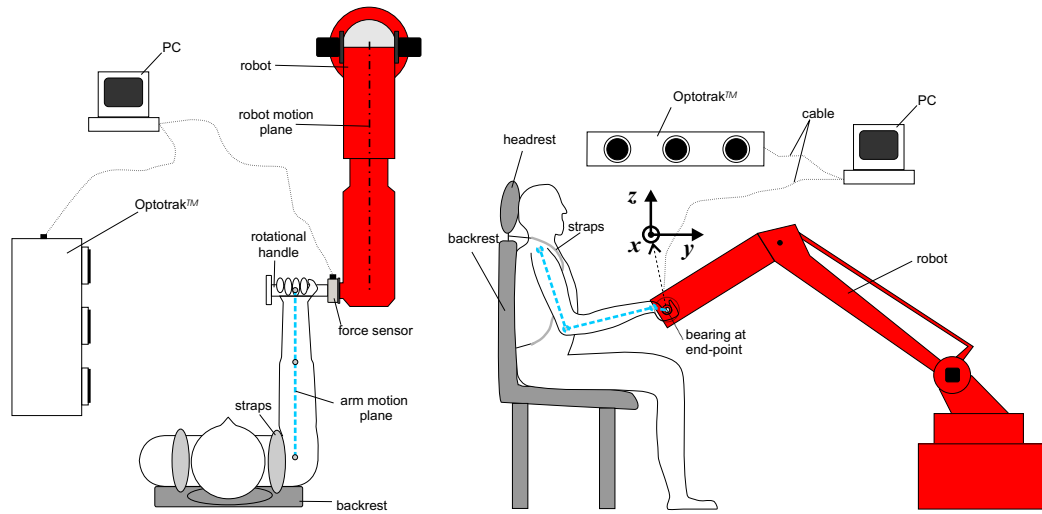


Figure 3.1: *The experimental setup from above (left) and a side view (right). The subject was seated on a strap equipped passenger type seat which minimizes trunk movements. Three IR markers were attached above joint rotation centers as recommended in [81]. The contact forces and moments $\mathbf{F}_{\text{end}} = [F_y, F_z, M_x]^T$ were measured with a 4D JR³ strain gauge force sensor. Due to a bearing at the robot attached handle, the torque value M_x was minimal.*

The handle was lightly strapped to the robot-attached handle in order to allow good contact during the movement (figure 3.3). The strapping also meant that there was no voluntary muscle activity due to gripping.

3.1 Mathematical modelling

In order to develop our upper extremity parameter estimation technique we first had to produce a mathematical model of the upper extremity. This enabled a mathematical description of joint torques in relation to the model kinematics and environmental forces. In the modelling phase we tried to keep the model as straightforward as possible in order to obtain method simplicity and due to the fact that complex modelling potentially leads to severe mathematical difficulties. Throughout the whole thesis the human arm was regarded as a 3DOF planar structure (Figure 3.4.1).

The segment lengths are denoted with a_j , their centers of mass with l_j while q_j indicate the positive angle directions with respect to the zero position (*dashed line*). Positive angle values are denoted with the arrow. The masses are presented with m_j . The centers of gravity were expressed as a distal distance from the joint



Figure 3.2: A photo showing the experimental environment.

marked with the same index.

As in every other manipulator system, the dynamic behavior, as a relationship between applied driving torques $\tau(\mathbf{u})$, environment forces \mathbf{F}_{end} and joint motion trajectories $\ddot{\mathbf{q}}, \dot{\mathbf{q}}, \mathbf{q}$ of mechanical joints can be described as [38]:

$$\mathbf{B}(\mathbf{q})\ddot{\mathbf{q}} + \mathbf{C}(\mathbf{q}, \dot{\mathbf{q}})\dot{\mathbf{q}} + \mathbf{G}(\mathbf{q}) + \mathbf{K}_v\dot{\mathbf{q}} + \mathbf{K}_d\text{sgn}(\dot{\mathbf{q}}) + \mathbf{K}_e\mathbf{q} = \tau(\mathbf{u}) - \mathbf{J}^T(\mathbf{q})\mathbf{F}_{\text{end}}$$

or equally,

$$\begin{aligned} \tau_{\mathbf{B}}(\ddot{\mathbf{q}}) + \tau_{\mathbf{C}}(\mathbf{q}, \dot{\mathbf{q}}) + \tau_{\mathbf{G}}(\mathbf{q}) + \tau_v(\dot{\mathbf{q}}, \mathbf{q}, \mathbf{u}) + \tau_d(\text{sgn}(\dot{\mathbf{q}}), \mathbf{q}, \mathbf{u}) + \tau_e(\mathbf{q}, \mathbf{u}) = \\ = \tau(\mathbf{u}) - \tau_{\text{end}} \end{aligned} \quad (3.1)$$

Variables \mathbf{q} , $\dot{\mathbf{q}}$ and $\ddot{\mathbf{q}}$ represent the angle, angular velocity and angular acceleration vectors and can be represented as:

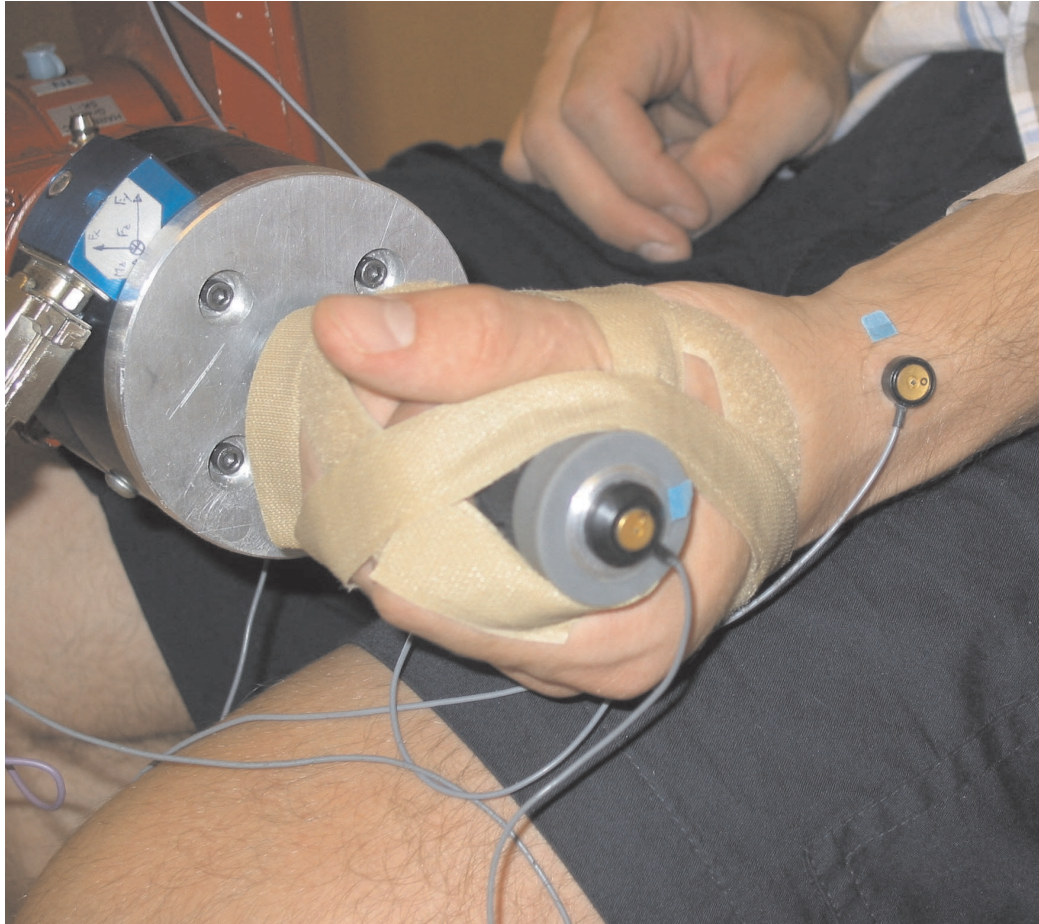


Figure 3.3: A detailed view of the contact between the strapped hand and the robot attached handle. The force sensor can be seen in the center of the photo (blue) while the robot is clearly visible on the left side (red). The wrist and handle attached IR markers can also be observed.

$$\begin{aligned}
 \mathbf{q} &= [q_1 \quad q_2 \quad q_3]^T \\
 \dot{\mathbf{q}} &= [\dot{q}_1 \quad \dot{q}_2 \quad \dot{q}_3]^T \\
 \ddot{\mathbf{q}} &= [\ddot{q}_1 \quad \ddot{q}_2 \quad \ddot{q}_3]^T
 \end{aligned} \tag{3.2}$$

The *moments of inertia* are represented as a (3×3) $\mathbf{B}(\mathbf{q})$ matrix. The diagonal elements b_{jj} of the matrix represent the moment of inertia at joint j axis, while the other two joints are fixed, whereas the non-diagonal ones b_{jk} account for the

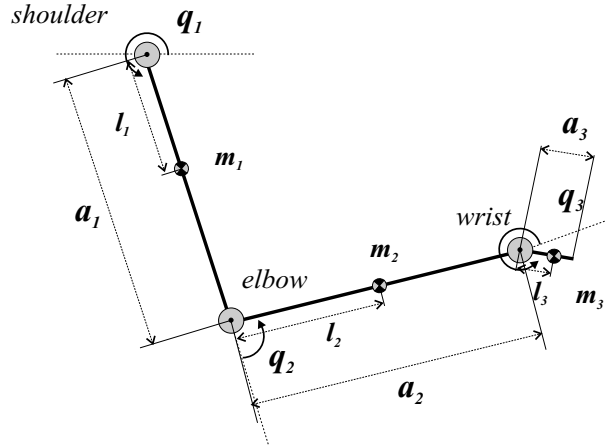


Figure 3.4: Geometric definitions for the assumed human arm structure, consisting of three rigid body segments. The segment lengths are denoted with a_j , their COGs with l_j while q_j indicates joint angle directions with respect to the zero position (dashed line). The segment masses are presented with m_j .

acceleration effect of joint j on an adjacent joint k . For a 3DOF planar manipulator the inertial matrix elements were derived as shown in equations 3.4. The variable I_j represents the transversal inertia tensor of a particular segment j . The trigonometric notation from equations 3.3 was used:

$$\begin{aligned}
 c_1 &= \cos(q_1) \\
 c_{12} &= \cos(q_1 + q_2) \\
 c_{123} &= \cos(q_1 + q_2 + q_3) \\
 s_1 &= \sin(q_1) \\
 s_{12} &= \sin(q_1 + q_2) \\
 s_{123} &= \sin(q_1 + q_2 + q_3)
 \end{aligned} \tag{3.3}$$

$$\mathbf{B}(\mathbf{q}) = \begin{bmatrix} b_{11} & b_{12} & b_{13} \\ b_{21} & b_{22} & b_{23} \\ b_{31} & b_{32} & b_{33} \end{bmatrix} \tag{3.4}$$

$$\begin{aligned}
b_{11} &= I_1 + I_2 + I_3 + l_1^2 m_1 + (a_1^2 + l_2^2) m_2 + (a_1^2 + a_2^2 + l_2^2) m_3 + \\
&\quad + 2a_1(l_2 m_2 + a_2 m_3) c_2 + 2l_3 m_3 (a_2 c_3 + a_1 c_{23}), \\
b_{12} &= I_2 + I_3 + l_2^2 m_2 + (a_2^2 + l_3^2) m_3 + a_1(l_2 m_2 + a_2 m_3) c_2 + \\
&\quad + 2a_2 l_3 m_3 c_3 + a_1 l_3 m_3 c_{23}, \\
b_{13} &= I_3 + l_3^2 m_3 + a_2 l_3 m_3 c_3 + a_1 l_3 m_3 c_{23}, \\
b_{21} &= I_2 + I_3 + l_2^2 m_2 + (a_2^2 + l_3^2) m_3 + a_1(l_2 m_2 + a_2 m_3) c_2 + \\
&\quad + 2a_2 l_3 m_3 c_3 + a_1 l_3 m_3 c_{23}, \\
b_{22} &= I_2 + I_3 + l_2^2 m_2 + (a_2^2 + l_3^2) m_3 + 2a_2 l_3 m_3 c_3, \\
b_{23} &= I_3 + l_3^2 m_3 + a_2 l_3 m_3 c_3, \\
b_{31} &= I_3 + l_3^2 m_3 + a_2 l_3 m_3 c_3 + a_1 l_3 m_3 c_{23}, \\
b_{32} &= I_3 + l_3^2 m_3 + a_2 l_3 m_3 c_3, \\
b_{33} &= I_3 + l_3^2 m_3.
\end{aligned}$$

Multiplying this matrix with the joint accelerations $\ddot{\mathbf{q}}$ yields a vector of *inertial contributions* in all three joints $\boldsymbol{\tau}_B = \mathbf{B}(\mathbf{q})\ddot{\mathbf{q}}$:

$$\boldsymbol{\tau}_B = [\tau_{b1} \quad \tau_{b2} \quad \tau_{b3}]^T \quad (3.5)$$

The second matrix, $\mathbf{C}(\mathbf{q}, \dot{\mathbf{q}})$ shows the *centrifugal effects* in its diagonal coefficients, while non-diagonal ones c_{jk} account for the *Coriolis effect* induced on joint j by the velocity of an adjacent joint k . For the given configuration the elements were specified as:

$$\mathbf{C}(\mathbf{q}, \dot{\mathbf{q}}) = \begin{bmatrix} c_{11} & c_{12} & c_{13} \\ c_{21} & c_{22} & c_{23} \\ c_{31} & c_{32} & c_{33} \end{bmatrix} \quad (3.6)$$

$$\begin{aligned}
c_{11} &= -\{a_1[(l_2 m_2 + a_2 m_3) s_2 + l_3 m_3 s_{23}] \dot{q}_2 + \\
&\quad + l_3 m_3 (a_2 s_3 + a_1 s_{23}) \dot{q}_3\}, \\
c_{12} &= 0.5\{-2a_1[(l_2 m_2 + a_2 m_3) s_2 + l_3 m_3 s_{23}] (\dot{q}_1 + \dot{q}_2) - \\
&\quad - 2l_3 m_3 (a_2 s_3 + a_1 s_{23}) \dot{q}_3\}, \\
c_{13} &= -l_3 m_3 (a_2 s_3 + a_1 s_{23}) q_1 \dot{q}_3, \\
c_{21} &= a_1[(l_2 m_2 + a_2 m_3) s_2 + l_3 m_3 s_{23}] \dot{q}_1 - a_2 l_3 m_3 s_3 \dot{q}_3, \\
c_{22} &= -a_2 l_3 m_3 s_3 \dot{q}_3, \\
c_{23} &= -a_2 l_3 m_3 s_3 q_1 \dot{q}_3, \\
c_{31} &= l_3 m_3 [(a_2 s_3 + a_1 s_{23}) \dot{q}_1 + a_2 s_3 \dot{q}_2], \\
c_{32} &= a_2 l_3 m_3 s_3 (\dot{q}_1 + \dot{q}_2), \\
c_{33} &= 0.
\end{aligned}$$

which after applying the velocity vector \dot{q} defines the joint torque dynamic contributions $\tau_C = \mathbf{C}(\mathbf{q}, \dot{\mathbf{q}})\dot{\mathbf{q}}$:

$$\tau_C = [\tau_{c1} \quad \tau_{c2} \quad \tau_{c3}]^T \quad (3.7)$$

The *gravitational contribution* is expressed with a three element column vector, where every element τ_{g_j} represents the moment generated at the joint j axis due to the presence of gravity:

$$\tau_G(\mathbf{q}) = [\tau_{g1} \quad \tau_{g2} \quad \tau_{g3}]^T, \quad (3.8)$$

where

$$\begin{aligned} \tau_{g1} &= g_0 \{ [l_1 m_1 + a_1(m_2 + m_3)]c_1 + (l_2 m_2 + a_2 m_3)c_{12} + l_3 m_3 c_{123} \}, \\ \tau_{g2} &= g_0 [(l_2 m_2 + a_2 m_3)c_{12} + l_3 m_3 c_{123}], \\ \tau_{g3} &= g_0 l_3 m_3 c_{123}. \end{aligned}$$

The gravitational acceleration constant is denoted with g_0 and was taken to be 9.81 m/s^2 .

The connection between the hand and the robot handle creates a closed chain kinematic linkage. Thus, the end-effector connection is described as a three dimensional vector with its horizontal and vertical forces (F_y, F_z) and the moment around the axis perpendicular to the plane of motion (M_x) (see figure 3.1):

$$\mathbf{F}_{\text{end}} = [F_y \quad F_z \quad M_x]^T \quad (3.9)$$

These forces have to be transformed to the joint level with the Jacobian matrix $\mathbf{J}^T(\mathbf{q})$ as seen in the product $\mathbf{J}^T(\mathbf{q})\mathbf{F}_{\text{end}}$ of equation 3.1 and are represented with the τ_{end} torque vector. The transpose of the Jacobian matrix $\mathbf{J}^T(\mathbf{q})$ for a 3DOF planar manipulator can be expressed as:

$$\mathbf{J}^T(\mathbf{q}) = \begin{bmatrix} -a_1 s_1 - a_2 s_{12} - a_3 s_{123} & a_1 c_1 + a_2 c_{12} + a_3 c_{123} & 1 \\ -a_2 s_{12} - a_3 s_{123} & a_2 c_{12} + a_3 c_{123} & 1 \\ a_3 s_{123} & -a_3 c_{123} & 1 \end{bmatrix} \quad (3.10)$$

The joint muscle activity is expressed in terms of the active joint contribution $\tau(\mathbf{u})$, which is a non-linear function of muscle activation \mathbf{u} .

The *viscous contribution* of the system is expressed in terms of $\mathbf{K}_v \dot{\mathbf{q}}$. This product yields a vector of three joint viscous torques $\tau_v(\dot{\mathbf{q}}, \mathbf{q}, \mathbf{u})$ which is not only a function of joint angular velocities $\dot{\mathbf{q}}$ as in other mechanical systems but also of joint angles \mathbf{q} and muscle activations \mathbf{u} . This relation is also a non-linear one:

$$\tau_v(\dot{\mathbf{q}}, \mathbf{q}, \mathbf{u}) = [\tau_{v1} \quad \tau_{v2} \quad \tau_{v3}]^T \quad (3.11)$$

$\mathbf{K}_d \text{sgn}(\dot{\mathbf{q}})$ indicates the velocity direction dependent *dissipative torques* and is in the literature usually denoted as the static friction torque [38, 86]. It can be expressed with the dissipative moment $\tau_d(\text{sgn}(\dot{\mathbf{q}}), \mathbf{q}, \mathbf{u})$ which is a function of the velocity direction $\text{sgn}(\dot{\mathbf{q}})$ and the \mathbf{q} and \mathbf{u} variables.

$$\tau_d(\text{sgn}(\dot{\mathbf{q}}), \mathbf{q}, \mathbf{u}) = [\tau_{d1} \quad \tau_{d2} \quad \tau_{d3}]^T \quad (3.12)$$

Finally, the *elastic torque* contributions in a particular joint are expressed with the product $\mathbf{K}_e \mathbf{q}$ which gives a joint elasticity vector $\tau_e(\mathbf{q}, \mathbf{u})$.

$$\tau_e(\mathbf{q}, \mathbf{u}) = [\tau_{e1} \quad \tau_{e2} \quad \tau_{e3}]^T \quad (3.13)$$

The reason why the $\tau_v(\dot{\mathbf{q}}, \mathbf{q}, \mathbf{u})$ and the $\tau_d(\text{sgn}(\dot{\mathbf{q}}), \mathbf{q}, \mathbf{u})$ vectors were also functions of the \mathbf{q} and \mathbf{u} variables lies in the nature of a biomechanical system where every body segment is surrounded with tissues ligaments and muscles. It should be known that these functions are usually non-linear in a biomechanical system making the system itself non-linear in nature. The various distribution of these structures is a direct result of the current angular configuration and muscle activation. The same could be said about the vector $\tau_e(\mathbf{q}, \mathbf{u})$ which would in a normal mechanical system only be a function of angle. Due to notation simplicity the variables \mathbf{q} and \mathbf{u} will from now on be omitted.

Due to the free handle rotation during movement the hand dynamic parameters were properly adjusted. The mass and all geometric dimensions of the handle were accurately measured before the experiment. The handle mass m_{handle} was then added to the one of the hand m_{hand} to yield a new third segment mass m_3 , while the center of gravity locations l_{handle} and l_{hand} were also considered in obtaining a new location l_3 :

$$\begin{aligned} m_3 &= m_{hand} + m_{handle}, \\ l_3 &= \frac{l_{hand}m_{hand} + l_{handle}m_{handle}}{m_{handle} + m_{hand}} \end{aligned} \quad (3.14)$$

In this equation m_{hand} and l_{hand} were taken from the literature [21] (0.61% of body mass and 79% of measured hand length respectively) while m_{handle} and l_{handle} were accurately measured before the experiment ($m_{handle} = 0.277$ kg and $l_{handle} = 0.844$ m).

The sum of elastic and dissipative contributions, $\tau_e + \tau_d$ has a special meaning when there is no muscle activation \mathbf{u} and can be described with a commonly accepted term *passive moments*.

$$\tau_p = \tau_e + \tau_d \quad (3.15)$$

3.2 General assumptions made in the experiments

Due to several reasons we have made some crucial assumptions in the modelling process in order to simplify the mathematical model:

1. Because of the extreme complexity in the upper extremity anatomical structure as already seen in chapter 1.1 we *simplified it to the extent of a 3DOF planar arm* presuming *axial rotations* and *rigid body segments* as seen in figure 3.4.1. This seemingly big simplification was justified for the straightforward movements which were performed during all types of movements in our experiments. We have based this assumption on the study of Veeger *et al.* [72] which shows that the flexion-extension rotational center translation of the glenohumeral joint was within just 4 mm of the geometric center. The same presumption was also extended to the other two joints despite the fact that we did not find a comparable study for these joints.
2. We decided to perform all experimental movements with the upper *extremity muscles in a relaxed condition*. Hence we can write the following relation:

$$\tau(\mathbf{u}) = 0 \quad (3.16)$$

It has been proven by numerous researchers in the past that muscle activation considerably alters the joint internal dynamic characteristics which are in active movement influenced by the CNS. According to the somewhat controversial *equilibrium point hypothesis* the CNS alters these properties in a way which allows the subject to optimally perform a movement [39,41]. On the other hand this assertion can also be based on a frequency identification technique done by Hollerbach *et al.* [59].

To prove that the subject induced no voluntary action during the course of the experiment we observed the EMG signals of four muscles in a typical elbow flexion-extension movement prior to doing any experimental work (Figure 3.5).

The surface EMG electrodes were placed on the four major flexion and extension muscles by a skilled professional (*i.e. biceps long head, biceps short head, triceps* and *brachioradialis*). The EMG data from a typical robot movement was then compared to those obtained in an active flexion-extension isotonic movement when the subject was asked to perform a similar movement without the robot being present (Figure 3.6).

It is evident that practically no EMG activity was present during inactivity, confirming equation 3.16. It needs to be noted that the described EMG measurement was done only once and served as a justification for presuming muscle inactivity in all further experimental work.

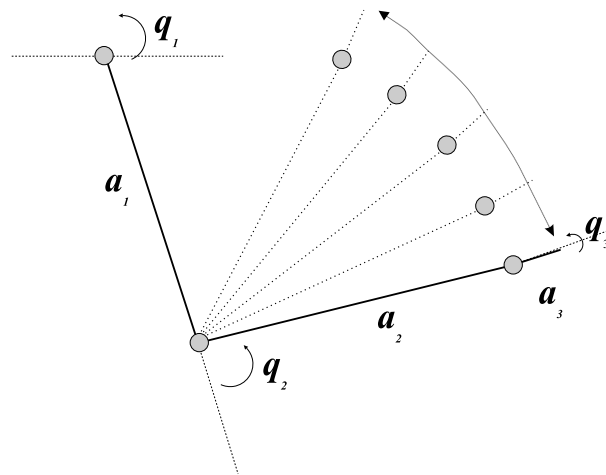


Figure 3.5: *The elbow flexion-extension trajectory along which the robot led the human arm.*

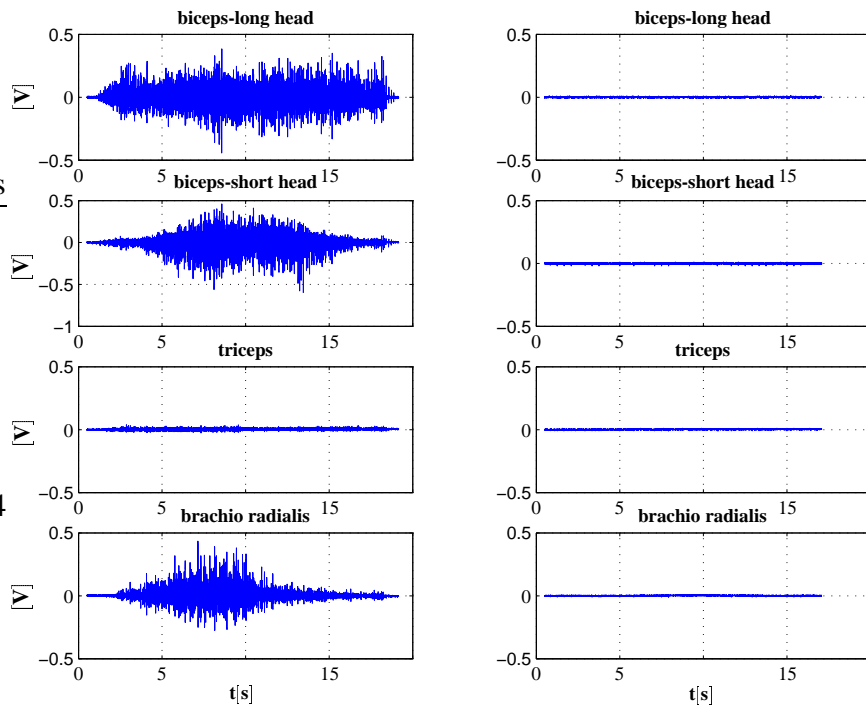


Figure 3.6: *The EMG signal during voluntary flexion attempt (left) and a passively held arm (right). Every row of figures represents a different muscle.*

3. All performed movements were *very slow* with angular velocities around 0.2 rad/s. This allowed us to assume that the experiment was always performed under quasi-static conditions. In these conditions all velocity and acceleration related terms influencing upper extremity dynamics could be discarded. In typical movements throughout our experiments the angular accelerations reached values of up to 1.2 rad/s² at points where the motion direction was changed, 0.6 rad/s² where the movement was started and ended, and almost zero elsewhere. Because these were all verified to be very low values, the contributions of all dynamic terms in equation 3.1, were negligible compared to the non velocity and acceleration dependent terms. To determine the most suitable joint velocity we have performed a pilot study where we studied the joint torques due to different dynamic contributions in a simple elbow movement which can be seen in figure 3.5 [16]. The observations were made at four different velocity trajectories.

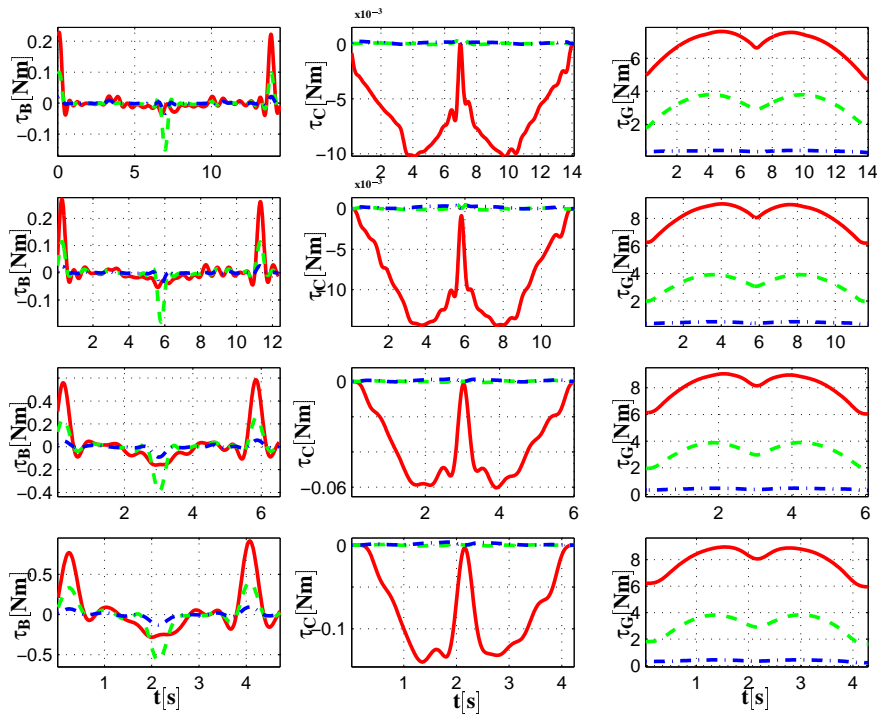


Figure 3.7: The inertial, Coriolis and gravity torque contributions as calculated from equations 3.4, 3.6 and 3.8 respectively. The elbow joint was displaced at different linear speed levels : $|\dot{q}_2| \approx 0.25$ rad/s (row 1), $|\dot{q}_2| \approx 0.3$ rad/s (row 2), $|\dot{q}_2| \approx 0.65$ rad/s (row 3) and $|\dot{q}_2| \approx 1$ rad/s (row 4) for the shoulder (-, red), elbow (-, green) and wrist (-., blue) respectively.

It can be observed from figure 3.7 that the gravity component τ_G remains constant at all times since it is not velocity dependent. However, the inertial and Coriolis components τ_B and τ_C reduce significantly with decreased velocity. In the slowest case (upper row in figure 3.7) they amount up to 0.2 Nm for τ_B and 0.001 Nm for τ_C , which is low compared to the major contribution of τ_G .

This lead us to the quasi-static assumption so that we could now write the following simplifications:

$$\tau_B = \mathbf{0}, \quad \tau_C = \mathbf{0}, \quad \tau_v = \mathbf{0} \quad (3.17)$$

4. For modelling-simplicity reasons all experiments were carried out in the *sagittal plane* of the subject. While this configuration required us to take gravity related contributions into account on one hand, it allowed us to use no particular fixation mechanisms for restraining the arm to the desired position. The method was therefore friendlier from the subjects' point of view and mechanically easier to implement.

3.3 An overview of the experimental setup

In order to implement all experiments we had to develop an experimental setup which enabled the collection and analysis of all desired quantities. The block diagram of the setup can be seen in figure 3.8.

- The *Client PC* was manipulated by the operator who initiated and terminated the experiment by running and stopping a Matlab-Simulink application. Before running the application the *required robot joint trajectory* \mathbf{q}_r had to be generated with an off-line simulation. This trajectory was then sent to the *robot server PC* through TCP/IP. The input to the application were force sensor data \mathbf{F}_{end} , Optotrak marker data \mathbf{m} and two load cell readings \mathbf{L} . The load cell data were only read when performing the mechanical arm experiment whereas they were not necessary while measuring on the human subject. Upon termination all variables were saved for later off-line processing.
- The *Robot Server PC* is in fact a robot controller running RT-Linux and runs at a sampling frequency of 4 kHz. A C++ based control algorithm determines the required voltage amplitude level for every particular motor. These voltages \mathbf{v} are then written to an output port of a D/A card and converted to the current motor reference by means of power amps in the

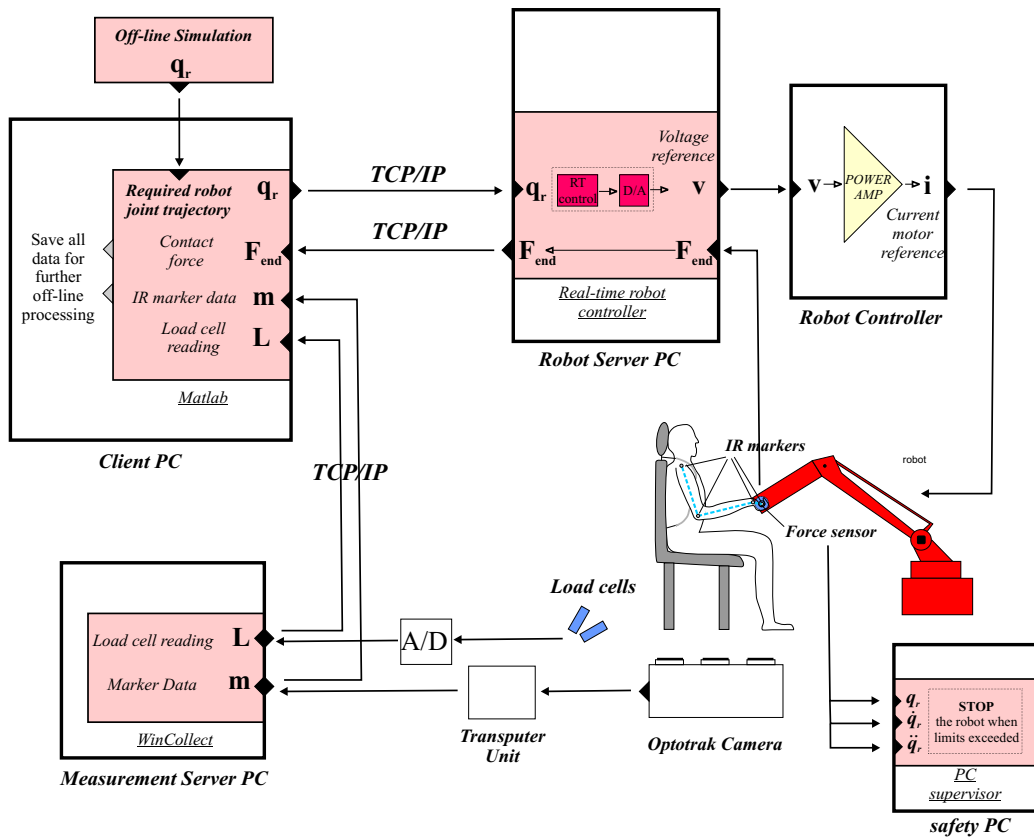


Figure 3.8: A block diagram of the experimental setup. Four different PC computers were arranged in a way which allowed reliable data collection. The Client PC was used by the operator for initiation and termination of the measurement. During the measurement the Robot Server PC and the Measurement Server PC were used for data collection and robot manipulation. The Safety PC assured that there were no safety violation during the process.

original robot controller. The Robot Server PC also serves as a collection point for contact forces \mathbf{F}_{end} from the JR^3 6D sensor. Out of the 6 measured quantities only the horizontal force, vertical force and one torque were used for the purposes of our studies due to the planar nature of the movement. The signal coming from the sensor was sampled by means of a 16-bit A/D converter inside the sensor. The sensor data was then sent through TCP/IP to the Client PC.

- The Measurement Server PC served as a collection point for the marker data \mathbf{m} coming from the Optotrak transputer unit. We developed an application

running on the *measurement server PC* which was used for collecting Optotrak data at a specified frequency and diverting the data to the TCP/IP. Apart from setting the collection frequency the software also enabled some other basic functions such as calibration and choosing a desired number of markers. Apart from the marker data the software could also collect up to 16 channels from an A/D converter. This feature was utilized when experimenting with the mechanical arm where we had to deal with two strain gauge load cells which presented two additional quantities - \mathbf{L} . This variable was also sent to the *Client PC* by means of TCP/IP.

- The *Safety PC* was added to the system for security purposes. The PC supervisor application which ran on it constantly scanned the current robot angles \mathbf{q}_r , angular velocities \dot{q}_r and angular accelerations \ddot{q}_r . When any of these values exceeded the previously determined safety limit, the robot controller was immediately stopped without causing any damage.

3.4 Shoulder and elbow joint passive moments

In the first experimental phase the goal was to determine passive moments of the human elbow and shoulder joints. We hence attempted to quantify the sum $\tau_e + \tau_d$ from equation 3.1. As it has already been mentioned in section 3.1 both these terms behave non-linearly, being a function of the velocity direction ($\text{sgn}(\dot{\mathbf{q}})$), angles (\mathbf{q}) and muscle activations (\mathbf{u}) and compose a more general passive moment torque τ_p .

3.4.1 A simplification of the biomechanical model

The assumptions 2 (*no muscle activity*) and 3 (*slow movement*) from section 3.2 were accounted for in equation 3.1, modifying now to a much more simple relationship:

$$\begin{aligned} \mathbf{K}_e \mathbf{q} + \mathbf{K}_d \text{sgn}(\dot{\mathbf{q}}) &= -\mathbf{G}(\mathbf{q}) - \mathbf{J}^T(\mathbf{q}) \mathbf{F}_{\text{end}} \\ \tau_e + \tau_d &= -\tau_G - \tau_{\text{end}} \\ \tau_p &= -\tau_G - \tau_{\text{end}} \end{aligned} \quad (3.18)$$

The passive moments can be summed up as a variable τ_p which is generally a function of three variables $\text{sgn}(\dot{\mathbf{q}})$, \mathbf{q} , \mathbf{u} . For simplicity reasons it will be denoted as τ_p :

$$\tau_p = [\tau_{p1} \quad \tau_{p2} \quad \tau_{p3}]^T \quad (3.19)$$

Two main sets of measurements were made during this experiment:

1. With the shoulder angle fixed at various angles, while the elbow angle was varied smoothly. The fixation of the shoulder was done without any fixation mechanisms.
2. With the elbow fixed, while the shoulder was moved through its range of motion. For fixating the elbow joint we used a simple plastic fixation mechanism - orthosis.

In both cases the wrist was not fixed and was allowed to move freely since the deviation from the neutral position was found to be only a few degrees. Before the particular measurements, ten different trajectories (not shown here) were programmed into the robot for each subject. The first five measurements concentrated on the elbow angle smooth variation from one boundary angle to the other and backwards, with the shoulder fixed at different angles (-68° , -40° , -16° , -10° , -36°). The shoulder angle was kept constant by programming an appropriate trajectory, using no additional fixation mechanisms (figure 3.9 - left side).

The second set of trials focused on movements of the shoulder joint, with the elbow kept at constant angles (27° , 40° , 50° , 60° , 70°). For fixating the elbow angle, a simple plastic orthosis was used, which allowed angle adjustments from almost complete extension to a flexion angle of 85 degrees. It was velcro-strapped to the upper side of the elbow joint and tightly fixed at a certain angle with a screw (figure 3.9 - right side).

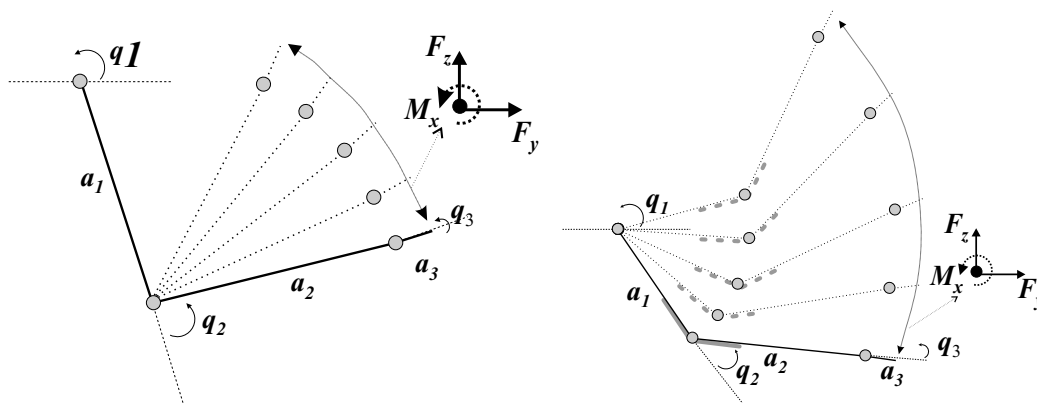


Figure 3.9: A typical programmed elbow trajectory (left) at a certain fixed shoulder angle q_1 and shoulder trajectory (right) at a fixed elbow angle q_2 . Note the elbow orthosis in fixed-elbow movements (right).

The mass of the orthosis utilized for shoulder movements was included into the calculation of the $\mathbf{G}(\mathbf{q})$ matrix from equation 3.8, which describes the new upper and forearm masses and center of gravity locations as m_j and l_j :

$$\begin{aligned} m_1 &= m_{ua} + m_{uo}, & m_2 &= m_{fa} + m_{lo} \\ l_1 &= a_1 - \frac{l_{ua}m_{ua} + l_{uo}m_{uo}}{m_{ua} + m_{uo}} \\ l_2 &= \frac{l_{fa}m_{fa} + l_{fo}m_{fo}}{m_{fa} + m_{fo}} \end{aligned} \quad (3.20)$$

Here the *ua* and *fa* indices refer to the *upper arm* and *forearm*, whereas *uo* and *fo* describe the *upper* and *lower orthosis* parts. The orthosis masses and centers of gravity were accurately determined before the experiment ($m_{lo} = 0.191$ kg, $m_{uo} = 0.200$ kg, $l_{lo} = 0.066$ m, $l_{uo} = 0.091$ m). Because the center of gravity lengths l_{fa} and l_{ua} were measured with respect to the joint rotational point, the parameter l_1 was obtained by subtracting from the upper arm length a_1 .

A typical elbow passive moment pattern as a function of the current joint angle can be seen in figure 3.10 at shoulder fixation of $q_1 \approx -68^\circ$. We can clearly observe a hysteresis arising due to muscle dissipative effects (τ_d) [18], where the upper part of the curve always indicates movements from extension to flexion. The hysteresis average is known to be the *passive elastic moment*, which was the topic of some earlier studies [17, 54]. The passive moment curve patterns show an ascending pattern most of the time, at small angles, however, this is sometimes a descending one resulting in a global minimum.

3.4.2 Implementation of the experiment

The IR markers were attached to the skin above the rotation points of the three arm joints in consideration to the handle and to the robot manipulator joints in order to allow for later verification and complete reconstruction of the measurement. All calculations from equations mentioned in the preceding sections were performed off-line using Matlab[®]. In order to eliminate high frequency noise the Optotrak and Force sensor data were both low-pass filtered at 5 Hz using a sixth order Butterworth filter provided by the Matlab Signal Processing toolbox.

Six healthy subjects were tested with body masses ranging from 64 kg to 77 kg (average weight = 70.2 kg, standard deviation = 7.1 kg). They were all right-handed males aged from 25 to 39 years (average age = 28.3 years, standard deviation = 5.3 years). None had ever suffered from any kind of neuromuscular disease. All were asked to sit in a chair, lightly grip the robot attached handle and not exert any voluntary muscle action. Before the experiment at least two preliminary movements were made to assure that the programmed trajectory was appropriate

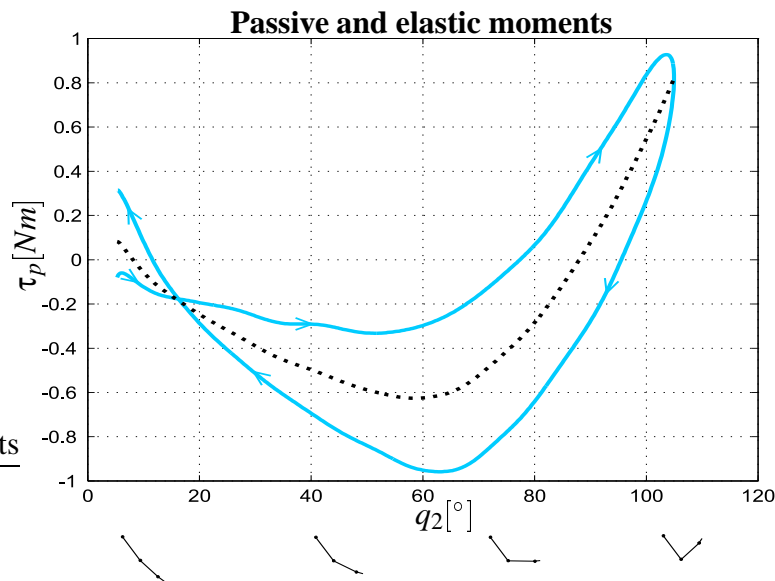


Figure 3.10: *Elbow passive moment hysteresis (solid blue line) with the elastic moment (dashed line) and the movement direction (arrow). Below the figure the arm movement is depicted. The shoulder angle was fixed at $q_1 \approx -68^\circ$.*

and that the subject was comfortable. After defining 10 different trajectories, a set of the first ten movements was made for the elbow and the second ten for the shoulder joint (two for each particular angular configuration).

Initially, six sets of measurements were made on only one particular subject (age 25, weigh 77 kg), with every one performed on a separate day. This gave a total of sixty measurements out of which six were made for the same angular configuration (*i.e.* extension to flexion and backwards). All other subjects were only measured twice for every particular angular configuration.

3.5 A technique for determining upper extremity joint and body segment parameters

As already mentioned in section 3.1 the upper extremity is a non-linear system in relation to variables \mathbf{q} , $\dot{\mathbf{q}}$ and \mathbf{u} . To avoid the problem of accounting for the $\dot{\mathbf{q}}$ and \mathbf{u} variables we again applied rules from 1 to 4.

3.5.1 Model linearization

The problem of angular non-linearities was confronted by imposing very small angular deviations into the movement. Within these angular regions the system was presumed to be planar.

We have experimentally deduced that when using angular deviations smaller than $\pm 12^\circ$ ($|\Delta q_j| < 12^\circ$) the τ_p nonlinearities were small enough to allow the value to be considered as constant. We can now express equation 3.18 as a linear relationship in a particular joint j at a certain time instant t_i [87]:

$$\begin{aligned}\tau_{pj} &= -\tau_{Gj} - \tau_{endj} \\ \tau_{pj} + \tau_{Gj} &= -\tau_{endj}\end{aligned}\quad (3.21)$$

By substituting the left side with a linear relationship $\mathbf{Y}_j \pi_j$ and the right side with a new generalized torque variable τ_j we can write [38, 86]:

$$\mathbf{Y}_j \pi_j = \tau_j \quad \text{at any given time instant } t_i \quad (3.22)$$

In this equation \mathbf{Y}_j represents the regression vector, π_j the corresponding vector of identification parameters for segment j and τ_j all other terms which are not related to the identified variables in π_j .

Let us now describe the system in equation 3.22 with three consecutive linear equations, describing the inverse dynamics of every particular joint of the 3DOF manipulator at a certain time instant t_i :

- *Wrist joint:*

$$g_0 \cos_{123} m_3 l_3 + \tau_{p3} = \tau_{end3}$$

or in matrix form,

$$\begin{aligned}\mathbf{Y}_3 \pi_3 &= [g_0 \cos_{123}, 1] [m_3 l_3, \tau_{p3}]^T = \\ &= \tau_{end3} = \tau_3\end{aligned}\quad (3.23)$$

Accounting for $m_3 l_3$ obtained from π_3 the elbow equation can now be expressed.

- *Elbow joint:*

$$g_0 \cos_{12} m_2 l_2 + g_0 a_2 \cos_{12} m_3 + \tau_{p2} = \tau_{end2} - g_0 \cos_{12} m_3 l_3$$

or in matrix form,

$$\begin{aligned} \mathbf{Y}_2\boldsymbol{\pi}_2 &= [g_0\cos_{12}, g_0a_2\cos_{12}, 1] [m_2l_2, m_3, \tau_{p2}]^T = \quad (3.24) \\ &= \tau_{end2} - g_0\cos_{12}m_3l_3 = \\ &= \tau_2 \end{aligned}$$

Accounting for m_3l_3 , m_2l_2 and m_3 from $\boldsymbol{\pi}_3$ and $\boldsymbol{\pi}_2$ we can write the third equation.

• **Shoulder joint:**

$$\begin{aligned} g_0\cos_1m_1l_1 + g_0a_1\cos_1m_2 + \tau_{p1} &= \tau_{end1} - \\ - g_0(a_1\cos_1 + a_2\cos_{12})m_3 - g_0\cos_{12}m_2l_2 - g_0\cos_{123}m_3l_3 \end{aligned}$$

or in matrix form,

$$\begin{aligned} \mathbf{Y}_1\boldsymbol{\pi}_1 &= [g_0\cos_1, g_0a_1\cos_1, 1] [m_1l_1, m_2, \tau_{p1}]^T = \quad (3.25) \\ &= \tau_{end1} - g_0(a_1\cos_1 + a_2\cos_{12})m_3 - g_0\cos_{12}m_2l_2 - g_0\cos_{123}m_3l_3 = \\ &= \tau_1 \end{aligned}$$

From all three joint equations it can be deduced that the identification vectors $\boldsymbol{\pi}_j$ were chosen as:

$$\begin{aligned} \boldsymbol{\pi}_3 &= [m_3l_3, \tau_{p3}]^T \quad (3.26) \\ \boldsymbol{\pi}_2 &= [m_2l_2, m_3, \tau_{p2}]^T \end{aligned}$$

and,

$$\boldsymbol{\pi}_1 = [m_1l_1, m_2, \tau_{p1}]^T \quad (3.27)$$

To obtain the segment COGs, l_j they had to be expressed from the identified parameters m_jl_j and m_j :

$$l_j = \frac{m_jl_j}{m_j} \quad (3.28)$$

However, for the uppermost segment l_1 could never be obtained since the procedure only gave the value of this parameter in linear combination with m_1 (i.e. m_1l_1).

By considering equation 5.6 and equation 3.25, for every π_j at N time instants t_i , a linearly dependent problem is formed [88, 89]. This is true since a_2 in vector \mathbf{Y}_2 and a_1 in vector \mathbf{Y}_1 are constants making the first two elements in these vectors a linear combination. Therefore the problem of identifying vectors π_j was described as an optimization problem, which minimizes the difference between both sides of equation 3.22. At t_i , this difference can be expressed with the following function:

$$F_{t_i}(\pi_j) = \tau_j - \mathbf{Y}_j \pi_j \quad (3.29)$$

The algorithm calculates π_j with a *constrained nonlinear least squares optimization* for all time samples $1 \leq t_i \leq N$ using the MatlabTM `lsqnonlin` function which solves the following minimization [90]:

$$\min_{\pi_j} \sum_{t_i=1}^N F_{t_i}(\pi_j)^2 \quad \text{such that} \quad \mathbf{l}_b \leq \pi_j \leq \mathbf{u}_b \quad (3.30)$$

The constraints \mathbf{l}_b and \mathbf{u}_b were chosen suitably for every particular identification vector.

3.5.2 Verification of the algorithm with a 2DOF mechanical model

To verify the accuracy of the described algorithm a preliminary experiment was made using a 2DOF mechanical arm. It was designed with CAD software (Autodesk - Mechanical Desktop[©]) which can calculate all dynamic parameters from geometry data. The segment lengths of the model were chosen comparably to the ones of the human arm as well as the segment masses (figure 3.11). To simulate joint passive moments, screw-adjustable rubber brakes were attached to every joint. These brakes produced a desirable Coulomb friction force by pressing on stainless steel disks from both sides. The friction force was directly measured with a load cell (HBM type PW2FC3, with a range of ± 360 N) mounted at a 45 degree angle which enabled the computation of brake-produced passive moments at every instant.

The mechanical arm was coupled with the robot using a bearing attached screw while motion trajectories and contact forces were measured in the same way as with a human subject.

The identification procedure used for this 2DOF manipulator, was the same as the one described at the beginning of this section, the only difference being the number of identification parameters. Since the model only consisted of two segments, only two identification vectors π_j had to be determined consisting of a total number of five identification parameters comprising vectors π_1 and π_2 :

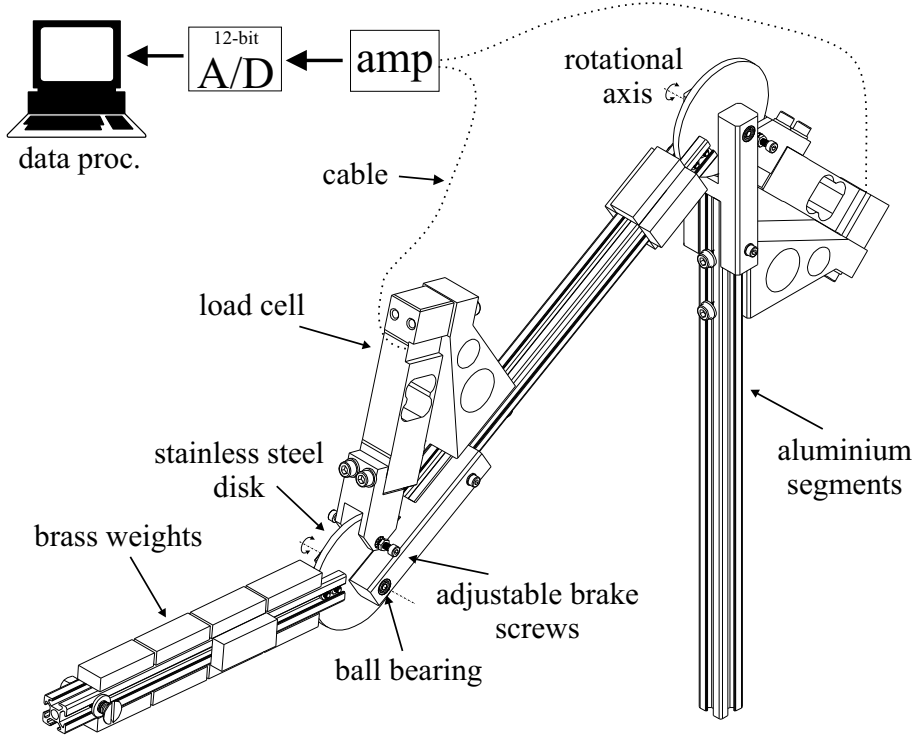


Figure 3.11: *The 2DOF mechanical model used for algorithm verification. Two HBM type PW2FC3 (with a range of ± 360 N) one dimensional aluminium strain gauge load cells were used for measuring mechanical friction. To obtain masses comparable to the human arm, brass weights were properly attached to the aluminium segments. The load cell signals were amplified, digitalized and processed together with contact forces and Optotrak motion data.*

$$\begin{aligned}\boldsymbol{\pi}_2 &= [m_2 l_2, \tau_{p2}]^T \\ \boldsymbol{\pi}_1 &= [m_1 l_1, m_2, \tau_{p1}]^T\end{aligned}\tag{3.31}$$

The best optimization results were obtained when the upper and lower optimization bounds (\mathbf{u}_b and \mathbf{l}_b in equation 3.30) for passive moments τ_{pj} were initially set to values around zero producing $\boldsymbol{\pi}_2 = [m_2 l_2, 0]^T$ and $\boldsymbol{\pi}_1 = [m_1 l_1, m_2, 0]^T$.

Let us now denote the identified passive moments for joint j with τ_{pjid} which were obtained by observing the absolute difference between the trajectory τ_j and the corresponding identified trajectory $\tau_{jid} = Y_j \boldsymbol{\pi}_j$ as:

$$\tau_{pjid} = \frac{1}{N} \sum_{i=1}^N |\tau_j(t_i) - \tau_{jid}(t_i)| \quad (3.32)$$

The imposed trajectory in this study was a flexion-extension movement as seen in a sequence of consecutive angular positions in figure 3.12.

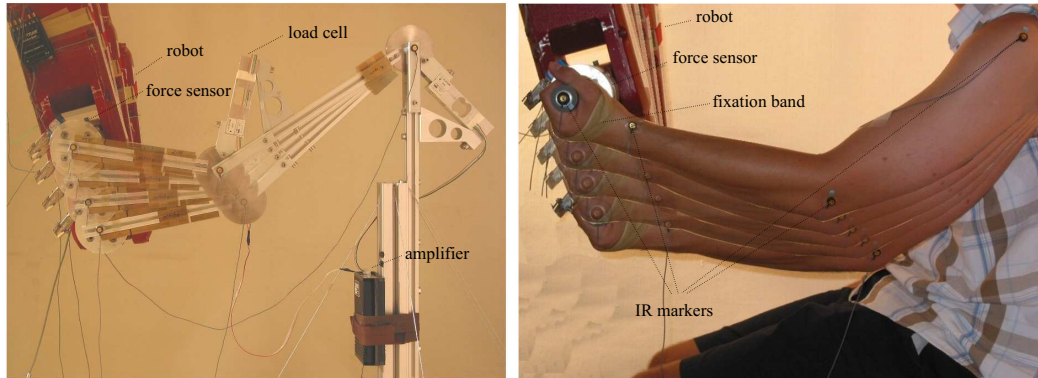


Figure 3.12: *Two composite images showing the complete courses of the mechanical arm trajectory with shoulder and elbow angular ranges of 11.4° and 11.5° respectively (left). The trajectory of the human arm (right) during the measurement with shoulder, elbow and wrist angular ranges of 12°, 3.4° and 1.8° respectively.*

The curve fitting optimization problem described in equation 3.30 was performed throughout all time samples of the τ_j trajectory. The Coulomb friction components in τ_j were then observed as the difference between the measured and identified trajectories. This technique gave satisfactory results which will be presented in the next section (see figures 4.21 and 4.22 in section 4).

3.5.3 Implementation of the experiment

The procedure described in the preceding section was then finally used with the real human arm. The actual movement can be seen from the right side of figure 3.12. All together ten equal measurements were performed for further analysis on the right arm of three different healthy individuals. The experimental apparatus was the same as the one explained at the beginning of this chapter. In order to prove the non-linear nature of the upper extremity the experiment, was performed in four different angular operation points. According to our reasoning the results should differ from point to point due to different levels of passive moments.

3.6 Simulation for calculating the required robot joint trajectory

When implementing experiments it was very important to program appropriate trajectories into the robot joints. For this the *required robot joint trajectory* \mathbf{q}_r had to be calculated in advance as already described when explaining the block diagram of the experimental setup in figure 3.8.

For calculation purposes a Matlab-Simulink based simulation was developed, which is shown as a block diagram in figure 3.13.

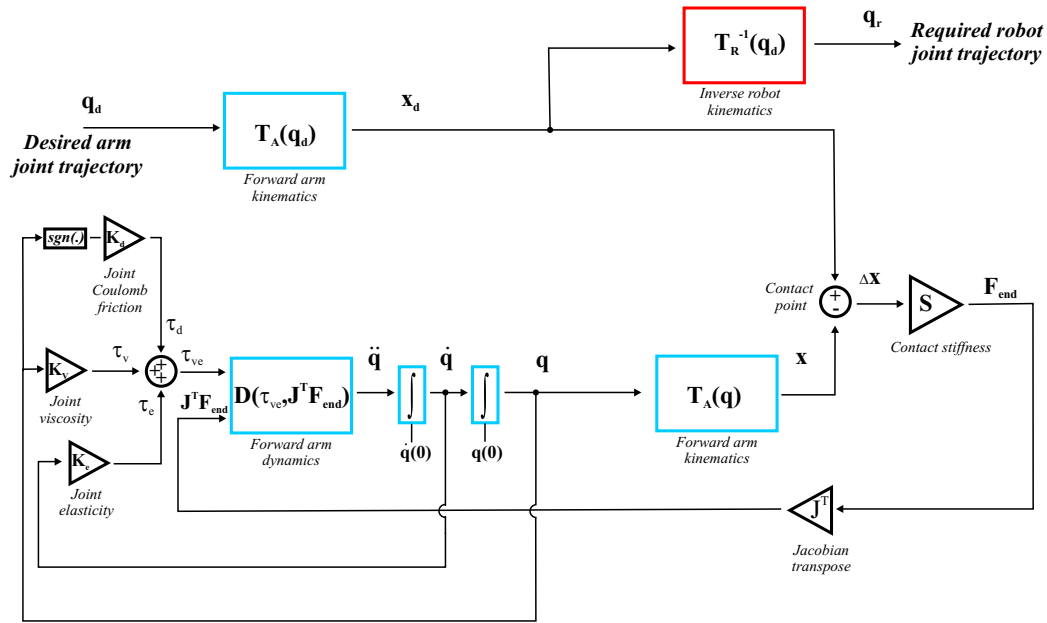


Figure 3.13: The block diagram of the experimental simulation. The desired arm trajectory \mathbf{q}_d which was specified by the user served as an input to the simulation whereas the output is represented by the required robot joint trajectory \mathbf{q}_r . The upper extremity (arm) forward dynamics was simulated from equation 3.1 whereas the contact was modelled as a simple spring (Contact point). The blocks for the arm are denoted in blue color ($\mathbf{D}(\tau_{ve}, \mathbf{J}^T \mathbf{F}_{end})$, $\mathbf{T}_A(\mathbf{q}_d)$, $\mathbf{T}_A(\mathbf{q})$) whereas the robot pertaining blocks are red ($\mathbf{T}_R^{-1}(\mathbf{q}_d)$).

- The simulation consists of the *forward arm kinematics* block $\mathbf{T}_A(\mathbf{q}_d)$ giving the desired global end-effector coordinates which the arm should follow. At first, however we had to specify the *desired arm joint trajectory* \mathbf{q}_d . A trajectory which fulfilled our angle, velocity and acceleration requirements

had to be generated. Theoretically any type of a continuous trajectory which did not exceed the safety and technical limits could be inserted.

- The *inverse robot kinematics* block $\mathbf{T}_R^{-1}(\mathbf{q}_d)$ was applied to \mathbf{x}_d in order to calculate the *required robot joint trajectory* \mathbf{q}_r . This vector was one of the most relevant simulation results because it was later used directly for driving the robot motors (see figure 3.8). These two blocks by itself would be enough to generate the necessary robot joint trajectory but the experimental simulation enabled us to have an insight into all relevant dynamic and kinematic parameters of the arm.
- The arm dynamics was accounted for in the *forward arm dynamics* $\mathbf{D}(\tau_{ve}\mathbf{J}^T\mathbf{F}_{end})$ block where the forward dynamics was calculated by expressing the arm joint acceleration vector $\ddot{\mathbf{q}}$ from equation 3.1. The *joint Coulomb (dissipative) friction* torques τ_d , *joint viscosity* τ_v and *joint elasticity* τ_e were adjusted with the \mathbf{K}_d , \mathbf{K}_v and \mathbf{K}_e matrices respectively. Their sum composed the vector of resistive properties τ . The angle initial condition $\mathbf{q}(\mathbf{0})$ was set arbitrarily whereas the velocity initial condition $\dot{\mathbf{q}}(\mathbf{0})$ was always 0. To obtain the end point position of the arm \mathbf{x} we again applied the *forward arm kinematics* block $\mathbf{T}_A(\mathbf{q})$.
- The *contact point* between the robot end-effector and the arm was modelled as a linear spring with stiffness \mathbf{S} . The contact force was then obtained as:

$$\mathbf{F}_{end} = \mathbf{S} \cdot \Delta \mathbf{x} \quad (3.33)$$

To acquire the arm joint torques we had to apply the *jacobian transpose* for the arm i.e. $\mathbf{J}^T\mathbf{F}_{end}$.

In the simulation we have presumed three rigid body segments for the upper extremity (arm) and two for the robot in a configuration similar to the one in reality. The segments had only the longitudinal dimension whereas rotations were presumed to be ideal. This configuration can be seen in figure 3.14 which shows the upper extremity simulation case where 3 segments were used for the arm. When simulating the mechanical arm, however, the simulation only accounted for 2 segments of the arm.

The body segment lengths of the arm are denoted with variables a_j and the robot segment lengths with Ra_j . The angles q_j of the arm and robot q_{rj} are denoted in accordance with the notation described in figure 3.4.1 on page 45. The horizontal force components are shown with F_x and the vertical ones with F_z . The robot and the arm together form a closed kinematic chain because their distal joints (at points of rotations q_1 and q_{r1}) are presumed to be fixated. While this is

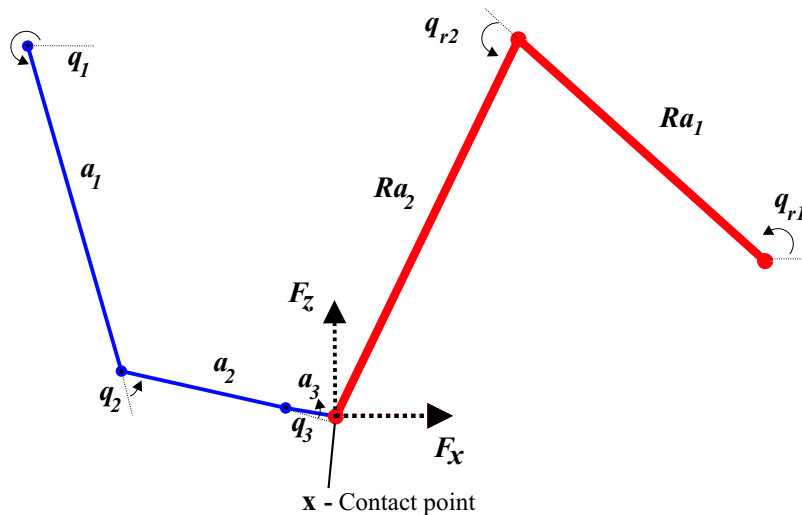


Figure 3.14: A stick figure scheme showing the two segments of the robot manipulator (blue line) and three segments of the human arm (red line). The segment lengths are denoted with a_j and Ra_j and the angles with q_j and q_{rj} respectively. The horizontal and vertical contact forces are also denoted (F_z , F_y).

true for the robot and the mechanical arm we attempted to keep the shoulder position in the upper extremity as constant as possible during experiments in order to fulfill this requirement.

After specifying the relevant model parameters we were capable of observing all relevant quantities during the course of the simulation (figure 3.15).

From figure 3.15 we can see that the operator first had to specify a certain number of simulation parameters before starting the simulation:

- The *number of arm DOF* was either 2 (in simulation of mechanical arm) or 3 (in simulation of upper extremity).
- The *arm kinematic parameters* were chosen according to accurate measurements made prior to the experiment. When determining upper extremity segment lengths we took the distances between the observed IR markers.
- The *arm dynamic parameters* such as segment COGs (l_j), segment masses (m_j) and segment transversal moments of inertia (I_j) were also set. They

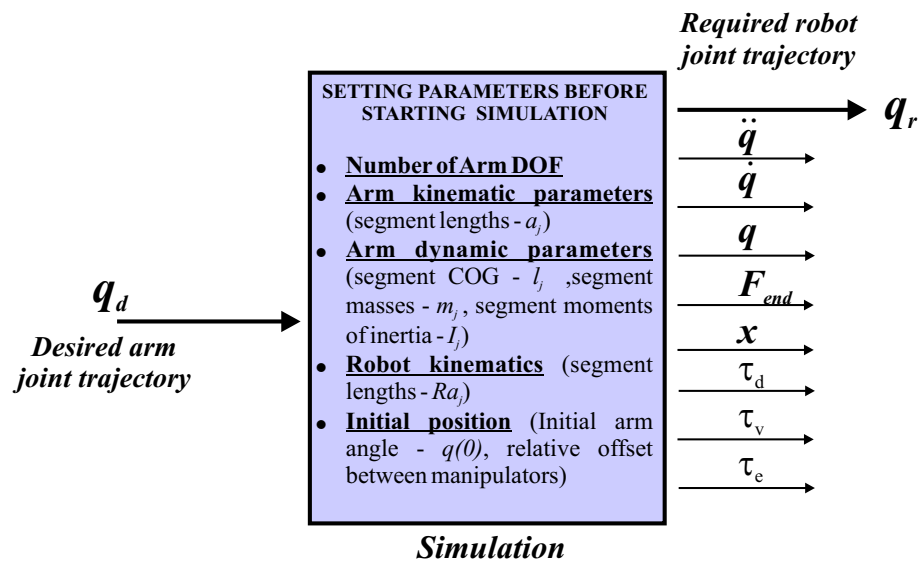


Figure 3.15: The input/output block showing the simulation which gives an overview of the whole procedure. The operator had to define the desired arm joint trajectory \mathbf{q}_d and define some model parameters which are stated inside the simulation block. On the right side all output variables are denoted.

were obtained from the CAD model in the mechanical arm case and from regression equations [81] for the case of the upper extremity.

- The *robot kinematic* parameters were also very important in order to generate proper results. Segment lengths Ra_j were carefully measured on the real robot.
- In order to generate results comparable to the actual ones we had to specify the *initial position* of the arm $\mathbf{q}(0)$ and the relative horizontal and vertical offsets between base points of the robot and arm. This completely described the angles of both manipulators at the beginning of the simulation.

Chapter 4

Results

We will try to present the results of all performed experiments as concisely as possible regardless of the vast amount of data. The result section is divided into three logical parts in the same way as it was done in the previous section. The results will first be presented for the *passive moment experiment*, then for the *experiment of determining body segment and joint parameters* and finally we will try to represent the quality of the results obtained with the developed *Matlab simulation*.

4.1 Determining shoulder and elbow joint passive moments

We have presented the results for this experiment in two different parts. First, a detailed overview of data acquired for one intact person (a person without any neuromuscular disorders) is given. Among checking the general trends, the purpose of this experiment was to assess the fidelity and repeatability of the method. The second part includes measurements on six persons to gain insight into data variability among several persons. Eventually the obtained results are evaluated and discussed.

It has to be noted that for these measurements the shoulder and elbow were not moved throughout their complete range of motion because of a limitation imposed by the workspace of the robot manipulator.

4.1.1 Passive moment results for one subject

Initially, six measurements of all ten movements were carried out on one particular subject (age 25, weigh 77 kg), with every one performed on a separate day.

In total six measurements were made for every movement (*i.e.* extension to flexion and backwards). In figures from 4.1 to 4.5 six trial average time courses

and standard deviations of force and kinematic data for five fixed-elbow and five fixed-shoulder configurations, are shown. The upper extremity movement is sketched below every figure.

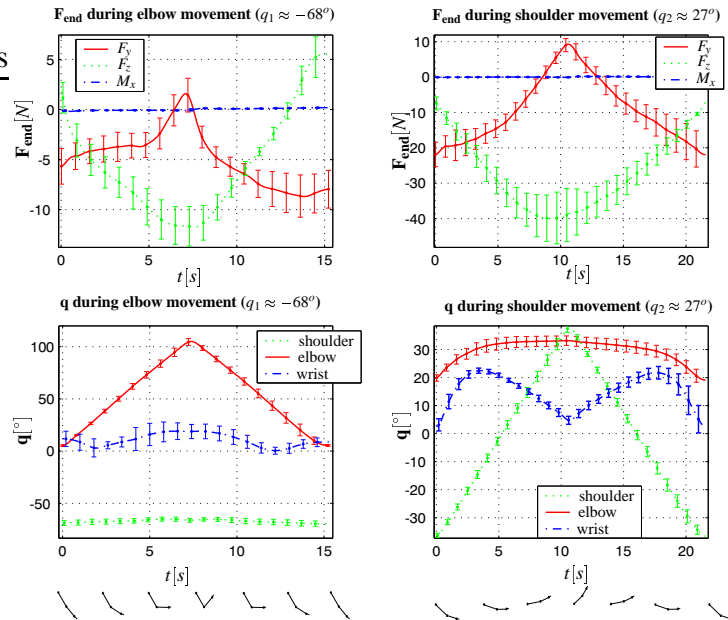


Figure 4.1: The average contact force \mathbf{F}_{end} and joint angle q_j trajectories with their standard deviation error bars obtained from six trials, in an elbow movement while the shoulder was fixed at $q_1 \approx -68^\circ$ (left column) and in a shoulder movement while the elbow was fixed at $q_2 \approx 27^\circ$ (right column). The arm movement is sketched below the figure.

Note that the force data deviations in figures from 4.1 to 4.5 (upper two subplots in every figure) are larger than the ones of kinematic data (lower two subplots in every figure) due to a bigger level of contact force sensitivity.

The x axis torque M_x seen in figures 4.1 to 4.5 was almost negligible due to a bearing attached in the mechanism of the handle. These averaged data were then applied to the equation 3.18, yielding a vector of average passive moments $\bar{\tau}_p$ for all 10 configurations as seen in figures from 4.6 through 4.10. These figures show the average passive moment time courses and their six trial standard deviations in all ten configurations.

It is sensible to represent the average passive moments in relation to the displaced angle which can be seen in figures from 4.11 to 4.16. The first figure 4.11 represents data from a subject on which a more extensive analysis of six measurements was made. The fixation angles of the elbow (q_2) and shoulder (q_1) as

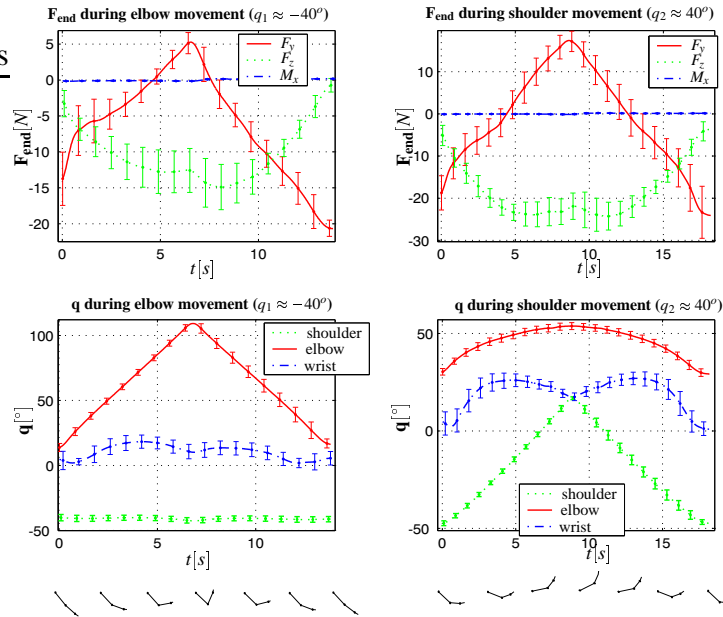


Figure 4.2: The average handle force \mathbf{F}_{end} and joint angle q_j trajectories with their standard deviation error bars obtained from six trials, in an elbow movement while the shoulder was fixed at $q_1 \approx -40^\circ$ (left column) and in a shoulder movement while the elbow was fixed at $q_2 \approx 40^\circ$ (right column). The arm movement is sketched below the figure.

measured by the Optotrak system are also denoted.

Clearly the passive moments of the shoulder are much less influenced by adjacent angle fixation than the ones of the elbow. This comes as a result of a smaller number of passive one and two-joint muscles spanning the elbow joint (7) compared to a much greater number of muscles in the shoulder (15). Apart from this the biceps and triceps muscles which are a major contributor to elbow passive properties are two-joint muscles and hence also influence the shoulder passive properties. The maximum standard deviations (σ_{max}) acquired for every passive moment seen in figures 4.6 to 4.10 can be seen in tables 4.1 and 4.2:

It is obvious that the standard deviations in vectors τ_{p1} and τ_{p2} are quite large, indicating a large error level. This error occurs mostly due to a large contact force standard deviation which could be observed in figures 4.1 to 4.5.

It has to be noted that in figure 4.11, the range of displaced angles was different for every particular movement because of different joint movement ranges at corresponding adjacent angle fixations. In all curves a hysteresis arising due to muscle dissipative effects can clearly be observed [18]. This hysteresis was

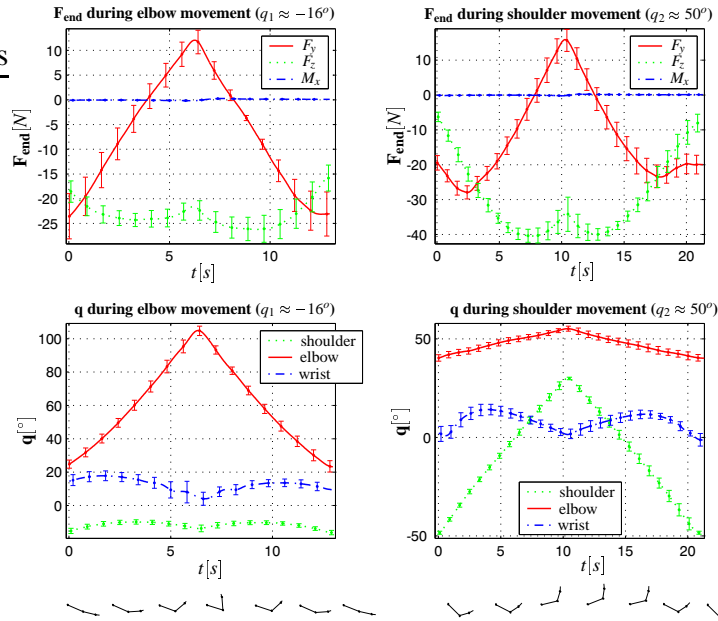


Figure 4.3: The average handle force \mathbf{F}_{end} and joint angle q_j trajectories with their standard deviation error bars obtained from six trials, in an elbow movement while the shoulder was fixed at $q_1 \approx -16^\circ$ (left column) and in a shoulder movement while the elbow was fixed at $q_2 \approx 50^\circ$ (right column). The arm movement is sketched below the figure.

discussed and shown in figure 3.10 of section 3.4.

4.1.2 Passive moment result comparison for six subjects

The same data analysis was used for all six subjects participating in the study and all measurements were made under the same conditions. For five subjects every movement was measured only twice whereas one particular subject was measured six times.

It needs to be emphasized that for practical reasons the shoulder and elbow angles were not fixed completely equally for all subjects (the deviations were less than $\pm 8^\circ$). This is mostly due to a fairly complex process of trajectory programming and different arm geometry among subjects. This fact inseparably results also in slightly different passive moments. The standard deviations of the other five subjects are presumed to resemble the ones observed in the previous section (tables 4.1 and 4.2 and figures 4.1 through 4.5) for one subject. They are not given here however, because the passive moments for these five subjects were produced

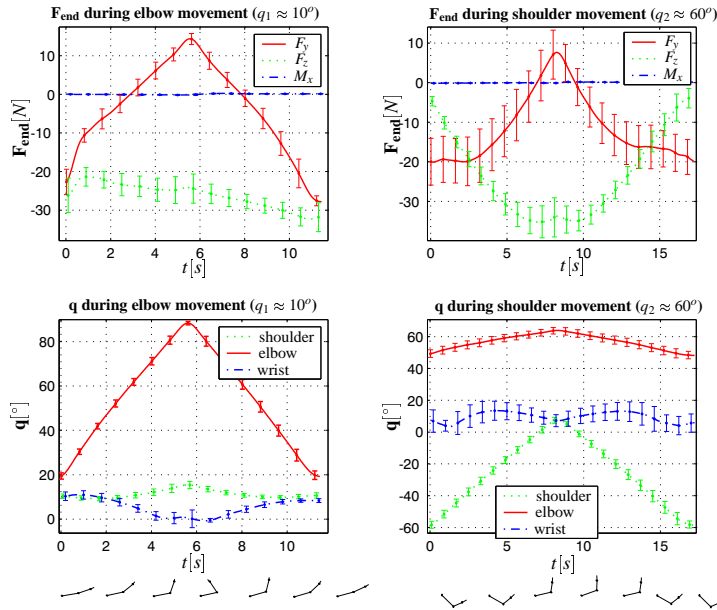


Figure 4.4: The average handle force \mathbf{F}_{end} and joint angle q_j trajectories with their standard deviation error bars obtained from six trials, in an elbow movement while the shoulder was fixed at $q_1 \approx 10^\circ$ (left column) and in a shoulder movement while the elbow was fixed at $q_2 \approx 60^\circ$ (right column). The arm movement is sketched below the figure.

from only *two independent measurements* which is a very low number for statistical analysis. Standard deviations were hence only observed for the passive moments of one subject which were produced from a larger number of *six independent measurements*. In figures from 4.12 to 4.16 all ten passive moment curves are given as a function of the displaced angle in the same way as it was done in figure 4.11 for the first subject.

It should again be noted that the scale of shoulder passive moments in all figures from 4.11 to 4.16 is larger than for elbow passive moments. Every curve in these plots represents an average of two measurements. Most subjects show a similar pattern, although some show quite obvious differences in the hysteresis size and slope.

4.1.3 Discussion of obtained results

In this experiment a method for estimating arm passive moments is proposed, which according to our knowledge has not been used before. Similar angle-

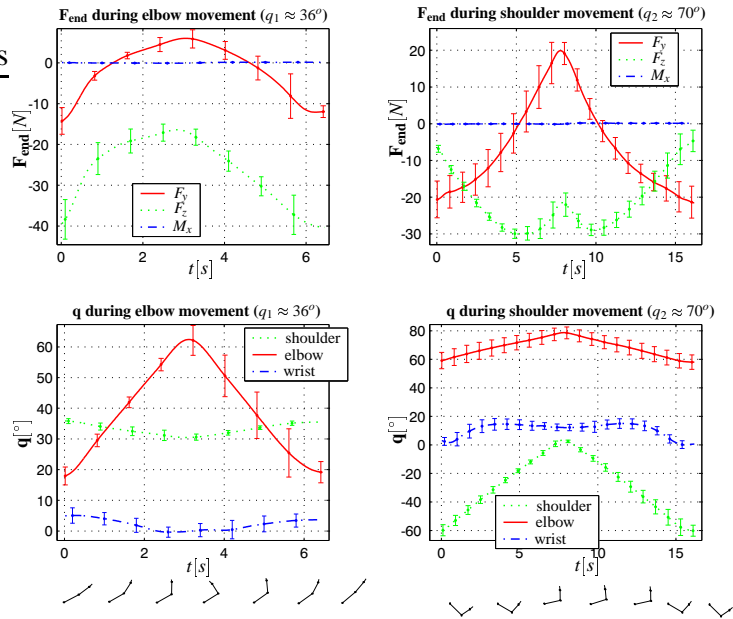


Figure 4.5: The average handle force \mathbf{F}_{end} and joint angle q_j trajectories with their standard deviation error bars obtained from six trials, in an elbow movement while the shoulder was fixed at $q_1 \approx 36^\circ$ (left column) and in a shoulder movement while the elbow was fixed at $q_2 \approx 70^\circ$ (right column). The arm movement is sketched below the figure.

dependent studies have been made for lower extremities [54, 55], while the upper extremity passive moments were not studied as much. In the measurement process, firstly one healthy individual was studied more in detail as described in section 3.4. The repeatability of data obtained from six measurements can be observed in figures from 4.1 to 4.5. While the angle data is very repeatable, the force sensor data on the other hand, shows more deviations. This is caused by a difficulty with which a subject is capable of maintaining the arm-robot connection fully equally in two successive trials. These raw data were then applied to equation 3.18, producing a passive moment vector $\tau_{\mathbf{p}}$, represented in figures from 4.6 to 4.10 as a function of time. From this vector the component τ_{p2} represents the elbow passive moment and τ_{p1} the shoulder passive moment. Five elbow and five shoulder passive moments were inspected for this individual, with adjacent joints being fixed at various angles (figure 4.11).

Furthermore, five more healthy subjects were measured in the same way. The force and kinematic data compared among different subjects show rather large differences due to geometrical and dynamical differences and due to differences in

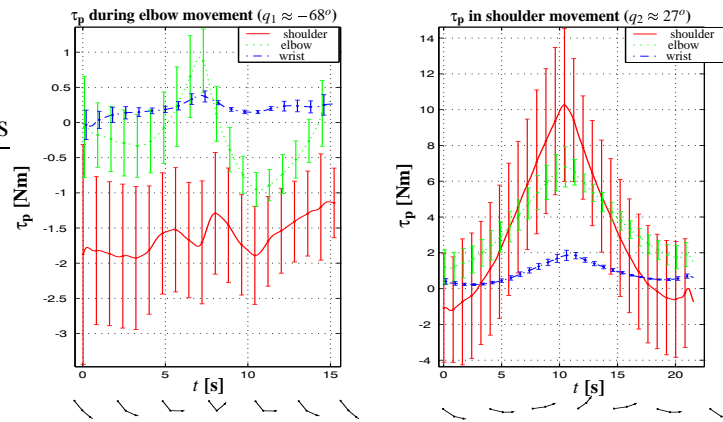


Figure 4.6: The average passive moments $\bar{\tau}_p$ in all three joints, computed from the force and angle data in figure 4.1 with their six-trial standard deviation error bars, in an elbow movement while the shoulder was fixed at $q_1 \approx -68^\circ$ (left) and in a shoulder movement while the elbow was fixed at $q_2 \approx 27^\circ$ (right). The arm movement is sketched below the figure.

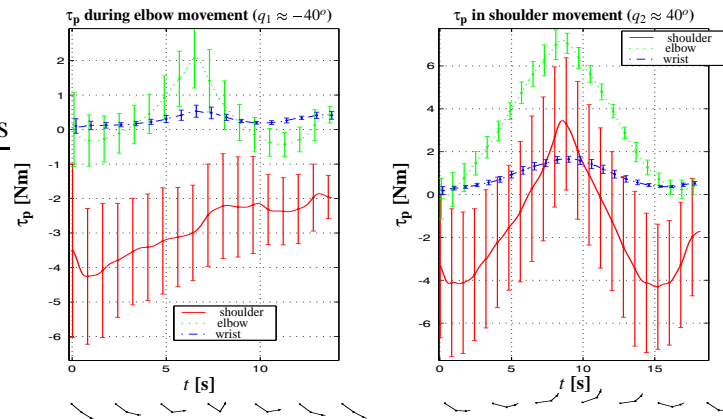


Figure 4.7: The average passive moments $\bar{\tau}_p$ in all three joints, computed from the force and angle data in figure 4.2 with their six-trial standard deviation error bars, in an elbow movement while the shoulder was fixed at $q_1 \approx -40^\circ$ (left) and in a shoulder movement while the elbow was fixed at $q_2 \approx 40^\circ$ (right). The arm movement is sketched below the figure.

the anatomical structure. This also explains why there is no straightforward correlation in the passive moments among all subjects (figures from 4.11 to 4.16). A large passive moment amplitude variation among different subjects was observed,

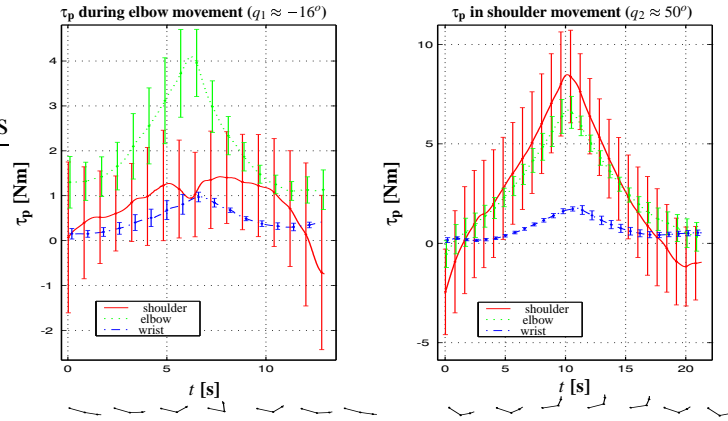


Figure 4.8: The average passive moments $\bar{\tau}_p$ in all three joints, computed from the force and angle data in figure 4.3 with their six-trial standard deviation error bars, in an elbow movement while the shoulder was fixed at $q_1 \approx -16^\circ$ (left) and in a shoulder movement while the elbow was fixed at $q_2 \approx 50^\circ$ (right). The arm movement is sketched below the figure.

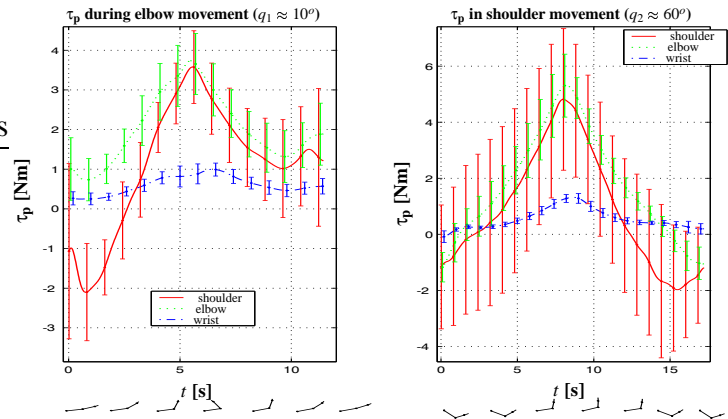


Figure 4.9: The average passive moments $\bar{\tau}_p$ in all three joints, computed from the force and angle data in figure 4.4 with their six-trial standard deviation error bars, in an elbow movement while the shoulder was fixed at $q_1 \approx 10^\circ$ (left) and in a shoulder movement while the elbow was fixed at $q_2 \approx 60^\circ$ (right). The arm movement is sketched below the figure.

especially in the shoulder joint.

When addressing the statistics issue it needs to be said that no comprehensive statistical analysis was performed. The major reason for this was the fact that

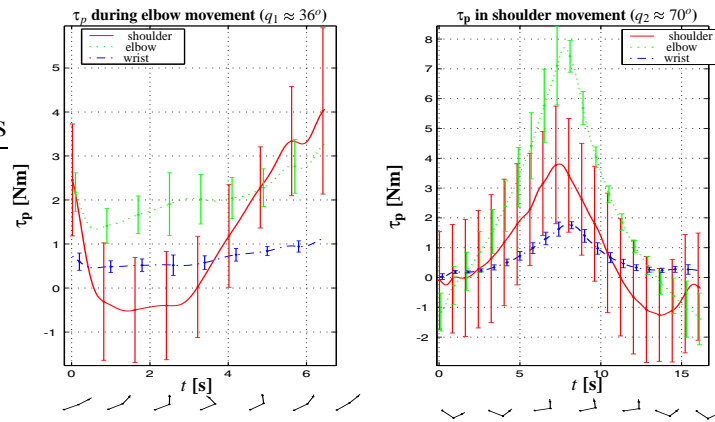


Figure 4.10: The average passive moments $\bar{\tau}_p$ in all three joints, computed from the force and angle data in figure 4.5 with their six-trial standard deviation error bars, in an elbow movement while the shoulder was fixed at $q_1 \approx 36^\circ$ (left) and in a shoulder movement while the elbow was fixed at $q_2 \approx 70^\circ$ (right). The arm movement is sketched below the figure.

Table 4.1: Maximum elbow passive moment six trial standard deviations σ_{max} (as observed from figures 4.6 to 4.10) at five different shoulder fixation angles for the first tested subject.

	σ_{max} ($q_1 = -68^\circ$)	σ_{max} ($q_1 = -40^\circ$)	σ_{max} ($q_1 = -16^\circ$)	σ_{max} ($q_1 = 10^\circ$)	σ_{max} ($q_1 = 36^\circ$)
elbow passive moment (τ_{p2})	0.7Nm	1.1Nm	1.0Nm	0.4Nm	1.1Nm

Table 4.2: Maximum shoulder passive moment six trial standard deviations σ_{max} (as observed from figures 4.6 to 4.10) at five different shoulder fixation angles for the first tested subject.

	σ_{max} ($q_2 = 27^\circ$)	σ_{max} ($q_2 = 40^\circ$)	σ_{max} ($q_2 = 50^\circ$)	σ_{max} ($q_2 = 60^\circ$)	σ_{max} ($q_2 = 70^\circ$)
shoulder passive moment (τ_{p1})	4.4Nm	3.6Nm	2.7Nm	3.0Nm	2.2Nm

the number of measurements was relatively low (six for one subject and only two for the other five). In analyzing the obtained passive moment results we tried to obtain a linear regression model of the curves which were presented in figures 4.11 to 4.16) by means of data mining [91]. The produced linear model rules

unequivocally reveal the fact that the inter-subject variability is larger than the test variability. The outcomes of this study are not shown in this thesis since they are very extensive and somewhat out of context with the topic of this thesis.

It can be seen that the passive moments are strongly influenced by adjacent joint angle fixation. However, this is much less evident for the shoulder joint, than it is for the elbow (figures from 4.11 to 4.16). It is also obvious that the shoulder passive moments are far larger than the ones obtained for the elbow. The reason lies in passive one and two-joint muscles which span over both joints and are very likely the major contributor to the passive properties. While there are only seven muscles producing elbow joint movements, there are fifteen which are involved in the shoulder, with a total physiological cross section area (PCSA) far greater than the one of the elbow muscles (see figures 1.2 and 1.3 in section 1.1). Apart from this, the biceps and triceps muscles which contribute to elbow joint motions are two-joint muscles spanning the whole upper arm and hence influence the passive properties of both the shoulder and the elbow joint.

In all similar works [17, 54, 57] the passive elastic moment was found to resemble a symmetrical double exponential curve with highly positive values at complete extension and negative ones at extreme flexion. Other parts of the curve were found to be almost linear. The exponential nature of these passive moments for intact population, which is more expressed near the articular boundaries, is in the presented (figures 4.11 through 4.16) results not always evident. Because of this we need to be aware of the fact that this results in passive moment values which are sometimes of very low value and therefore realistically also a subject to larger errors. We need to be aware of the fact that the passive moments τ_p in this study, contain elastic and dissipative contributions as explained in equation 3.18 and seen in figure 3.10. The calculated average passive moment patterns observed in figures 4.11 through 4.16, sometimes show a descending tendency at low angles. The reasons for this lies in the fact that the gravity contributions $G(q)$ from equation 3.18 have a larger inverse tendency than the environment contributions $J^T(q)F_{end}$ in that particular angular region. With the continuing flexion motion, however, the passive moments always show an increasing trend.

It has to be underlined that the flexion-extension movement limits in this study never reached the articular boundaries of either the elbow or the shoulder joint. This occurs due to a limited robot workspace and almost no physical constraining of the arm. Therefore the passive moments were quantified only in the central region of the movement range. The calculated passive moments here are also opposite in sign and show an inverse tendency compared to many other studies because the angle notation is different.

Apart from the relatively large force sensor data deviations (figures from 4.1 to 4.5), another source of error is also the gravity term $\mathbf{G}(\mathbf{q})$ in equation 3.18 which was calculated by using the segment masses m_j , lengths a_j and centers of gravity

l_j , from the literature [81] as seen in equation 3.8. Because the segment mass estimation m_j affects only the term $\mathbf{G}(\mathbf{q})$ in this equation, the inexact value causes significant errors to the passive moment calculation. The standard deviations of calculated passive moments τ_p in figures 4.6 to 4.10 can be seen as a good error indicator. They are obviously always larger for the shoulder and smallest from the wrist joint. The reason for this can be seen by observing the product $\mathbf{J}^T(\mathbf{q})\mathbf{F}_{\text{end}}$ in equation 3.15 which incorporates errors from the end force vector F_{end} and angles q (as seen in figures from 4.1 to 4.5). The first element of this product which corresponds to shoulder passive properties τ_{p1} involves six multiplications between the angle dependent terms in $\mathbf{J}^T(\mathbf{q})$ and the elements of the force vector \mathbf{F}_{end} , the second one (τ_{p2}) four and the third one τ_{p3} only two. This fact consequently implies higher standard deviations.

On the other hand, segment length and center of gravity location errors do not affect the result greatly. The effect they have on the term $\mathbf{G}(\mathbf{q})$ cancels itself with that from the environment contribution term $\mathbf{J}^T(\mathbf{q})\mathbf{F}_{\text{end}}$ (equation 3.18). The reason lies in the Jacobian matrix $\mathbf{J}^T(\mathbf{q})$ (equation 3.10) which also depends on a_j . Hence, the error imposed by a marker misalignment, is not very prominent, resulting in low percentage changes in segment lengths a_j and subsequently centers of gravity l_j .

Owing to the fact that the planar model structure is mathematically far less complex to describe than any other alternative, some studies suggest that the motor control system in the human brain actually uses a simplified version of such a model in determining the inverse dynamics problem [15]. In the model used in this study, the segments are presumed to be rigid, while the joints include pure rotations without any translation. Apart from that, the shoulder complex also includes two translational degrees of freedom. The study of Veeger *et al.* [72] shows that the flexion-extension rotational center translation of the glenohumeral joint was within just 4 mm of the geometric center, making our assumption reasonably justified.

The study presented here simultaneously determines all three passive moments from the inverse dynamics model by using a robot manipulator. If compared to other studies on passive moments, the method seems to be elegant from the subject point of view, with less physical constraining of particular arm segments required. The single required constraining mechanism in the process is the elbow orthosis, utilized for all shoulder movement trajectories, whereas all elbow motion trajectories are performed with all arm joints being completely unconstrained. Moreover the methods used for assessing the passive moments in other studies concentrate on masses and other dynamic parameters of the body segment in motion, enabling the determination of passive moments for only one considered joint.

The experimental results shown here were obtained for healthy individuals with an experimental setup using a robot manipulator as the main apparatus. Ac-

According to our expectations impaired subjects should show values which are distinguishable from the results on intact subjects. We are aware of the fact that the EMGs of such subjects would be very unpredictable which would not allow us to make the assumption 3.16. Despite this fact the results could still be interesting from the clinical point of view since they could allow the monitoring of this particular unpredictable activity itself. We should be aware, however that not all neurological impairments imply such unpredictable activity. Patients with neurological impairments are considered to be good candidates for treatment with new rehabilitation treatment devices such as haptic robots which allow human-machine interaction by means of force and touch. In such novel rehabilitation environments the methodology shown here could be used as a measurement module. We speculate that the presented joint parameter estimation method could provide a potential upper extremity clinical evaluation method which provides data on joint properties instantaneously during the rehabilitation practice itself.

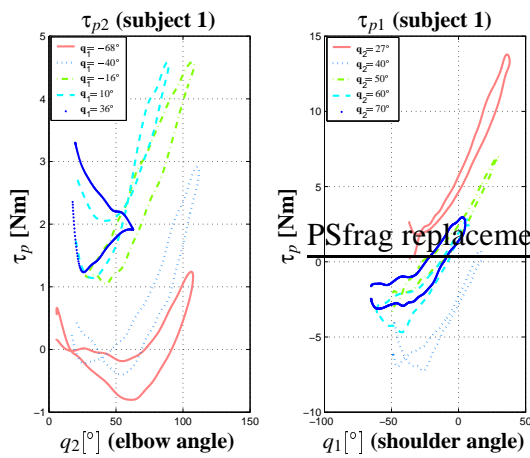


Figure 4.11: All five average elbow (left) and shoulder (right) passive moments as a function of both angles for subject 1. Every curve is an average of six measurements.

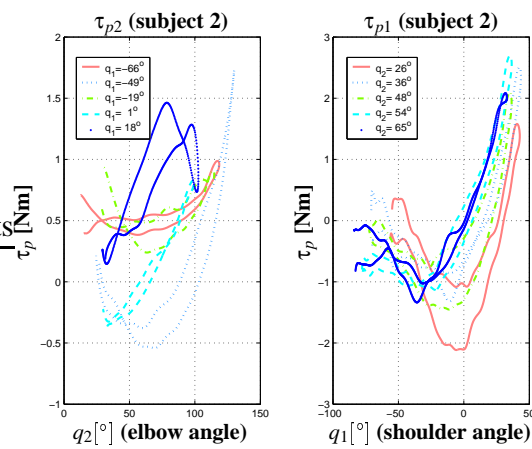


Figure 4.12: All five average elbow (left) and shoulder (right) passive moments as a function of both angles for subject 2. Every curve is an average of six measurements.

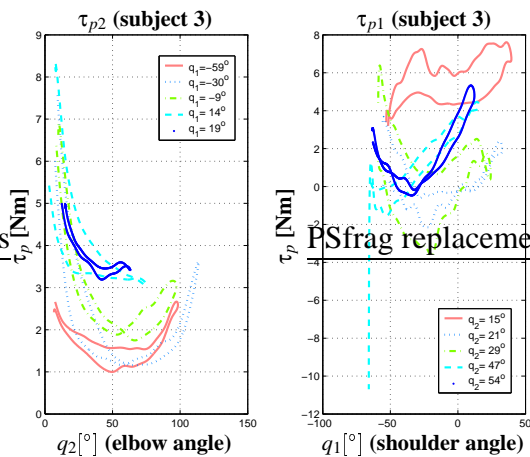


Figure 4.13: All five average elbow (left) and shoulder (right) passive moments as a function of both angles for subject 3. Every curve is an average of two measurements.

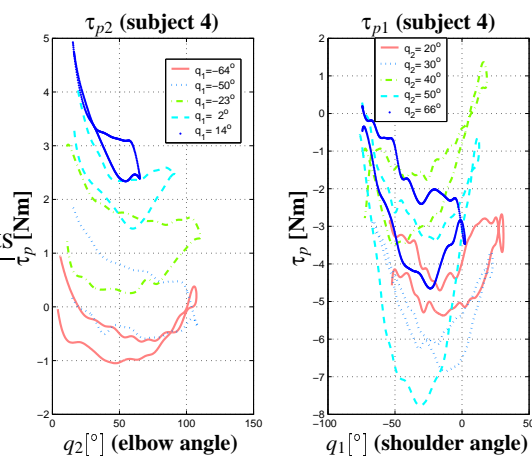


Figure 4.14: All five average elbow (left) and shoulder (right) passive moments as a function of both angles for subject 4. Every curve is an average of two measurements.

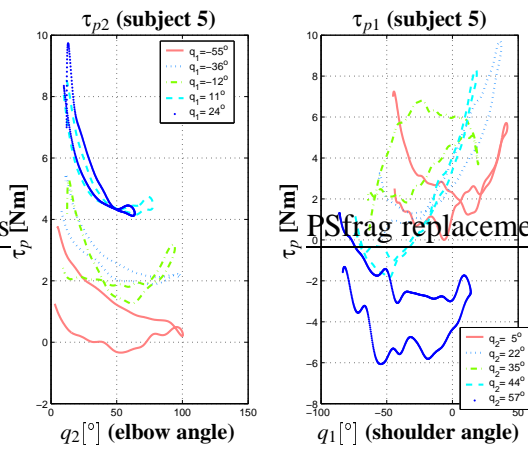


Figure 4.15: All five average elbow (left) and shoulder (right) passive moments as a function of both angles for subject 5. Every curve is an average of two measurements.

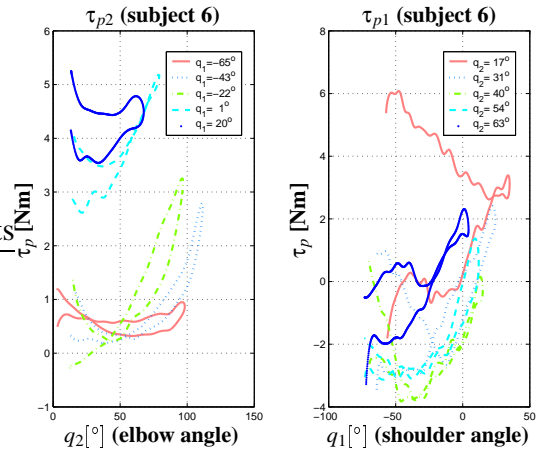


Figure 4.16: All five average elbow (left) and shoulder (right) passive moments as a function of both angles for subject 6. Every curve is an average of two measurements.

4.2 Upper extremity joint and body segment parameter identification

As shown in section 3.5, the second experiment was focused on determining joint and body segment parameters in the upper extremity and in a mechanical arm for verification purposes. We will first present results obtained in the mechanical arm experiment and later on the outcomes of the method performed on three right upper extremities of healthy individuals in four different configurations for every one of them. Finally we will discuss the results obtained with this method.

4.2.1 Results obtained in the mechanical arm experiment

As seen in section 3.5.2 we have developed a mechanical arm for verification of our identification method. The arm structure has already been presented in figure 3.11. We have obtained the reference values for mass ($m_{j_{ref}}$), COG ($l_{j_{ref}}$) and segment length ($a_{j_{ref}}$) parameters from the CAD model and the passive moment references ($\tau_{pj_{ref}}$) from the load cell readings. It needs to be emphasized that unlike in the human upper extremity, the passive moments τ_{pj} in the mechanical model were not a function of adjacent angles q_j . The numerical reference values are summed in the following table:

Table 4.3: *Significant parameters of the mechanical arm as obtained from the CAD model.*

$m_{1_{ref}}$ [kg]	$l_{1_{ref}}$ [m]	$a_{1_{ref}}$ [m]	$\tau_{p1_{ref}}$ [Nm]	$m_{2_{ref}}$ [kg]	$l_{2_{ref}}$ [m]	$a_{2_{ref}}$ [m]	$\tau_{p2_{ref}}$ [Nm]
1.440	0.184	0.376	0.139	1.160	0.115	0.239	0.161

The reference value of both identification vectors $\pi_{1_{ref}}$ and $\pi_{2_{ref}}$ from equation 3.31 can now be expressed numerically as:

$$\begin{aligned}\pi_{2_{ref}} &= [0.130 \text{ kgm}, 0.161 \text{ Nm}]^T \\ \pi_{1_{ref}} &= [0.260 \text{ kgm}, 1.160 \text{ kg}, 0.139 \text{ Nm}]^T\end{aligned}\tag{4.1}$$

Before looking at the identification results we should observe the contact forces \mathbf{F}_{end} and both joint torques from vector $\mathbf{J}^T \mathbf{F}_{\text{end}}$. The values of τ_j in particular joints were crucially important because they defined the optimization function as shown in equation 3.29. Figure 4.17 shows the 10 trial average values and their standard deviations for the case when the brakes were not activated.

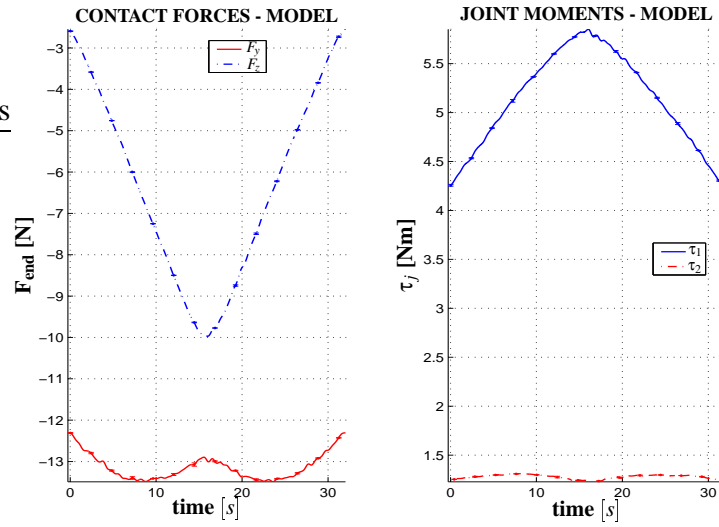


Figure 4.17: The mechanical model average horizontal (F_y) and vertical (F_z) contact forces with standard deviations from 10 different measurements (left) when the brakes were not activated. The right figure gives average values of τ_j for both joints and their standard deviations. Note that standard deviations are very small and therefore hardly visible.

When wanting to perform the identification process effectively, however the brakes had to be activated. The effect of braking on the contact forces and joint moments can be seen from figure 4.18.

The identification results for the case when the brakes were not activated are presented in graphical form in figures 4.19 (shoulder) and 4.20 (elbow). These figures give an insight into the identified joint torques τ_{jid} which were fitted to the measured torques τ_j shown in figure 4.17 for every particular joint. The identified passive moments τ_{pjid} are also presented against their measured values τ_{pjref} .

The same graphical results are also presented for the more general case when the brakes were activated in figures 4.21 and 4.22.

The parameter values will now be presented as bar plots which show the difference between identified numerical values of parameters m_2l_2 , m_2 , l_2 , m_1l_1 , τ_{p1} and τ_{p2} from identification vectors π_1 and π_2 (equation 3.31) against the reference values of these parameters in equation 4.1. These parameters can be seen in figure 4.23 for the case where there was no braking and 4.25 when brakes were activated. The units we used in these plots are [kgm], [kg], [m] and [Nm] for parameters m_jl_j , m_j , l_j and τ_{pj} respectively. Apart from this the relative errors are also denoted in separate bar plots for each particular case in figures 4.24 and 4.26.

The numerical results for the mechanical arm are represented separately for the case when there were no brakes (table 4.4) and for the case when brakes were

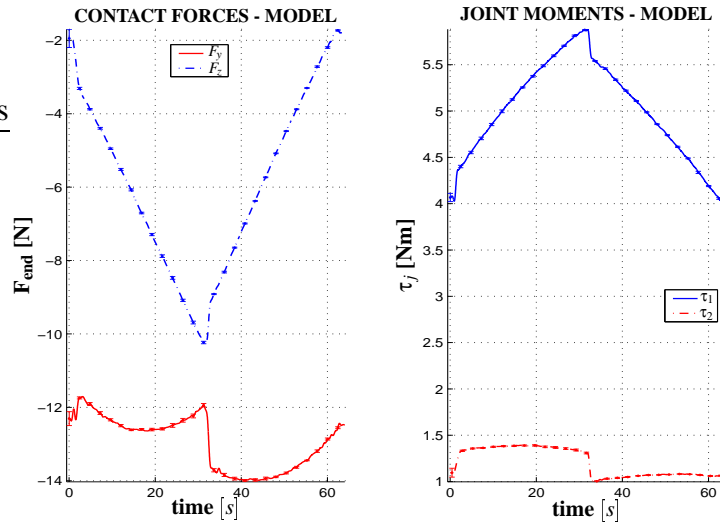


Figure 4.18: The mechanical model average horizontal (F_y) and vertical (F_z) contact forces with standard deviations from 10 different measurements (left) when the brakes were activated. The right figure gives average values of τ_j for both joints and their standard deviations. Note the force and moment steps which are due to Coulomb friction. Note that standard deviations are very small and therefore hardly visible.

activated (table 4.5). The value of x_{ref} denotes the CAD obtained parameter values from equations 4.1. The identified parameter values are represented with \bar{x} as average values from 10 measurements. The 10 measurement standard deviations (σ_x) and differences in relative form $\left(\frac{x_{ref}-\bar{x}}{\bar{x}}\right)$ are also given in both tables.

Table 4.4: Identified parameters obtained for the mechanical arm when passive moments τ_{pj} were zero. \bar{x} denotes the average values from 10 measurements, measurement standard deviations are σ_x and differences in relative form $\left(\frac{x_{ref}-\bar{x}}{\bar{x}}\right)$.

parameter	x_{ref}	\bar{x}	σ	$\frac{x_{ref}-\bar{x}}{x_{ref}}[\%]$
m_2l_2 [kgm]	0.130	0.132	0.001	1.8
m_2 [kg]	1.160	1.207	0.001	4.0
l_2 [m]	0.115	0.110	0.001	-4.6
m_1l_1 [kgm]	0.260	0.265	0.001	2.1
τ_{p2} [Nm]	0.005	0.003	0.001	-76.3
τ_{p1} [Nm]	0.002	0.008	0.001	73.3

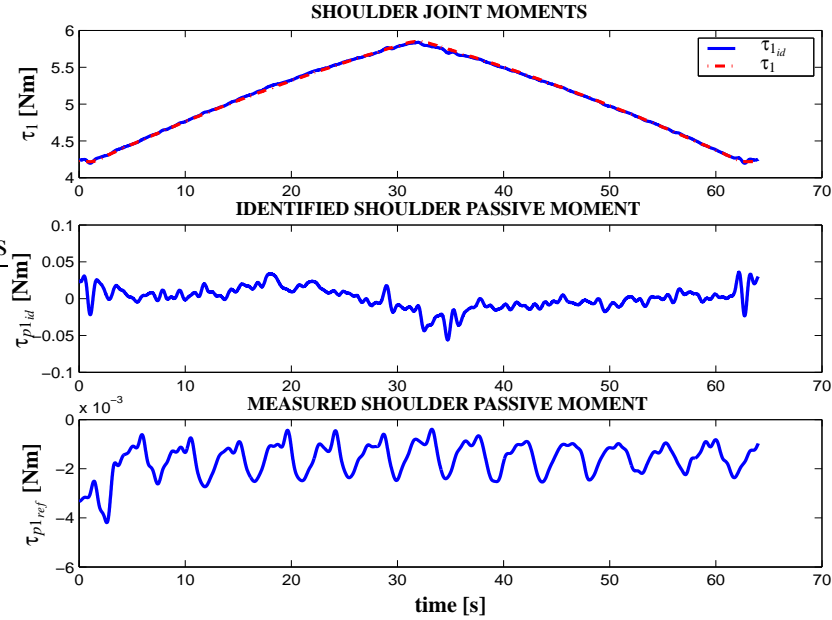


Figure 4.19: *Above* - The mechanical model shoulder moment τ_1 as measured (blue line) and the moment curve obtained as a result of the identification procedure $\tau_{1_{id}}$ (red line) without any brakes activated. *Middle* - The identified shoulder passive moment $\tau_{p1_{id}}$. *Below* - The measured shoulder passive moment $\tau_{p1_{ref}}$ as the outcome of load cell readings.

Table 4.5: *Identified parameters obtained for the mechanical arm when passive moments τ_{pj} were non zero.* \bar{x} denotes the average values from 10 measurements, measurement standard deviations are σ_x and differences in relative form $\left(\frac{x_{ref} - \bar{x}}{\bar{x}}\right)$.

parameter	x_{ref}	\bar{x}	σ	$\frac{x_{ref} - \bar{x}}{x_{ref}} [\%]$
$m_2 l_2$ [kgm]	0.130	0.125	0.001	-3.8
m_2 [kg]	1.160	1.206	0.001	3.9
l_2 [m]	0.115	0.104	0.001	-9.8
$m_1 l_1$ [kgm]	0.260	0.265	0.001	1.8
τ_{p2} [Nm]	0.161	0.145	0.006	-7.7
τ_{p1} [Nm]	0.139	0.151	0.007	10.6

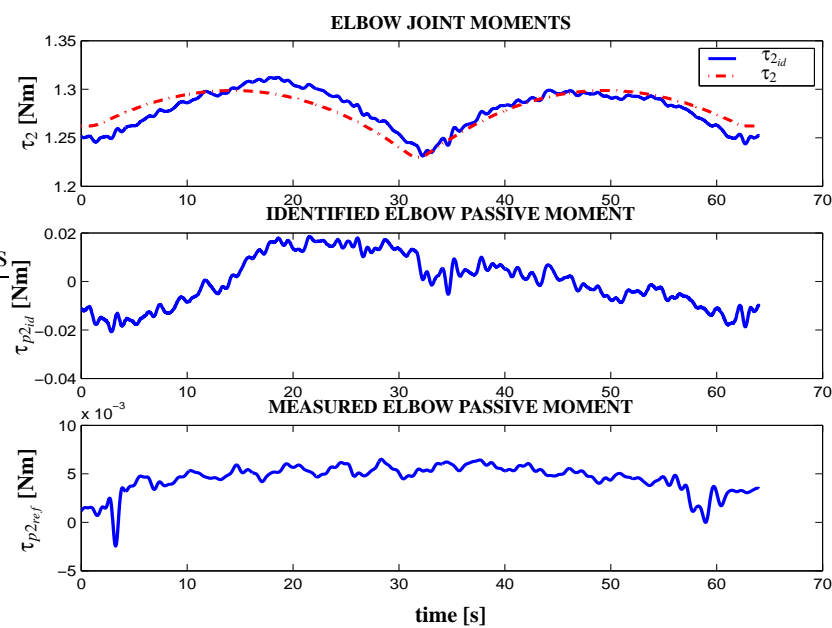


Figure 4.20: *Above* - The mechanical model elbow moment τ_2 as measured (blue line) and the moment curve obtained as a result of the identification procedure $\tau_{2_{id}}$ (red line) without any brakes activated. *Middle* - The identified elbow passive moment $\tau_{p2_{id}}$. *Below* - The measured elbow passive moment $\tau_{p2_{ref}}$ as the outcome of load cell readings.

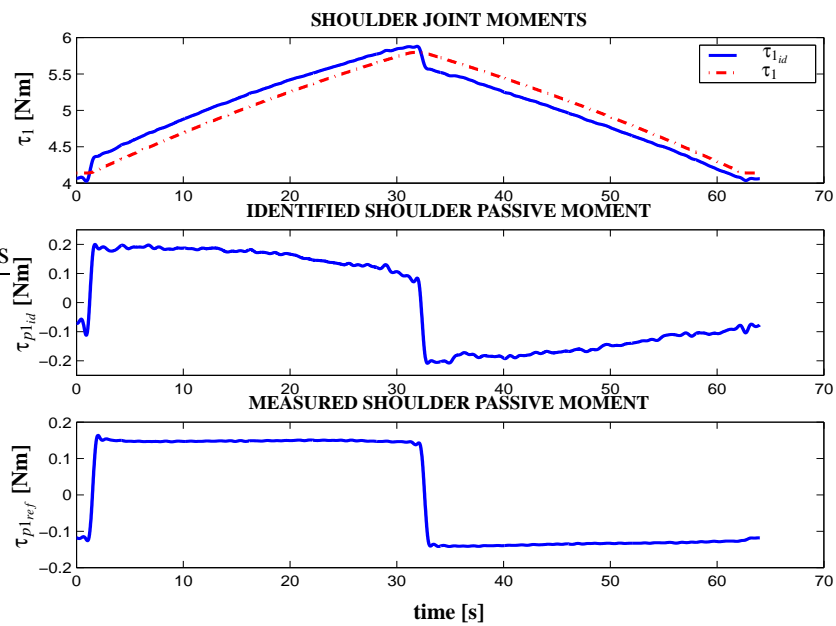


Figure 4.21: *Above* - The *mechanical model shoulder moment* τ_1 as measured (blue line) and the moment curve obtained as a result of the identification procedure $\tau_{1_{id}}$ (red line) when the *brakes were activated* to a certain level. *Middle* - The identified shoulder passive moment $\tau_{p1_{id}}$. *Below* - The measured shoulder passive moment $\tau_{p1_{ref}}$ as the outcome of load cell readings.

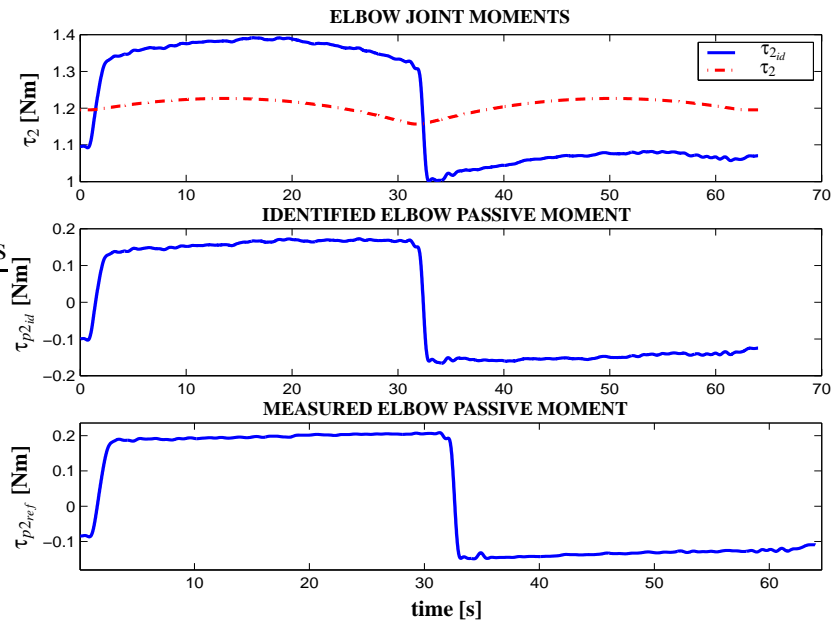


Figure 4.22: *Above* - The mechanical model elbow moment τ_2 as measured (blue line) and the moment curve obtained as a result of the identification procedure τ_{2id} (red line) when the brakes were activated to a certain level. *Middle* - The identified elbow passive moment τ_{p2id} . *Below* - The measured elbow passive moment τ_{p2ref} as the outcome of load cell readings.

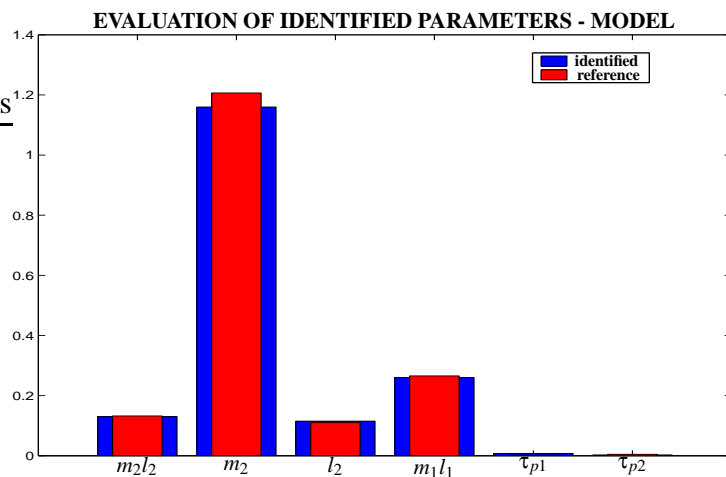


Figure 4.23: The comparison between measured and identified parameters for cases from figures 4.19 and 4.20 where brakes were not activated. The blue bars show identified values and the red ones the reference values from table 4.3.

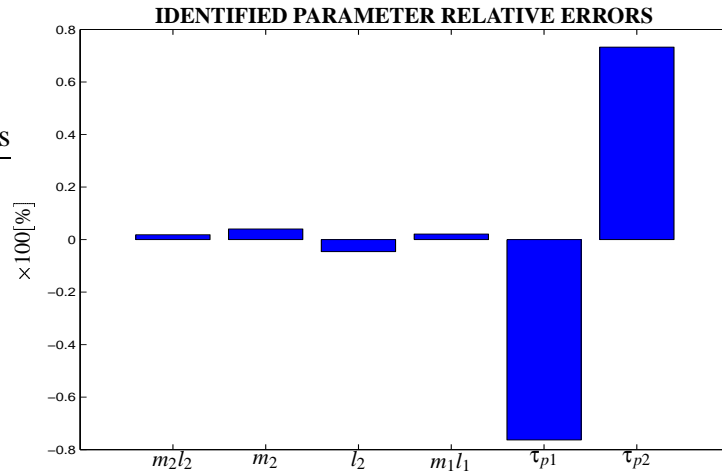


Figure 4.24: Relative errors for all identified parameters in figure 4.23.

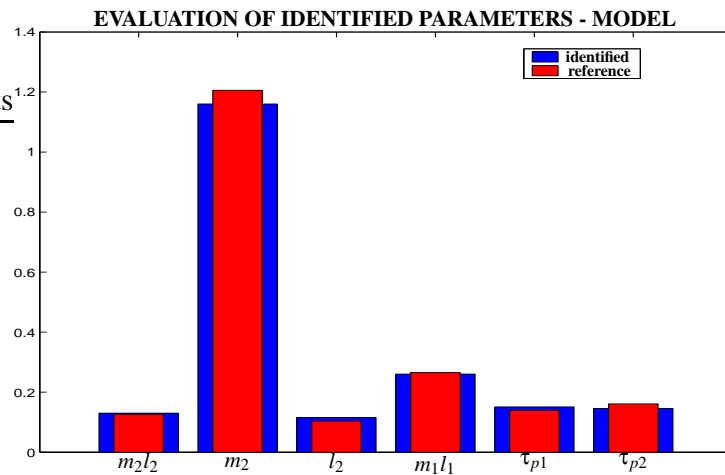


Figure 4.25: The comparison between measured and identified parameters for cases from figures 4.21 and 4.22 where brakes were activated. The blue bars show identified values and the red ones the reference values from table 4.3.

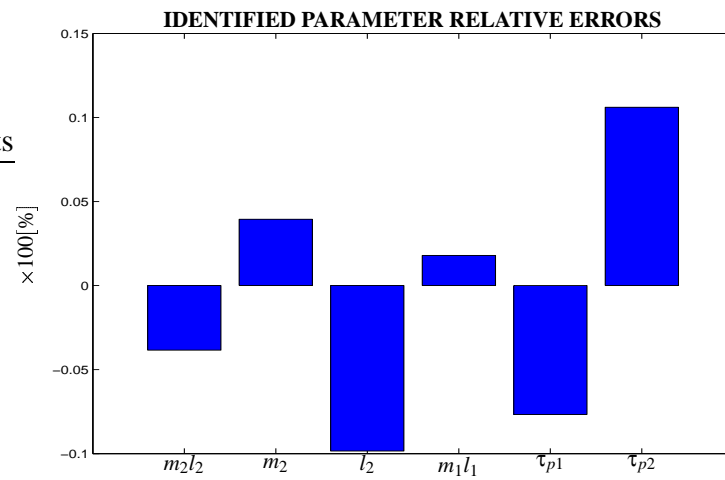


Figure 4.26: Relative errors for all identified parameters in figure 4.25.

4.2.2 Results obtained in the upper extremity experiment

Let us again observe typical contact forces \mathbf{F}_{end} in a typical upper extremity experiment and all joint torques from vector $\boldsymbol{\tau} = \mathbf{J}^T \mathbf{F}_{\text{end}}$ with average values obtained from 10 measurements and their standard deviations (figure 4.27) in a healthy human arm. The graphical identification results are shown in figures 4.28 through 4.30. The difference between the measured and identified curves in these figures gives an indication on joint passive moment values τ_{pj} .

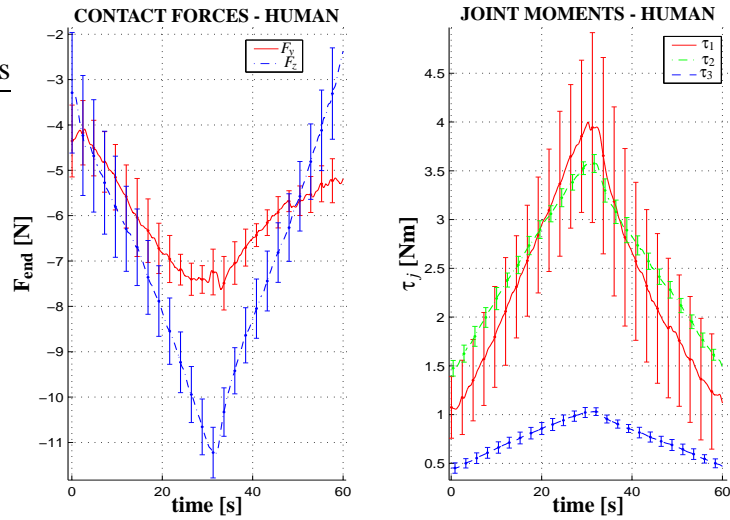


Figure 4.27: *The human arm average horizontal (F_y) and vertical (F_z) contact forces with standard deviations from 10 different measurements (left). The right figure gives average values of τ_j and their standard deviations.*

The evaluation of numerical results is again represented in the form of bar plots for every particular identified parameter from equation 3.26. As reference values we took those obtained from regression equations proposed by Zatsiorsky [21, 81] making the reference identification vectors look like this:

$$\begin{aligned}
 \pi_3 &= [0.047\text{kgm}, /]^T \\
 \pi_2 &= [0.154\text{kgm}, 0.663\text{kg}, /]^T \\
 \pi_1 &= [0.393\text{kgm}, 1.247\text{kg}, /]^T
 \end{aligned} \tag{4.2}$$

The identification procedure for every one of the three tested subjects was performed in four different angular configurations (figures 4.31, 4.33 and 4.35). Every one of these figures is accompanied by the relative error bar plots showing the differences between the identified and literature parameters (figures 4.32, 4.34 and 4.36).

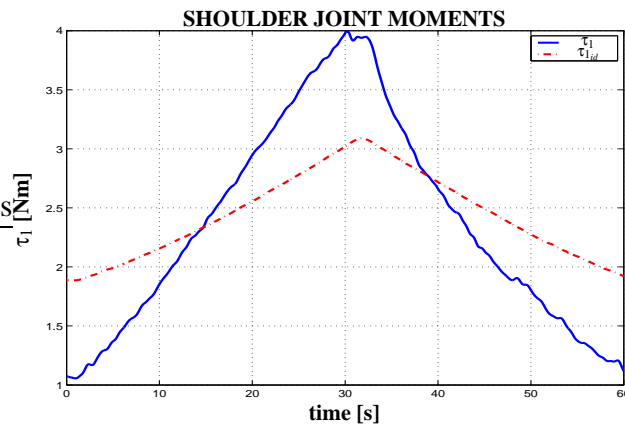


Figure 4.28: The upper extremity shoulder generalized torque τ_1 as measured (blue line) and the moment curve obtained as a result of the identification procedure $\tau_{1_{id}}$ (red line).

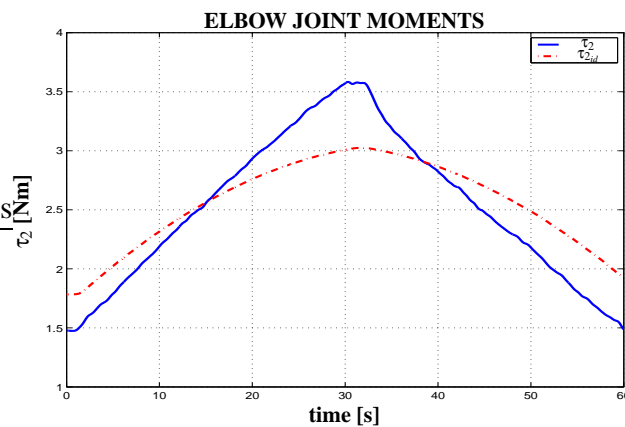


Figure 4.29: The upper extremity elbow moment τ_2 as measured (blue line) and the moment curve obtained as a result of the identification procedure $\tau_{2_{id}}$ (red line).

All numerical results are also given in tables 4.6, 4.7 and 4.8 respectively. The identified parameter values are again represented with \bar{x} as average values from 2 measurements. Despite the fact that we are dealing with a group of only 2 measurements we are also stating standard deviations (σ_x). Furthermore the value $\left(\frac{x_{ref} - \bar{x}}{\bar{x}}\right)$ denotes the differences in relative form.

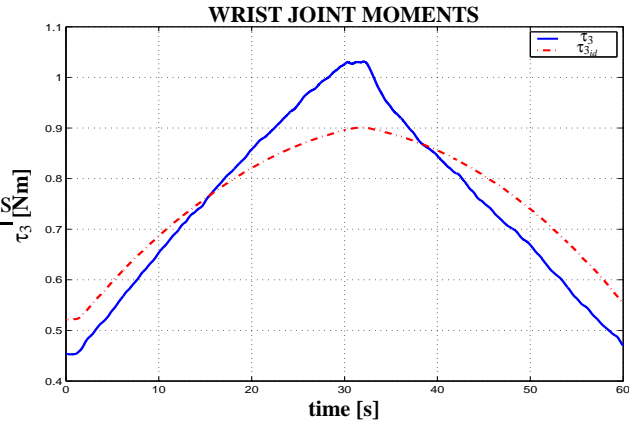


Figure 4.30: The upper extremity wrist moment τ_3 as measured (blue line) and the moment curve obtained as a result of the identification procedure $\tau_{3,id}$ (red line).

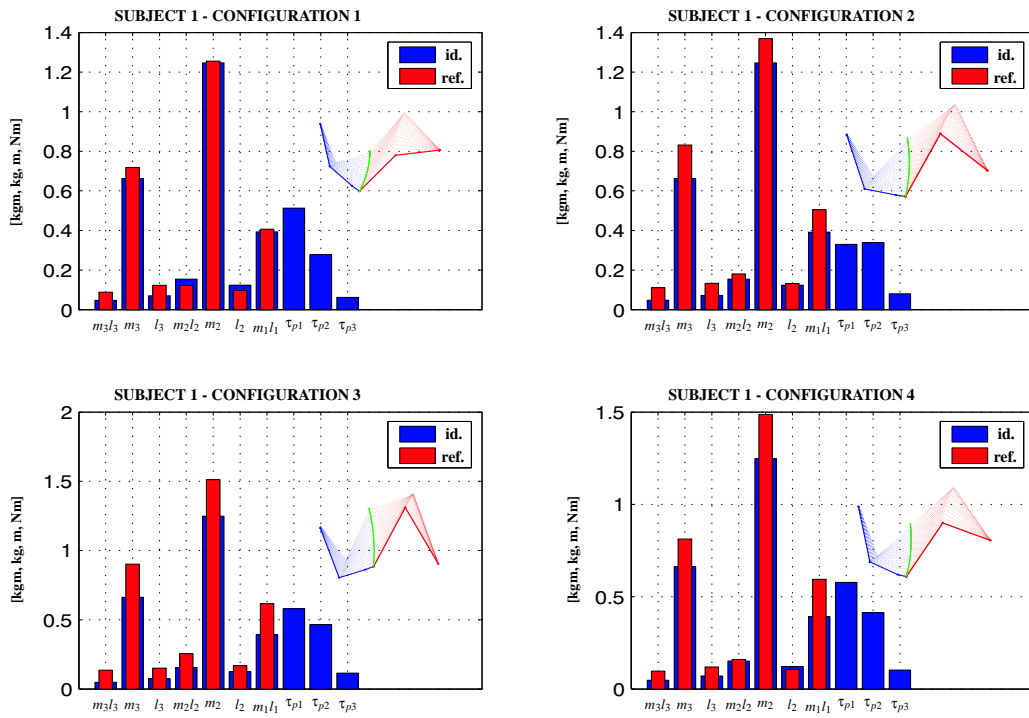


Figure 4.31: The comparison between reference parameters values taken from [81] and identified parameters for four different angular configuration in subject 1. The angular configurations are shown as a sketch in the upper right corner of every subplot. Blue bars show identified parameter values and the red ones the reference values. There are no reference values for passive moments because they could not be obtained from the literature.

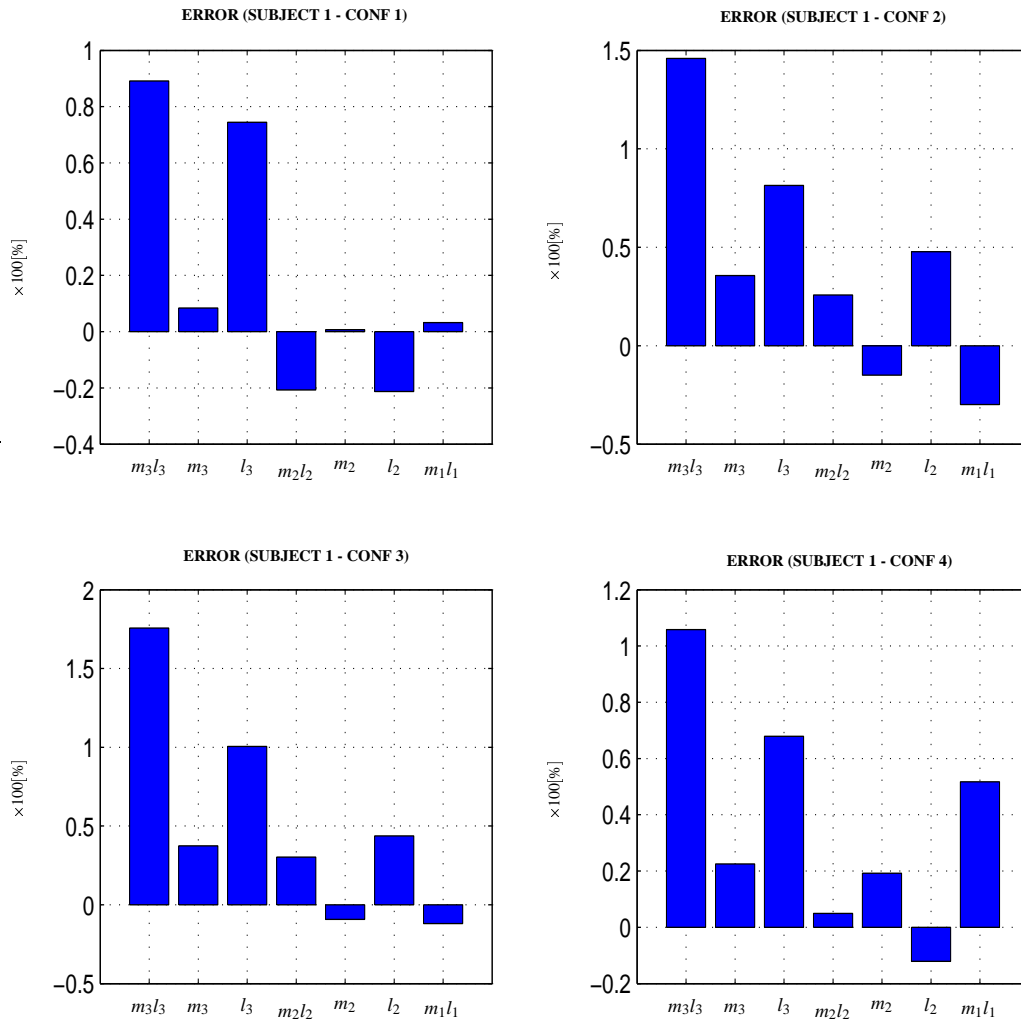


Figure 4.32: Relative errors for all identified parameters in figure 4.31.

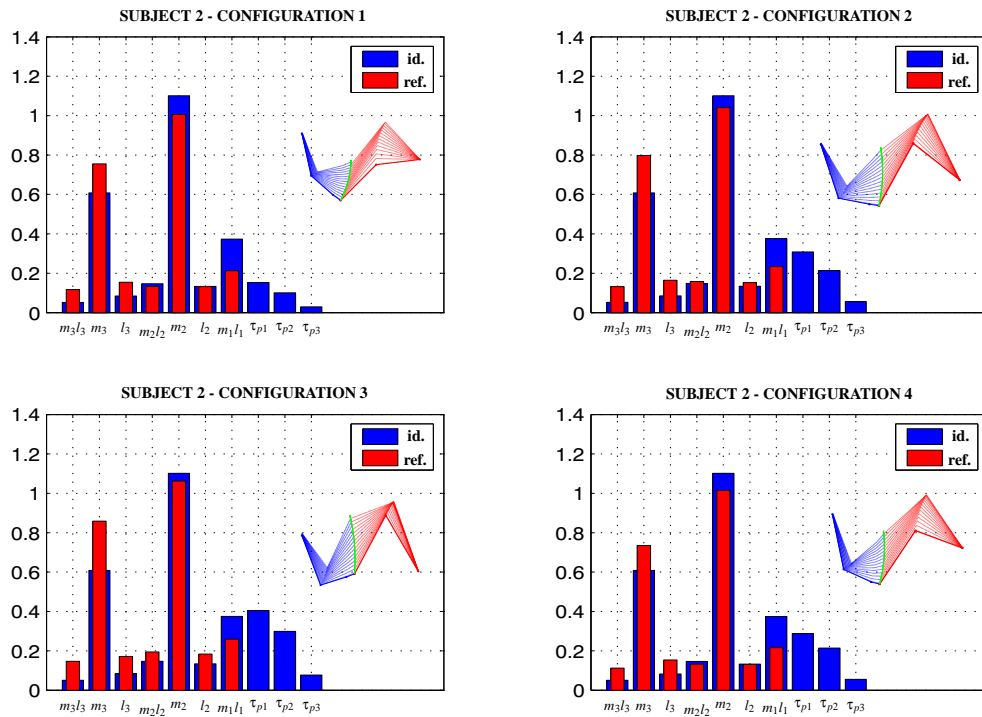


Figure 4.33: The comparison between reference parameters values taken from [81] and identified parameters for four different angular configuration in subject 2. The angular configurations are shown as a sketch in the upper right corner of every subplot. Blue bars show identified parameter values and the red ones the reference values. There are no reference values for passive moments because they could not be obtained from the literature.

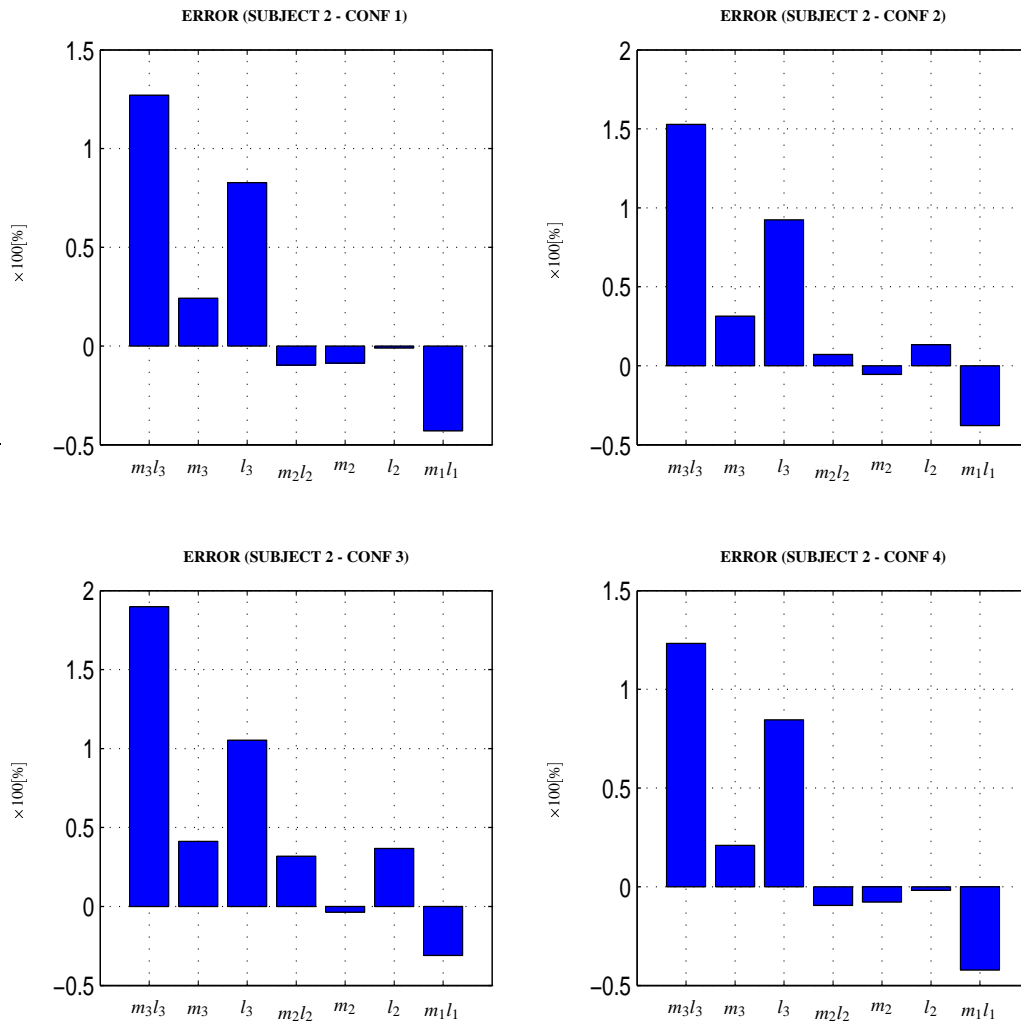


Figure 4.34: Relative errors for all identified parameters in figure 4.33.

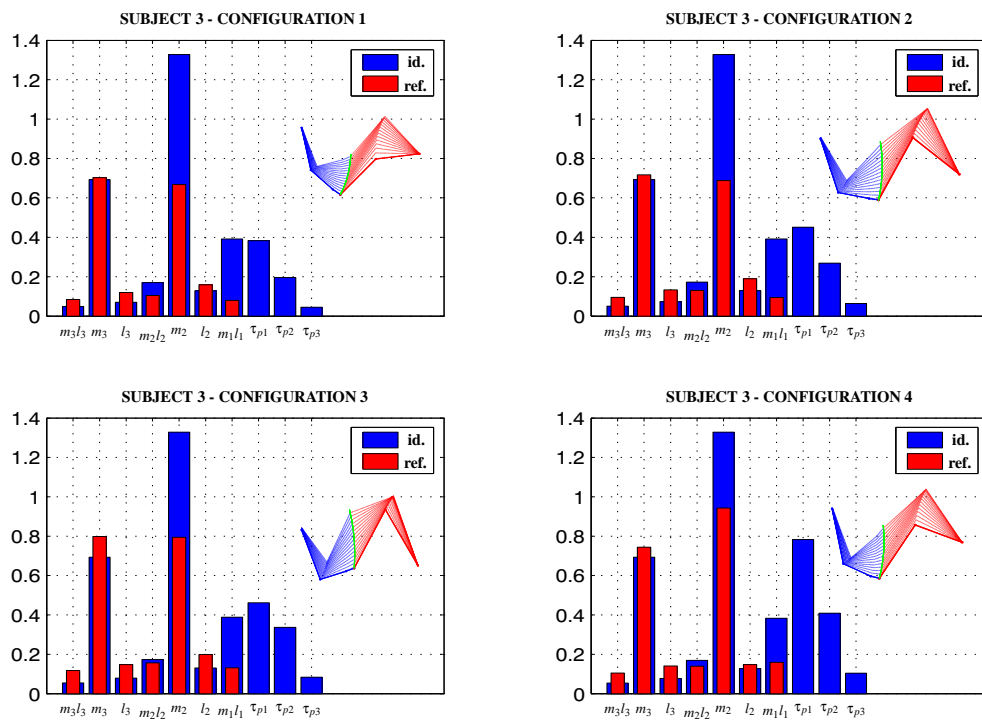


Figure 4.35: The comparison between reference parameters values taken from [81] and identified parameters for four different angular configuration in subject 3. The angular configurations are shown as a sketch in the upper right corner of every subplot. Blue bars show identified parameter values and the red ones the reference values. There are no reference values for passive moments because they could not be obtained from the literature

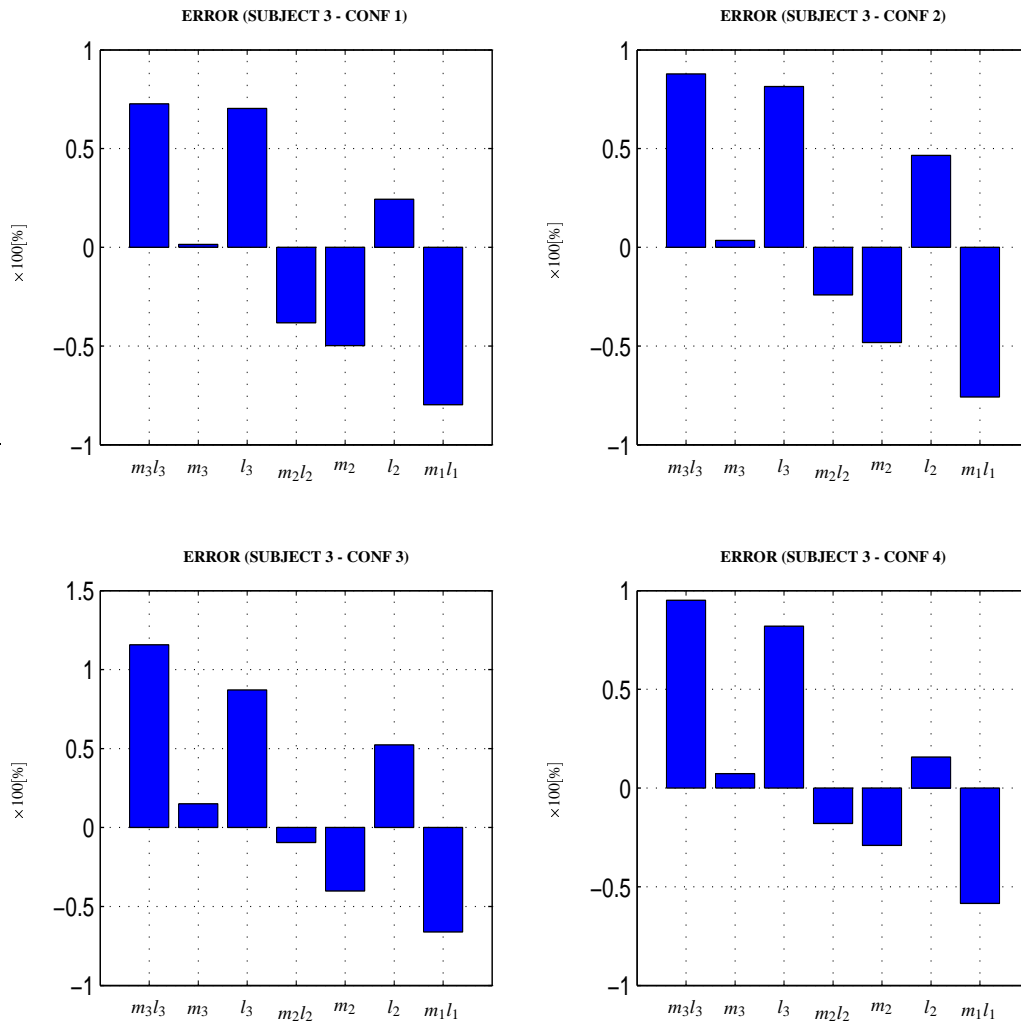


Figure 4.36: Relative errors for all identified parameters in figure 4.35.

Table 4.6: *Identified parameters obtained for subject 1. \bar{x} denotes the average values from 2 measurements. Measurement standard deviations are σ_x and differences in relative form $\left(\frac{x_{ref} - \bar{x}}{\bar{x}}\right)$.*

parameter	x_{ref}^a	\bar{x}	x_1 x_2	σ_x	$\frac{x_{ref} - \bar{x}}{\bar{x}}[\%]$	x_{ref}^a	\bar{x}	x_1 x_2	σ_x	$\frac{x_{ref} - \bar{x}}{\bar{x}}[\%]$
Configuration 1						Configuration 2				
$m_3 l_3$ [kgm]	0.047	0.088	0.086 0.090	0.002	89	0.047	0.111	0.104 0.117	0.009	133
m_3 [kg]	0.663	0.719	0.720 0.717	0.002	8	0.663	0.832	0.801 0.861	0.042	25
l_3 [m]	0.070	0.123	0.120 0.125	0.004	74	0.070	0.133	0.130 0.136	0.005	85
$m_2 l_2$ [kgm]	0.154	0.122	0.112 0.133	0.015	-21	0.154	0.180	0.160 0.201	0.012	1
m_2 [kg]	1.247	1.256	1.253 1.259	0.004	1	1.247	1.369	1.300 1.437	0.097	10
l_2 [m]	0.124	0.097	0.089 0.105	0.011	-21	0.124	0.132	0.123 0.140	0.012	6
$m_1 l_1$ [kgm]	0.393	0.406	0.404 0.408	0.003	3	0.393	0.505	0.451 0.558	0.076	29
τ_{p3} [Nm]	/	0.062	0.064 0.060	0.014	/	/	0.080	0.074 0.087	0.037	/
τ_{p2} [Nm]	/	0.277	0.287 0.268	0.014	/	/	0.339	0.313 0.365	0.037	/
τ_{p1} [Nm]	/	0.513	0.515 0.511	0.003	/	/	0.330	0.288 0.371	0.059	/
Configuration 3						Configuration 4				
$m_3 l_3$ [kgm]	0.047	0.136	0.138 0.135	0.002	180	0.047	0.097	0.093 0.102	0.006	106
m_3 [kg]	0.663	0.902	0.919 0.885	0.024	36	0.663	0.812	0.792 0.833	0.029	22
l_3 [m]	0.070	0.151	0.150 0.152	0.001	106	0.070	0.120	0.118 0.122	0.003	68
$m_2 l_2$ [kgm]	0.154	0.255	0.261 0.249	0.008	64	0.154	0.159	0.149 0.169	0.014	5
m_2 [kg]	1.247	1.511	1.547 1.476	0.051	21	1.247	1.487	1.436 1.538	0.072	19
l_2 [m]	0.124	0.169	0.169 0.169	0.000	35	0.124	0.107	0.104 0.110	0.004	-12
$m_1 l_1$ [kgm]	0.393	0.616	0.643 0.590	0.038	58	0.393	0.594	0.555 0.633	0.056	52
τ_{p3} [Nm]	/	0.115	0.117 0.112	0.023	/	/	0.103	0.107 0.099	0.036	/
τ_{p2} [Nm]	/	0.464	0.480 0.449	0.023	/	/	0.414	0.439 0.388	0.036	/
τ_{p1} [Nm]	/	0.579	0.673 0.485	0.133	/	/	0.578	0.653 0.503	0.106	/

^aTaken from the study of Zatsiorsky [21]

Table 4.7: Identified parameters obtained for subject 2. \bar{x} denotes the average values from 2 measurements. Measurement standard deviations are σ_x and differences in relative form $\left(\frac{x_{ref} - \bar{x}}{\bar{x}}\right)$.

parameter	x_{ref}^a	\bar{x}	$\begin{matrix} x_1 \\ x_2 \end{matrix}$	σ_x	$\frac{x_{ref} - \bar{x}}{\bar{x}}[\%]$	x_{ref}^a	\bar{x}	$\begin{matrix} x_1 \\ x_2 \end{matrix}$	σ_x	$\frac{x_{ref} - \bar{x}}{\bar{x}}[\%]$
Confi guration 1						Confi guration 2				
m_3l_3 [kgm]	0.051	0.117	$\begin{matrix} 0.117 \\ 0.117 \end{matrix}$	0.000	127	0.051	0.131	$\begin{matrix} 0.129 \\ 0.133 \end{matrix}$	0.002	153
m_3 [kg]	0.608	0.755	$\begin{matrix} 0.755 \\ 0.755 \end{matrix}$	0.000	24	0.608	0.798	$\begin{matrix} 0.794 \\ 0.803 \end{matrix}$	0.007	31
l_3 [m]	0.085	0.154	$\begin{matrix} 0.155 \\ 0.154 \end{matrix}$	0.000	83	0.085	0.164	$\begin{matrix} 0.163 \\ 0.165 \end{matrix}$	0.002	92
m_2l_2 [kgm]	0.147	0.132	$\begin{matrix} 0.133 \\ 0.132 \end{matrix}$	0.000	-10	0.147	0.158	$\begin{matrix} 0.155 \\ 0.161 \end{matrix}$	0.004	7
m_2 [kg]	1.102	1.006	$\begin{matrix} 1.004 \\ 1.009 \end{matrix}$	0.003	-9	1.102	1.041	$\begin{matrix} 1.027 \\ 1.056 \end{matrix}$	0.020	-5
l_2 [m]	0.133	0.132	$\begin{matrix} 0.132 \\ 0.131 \end{matrix}$	0.001	-1	0.133	0.152	$\begin{matrix} 0.151 \\ 0.152 \end{matrix}$	0.001	13
m_1l_1 [kgm]	0.373	0.213	$\begin{matrix} 0.208 \\ 0.217 \end{matrix}$	0.006	-43	0.373	0.233	$\begin{matrix} 0.221 \\ 0.246 \end{matrix}$	0.018	-38
τ_{p3} [Nm]	/	0.029	$\begin{matrix} 0.027 \\ 0.032 \end{matrix}$	0.003	/	/	0.056	$\begin{matrix} 0.047 \\ 0.064 \end{matrix}$	0.046	/
τ_{p2} [Nm]	/	0.101	$\begin{matrix} 0.099 \\ 0.103 \end{matrix}$	0.003	/	/	0.213	$\begin{matrix} 0.181 \\ 0.246 \end{matrix}$	0.046	/
τ_{p1} [Nm]	/	0.153	$\begin{matrix} 0.146 \\ 0.159 \end{matrix}$	0.009	/	/	0.308	$\begin{matrix} 0.252 \\ 0.365 \end{matrix}$	0.079	/
Confi guration 3						Confi guration 4				
m_3l_3 [kgm]	0.051	0.147	$\begin{matrix} 0.147 \\ 0.147 \end{matrix}$	0.000	90	0.051	0.113	$\begin{matrix} 0.112 \\ 0.113 \end{matrix}$	0.001	123
m_3 [kg]	0.608	0.858	$\begin{matrix} 0.859 \\ 0.857 \end{matrix}$	0.001	41	0.608	0.736	$\begin{matrix} 0.721 \\ 0.750 \end{matrix}$	0.021	21
l_3 [m]	0.085	0.171	$\begin{matrix} 0.171 \\ 0.172 \end{matrix}$	0.000	105	0.085	0.153	$\begin{matrix} 0.155 \\ 0.151 \end{matrix}$	0.003	85
m_2l_2 [kgm]	0.147	0.194	$\begin{matrix} 0.195 \\ 0.194 \end{matrix}$	0.001	32	0.147	0.133	$\begin{matrix} 0.135 \\ 0.130 \end{matrix}$	0.004	-9
m_2 [kg]	1.102	1.062	$\begin{matrix} 1.054 \\ 1.070 \end{matrix}$	0.010	-4	1.102	1.015	$\begin{matrix} 1.008 \\ 1.023 \end{matrix}$	0.011	-8
l_2 [m]	0.133	0.183	$\begin{matrix} 0.185 \\ 0.181 \end{matrix}$	0.003	37	0.133	0.131	$\begin{matrix} 0.134 \\ 0.127 \end{matrix}$	0.005	-2
m_1l_1 [kgm]	0.373	0.259	$\begin{matrix} 0.247 \\ 0.270 \end{matrix}$	0.016	-31	0.373	0.216	$\begin{matrix} 0.216 \\ 0.217 \end{matrix}$	0.001	-42
τ_{p3} [Nm]	/	0.077	$\begin{matrix} 0.073 \\ 0.081 \end{matrix}$	0.015	/	/	0.055	$\begin{matrix} 0.057 \\ 0.053 \end{matrix}$	0.009	/
τ_{p2} [Nm]	/	0.299	$\begin{matrix} 0.288 \\ 0.309 \end{matrix}$	0.015	/	/	0.214	$\begin{matrix} 0.221 \\ 0.208 \end{matrix}$	0.009	/
τ_{p1} [Nm]	/	0.404	$\begin{matrix} 0.367 \\ 0.442 \end{matrix}$	0.053	/	/	0.288	$\begin{matrix} 0.304 \\ 0.272 \end{matrix}$	0.022	/

^aTaken from the study of Zatsiorsky [21]

Table 4.8: *Identified parameters obtained for subject 3. \bar{x} denotes the average values from 2 measurements. Measurement standard deviations are σ_x and differences in relative form $\left(\frac{x_{ref} - \bar{x}}{\bar{x}}\right)$.*

parameter	x_{ref}^a	\bar{x}	x_1 x_2	σ_x	$\frac{x_{ref} - \bar{x}}{\bar{x}}[\%]$	x_{ref}^a	\bar{x}	x_1 x_2	σ_x	$\frac{x_{ref} - \bar{x}}{\bar{x}}[\%]$
Configuration 1						Configuration 2				
$m_3 l_3$ [kgm]	0.049	0.084	0.086 0.083	0.002	72	0.049	0.096	0.094 0.097	0.002	88
m_3 [kg]	0.693	0.703	0.706 0.701	0.004	1	0.693	0.718	0.716 0.719	0.002	3
l_3 [m]	0.075	0.120	0.121 0.118	0.002	70	0.075	0.133	0.131 0.135	0.003	81
$m_2 l_2$ [kgm]	0.170	0.105	0.110 0.100	0.007	-38	0.170	0.130	0.128 0.133	0.004	-24
m_2 [kg]	1.328	0.667	0.758 0.577	0.128	-50	1.328	0.688	0.659 0.717	0.041	-48
l_2 [m]	0.128	0.159	0.145 0.173	0.020	24	0.128	0.190	0.194 0.188	0.006	47
$m_1 l_1$ [kgm]	0.391	0.079	0.099 0.060	0.028	-80	0.391	0.095	0.092 0.097	0.004	-76
τ_{p3} [Nm]	/	0.045	0.052 0.037	0.049	/	/	0.064	0.053 0.076	0.066	/
τ_{p2} [Nm]	/	0.196	0.230 0.162	0.049	/	/	0.269	0.222 0.316	0.066	/
τ_{p1} [Nm]	/	0.383	0.474 0.291	0.130	/	/	0.451	0.319 0.583	0.186	/
Configuration 3						Configuration 4				
$m_3 l_3$ [kgm]	0.049	0.118	0.109 0.128	0.013	116	0.049	0.105	0.104 0.106	0.002	95
m_3 [kg]	0.693	0.798	0.776 0.820	0.031	15	0.693	0.744	0.723 0.764	0.029	7
l_3 [m]	0.075	0.148	0.140 0.156	0.011	87	0.075	0.141	0.143 0.139	0.003	82
$m_2 l_2$ [kgm]	0.170	0.157	0.144 0.170	0.018	-9	0.170	0.139	0.141 0.138	0.002	-18
m_2 [kg]	1.328	0.794	0.691 0.898	0.146	-40	1.328	0.943	0.925 0.961	0.025	-29
l_2 [m]	0.128	0.199	0.208 0.189	0.013	52	0.128	0.148	0.152 0.143	0.006	16
$m_1 l_1$ [kgm]	0.391	0.132	0.107 0.156	0.035	-66	0.391	0.159	0.157 0.161	0.003	-58
τ_{p3} [Nm]	/	0.084	0.077 0.091	0.038	/	/	0.104	0.099 0.109	0.025	/
τ_{p2} [Nm]	/	0.338	0.311 0.364	0.038	/	/	0.409	0.391 0.427	0.025	/
τ_{p1} [Nm]	/	0.462	0.465 0.459	0.004	/	/	0.783	0.791 0.774	0.012	/

^aTaken from the study of Zatsiorsky [21]

4.2.3 Discussion of obtained results

The proposed identification method enables a simultaneous computation of some upper extremity body segment parameters based on one single experimental trial. Because the experiment was carried out quasi-statically we did not focus into those parameters which have no effect on the upper extremity at lower velocities. The method is friendly from the subjects point of view as it does not require any special fixation mechanisms and can be performed very quickly. In fact the results can be computed almost immediately after a movement is completed.

It should be emphasized that this technique was developed with having in mind that this parameter estimation method could also be used in future rehabilitation practice. These parameters would be determined for a particular person in one configuration on a particular day just as we have shown in our study. The parameter values could be tracked for the same subject vs. time as a diagnostic tool that provides online insight into mechanic properties while the patients could primarily be doing their occupational task which is exercise. Apart from this the obtained parameter values could also be used in biomechanical modelling studies.

The accuracy of the method can be deduced from the results obtained on the mechanical arm experiment as seen from tables 4.4 and 4.5 and bar plots 4.24 and 4.26. The highest error rate of just under 80% can be observed for parameter τ_{p1} in the case when there was no braking, meaning at discardable passive moments in joints. Since the passive moment was almost zero in this case, we should not see this seemingly bad result as important. The significant error levels however are those seen from the mechanical arm with activated brakes (table 4.5 and figure 4.24). The highest error levels here are around 10% for parameters τ_{p2} and l_2 . We attribute these errors mostly to a non-ideal mechanical model. The explanation for errors in the mechanical model passive properties τ_{p1} and τ_{p2} can be that they are not only brake produced but arise also from small mechanical jitter and non ideal bearings. It should be noted, however that this is not the only source of error.

Measurement error analysis is a complex issue since we need to account for errors in every measured quantity such as contact force measurements and angle measurements. Apart from this the identification for inner segments in the second or third identification step (equations 5.6 and 5.1) also imparts errors made in the previous steps of the process (For mathematical proof of this fact see Appendix A).

The human arm parameter errors were given in relation to literature estimates which can not be viewed as an objective source since the errors there are of unpredictable nature. Among the reasons contributing to errors in the human arm parameter estimates we speculate that the most important ones arise as a consequence of the rigid segment and axial rotation assumptions (see figure 3.4.1) and the fact that the study of Zatsiorsky [21] was done for general population whereas

this study estimates parameters individually. Unlike in our assumption the real human arm is not composed of rigid bodies and has more DOF than just one single rotation in every joint [11, 13, 32]. The other important error source can be attributed to inaccuracies in the measurement of joint angles and contact forces which can roughly be deduced from standard deviations in figure 4.27. This also comes as a result of larger standard deviations of forces \mathbf{F}_{end} and generalized joint torques τ_j seen from figure 4.27. While joint angle errors can be explained by an inaccurate marker fixation, contact force errors on the other hand come as a result of worse repeatability of human arm trajectories in comparison to the model.

A good indicator of the identification method accuracy is also the observation of the identified joint passive moments τ_{pjid} in comparison to the measured values τ_{pjref} in the mechanical model. These can be observed in figures 4.19 and 4.20 for the case when brakes are not attached and figures 4.21 and 4.22 when braking is activated. The difference between the identified and the reference values comes as a result of the fact that τ_{pjid} is subject to noise from both the angle (\mathbf{q}) measurements and end force data \mathbf{F}_{end} as seen from equations 3.25 and 5.6. The other reason contributing to this difference is also the non-ideal mechanical model. As a contrary to τ_{pjid} the quantity τ_{pjref} is being directly measured and is therefore only a subject to load cell noise. A similar error source can also be seen as an explanation of differences in the human joint generalized torque curve τ_j as seen in figures 4.28, 4.29 and 4.30. In this case the differences between the real arm and the presumed mathematical model are even larger than with the mechanical model explaining larger errors.

When observing identified parameter errors for all three healthy subjects in bar plots 4.31 to 4.35 and tables 4.6 to 4.8 we can see that their general trend (blue bars) correlates with the reference values (red bars) obtained from the literature. Some parameters obviously show larger relative errors which could be contributed to the inaccuracies in the measurement process. This is particularly true for subject 3 in table 4.8 and figure 4.35. We are stating the standard deviations σ_x despite the fact being aware of the fact that low number of measurements (2) is too small for any serious statistical analysis. Nevertheless we think that this parameter still gives some insight into the difference between values of particular measurement x_1 and x_2 .

Every particular configuration of the same subject obviously gives slightly different results. This did not come as a surprise because of nonlinearities in passive moments which have already been observed in figures 4.11 through 4.16 of section 4.1. Every different angular configuration therefore implies a different passive moment value which was proven in section 4.1. Passive moment references were not given since they could not be reliably obtained from any available study. Their values severely depend on the anatomical structure of the upper extremity which is very subject-dependent.

4.3 Simulation

As we have already explained in section 3.6 we have developed a simulation in Matlab-Simulink for the purpose of calculating the required robot joint trajectory \mathbf{q}_r (see figure 3.13). Apart from this the simulation also enabled testing prior to the experiment in order to get an insight into kinematic and dynamic variables.

This section will try to present some results of the developed simulation, especially from the point of view of comparing the results to those obtained in the experimental measurements. As already explained in figure 3.15 many simulation parameters had to be set prior to running the simulation. The crucial ones were undoubtedly those which determined the kinematics and dynamics of the arm and are presented in tables 4.9 and 4.10. The mechanical arm parameters were again taken from the CAD model while those of the upper extremity were taken from measuring segment lengths and from the literature [81]. Only the parameters which were important to our study are shown below.

Table 4.9: *The kinematic and dynamic parameters of the 2DOF mechanical arm mechanism.*

parameter name	upper arm	lower arm
a_1 [m]	0.376	0.239
l_1 [m]	0.184	0.115
m_1 [kg]	1.440	1.160

Table 4.10: *The kinematic and dynamic parameters for the upper extremity of the first tested subject as obtained from regression curves.*

parameter name	upper arm	lower arm	hand
a_1 [m]	0.322	0.264	0.093
l_1 [m]	0.186	0.121	0.081
m_1 [kg]	2.114	1.264	0.753

The robot kinematics parameters were set as $Ra_1 = Ra_2 = 0.45$ m. The initial arm position $\mathbf{q}(\mathbf{0})$ was taken as the first point of the joint desired vector \mathbf{q}_d (figure 3.13). This trajectory was created by integrating a trapezoidal velocity profile. The velocity levels and the gradients (accelerations) of the trapezoidal trajectory were set to a desired value. This produced a very smooth second order, continuous joint angle trajectory which could easily be executed by the robot manipulator. The relative offset between the fixed points of both manipulators was measured in

the experimental setup (figure 3.15). In order to obtain simulation results which would be as realistic as possible we also had to properly set other parameters from block diagram 3.13. They were set in the following way:

parameter	description	size	value	comment
\mathbf{S} [N/m]	<i>contact stiffness</i>	6×6	10000	<i>2 diagonal elements</i>
\mathbf{K}_v [Nms/rad]	<i>arm joint viscosity</i>	$n \times n$	-0.2	<i>diagonal matrix</i>
\mathbf{K}_e [Nm/rad]	<i>arm joint elasticity</i>	$n \times n$	0.5	<i>diagonal matrix</i>
\mathbf{K}_d [Nm]	<i>arm joint Coulomb friction</i>	$n \times n$	0	<i>diagonal matrix</i>

The variable n denotes the DOF number of the arm which was either 2 for the mechanical model or 3 for the upper extremity. The contact point stiffness was only set for the horizontal and vertical directions because we assumed a fully planar model. In order to obtain stable simulation results the arm joint damping parameters in \mathbf{K}_D also had to be non zero. The Coulomb frictions were set to zero for testing purposes.

To get an insight into the quality of the simulation results, figures 4.38 and 4.39 give a comparison between the joint angles \mathbf{q} and contact forces \mathbf{F}_{end} for the mechanical model. Figure 4.37 gives a stick figure animation of the particular movement trajectory under which the comparison was performed.

Figures 4.40 and 4.41 give a comparison between the simulation and measurement results for the human upper extremity.

4.3.1 Discussion of obtained results

As we have already explained in section 3.6 the primary purpose of the simulation was the calculation of the robot joint angle vector \mathbf{q}_r under which the arm would follow the desired joint trajectory \mathbf{q}_d . The simulation quality was indicated by only presenting the results obtained on the mechanical model. The comparison between the mechanical model force and kinematic data from figures 4.38 and 4.39 shows reasonable correlation. The observed offset is a consequence of the fact that the mathematical model doesn't completely match the real system. The discrepancy is most likely a result of some unknown components in the simulation which are not accounted for in the simulation model. It needs to be emphasized that the simulation results depended very much upon the values of simulation parameters in table 4.3. The contact stiffness \mathbf{S} was set to a high value to account to a relatively stiff contact between the end points of the arm and robot. The stiffness is in reality determined by the contact material. The fact that the contact was made by using a steel screw explains the high stiffness level. Other parameters

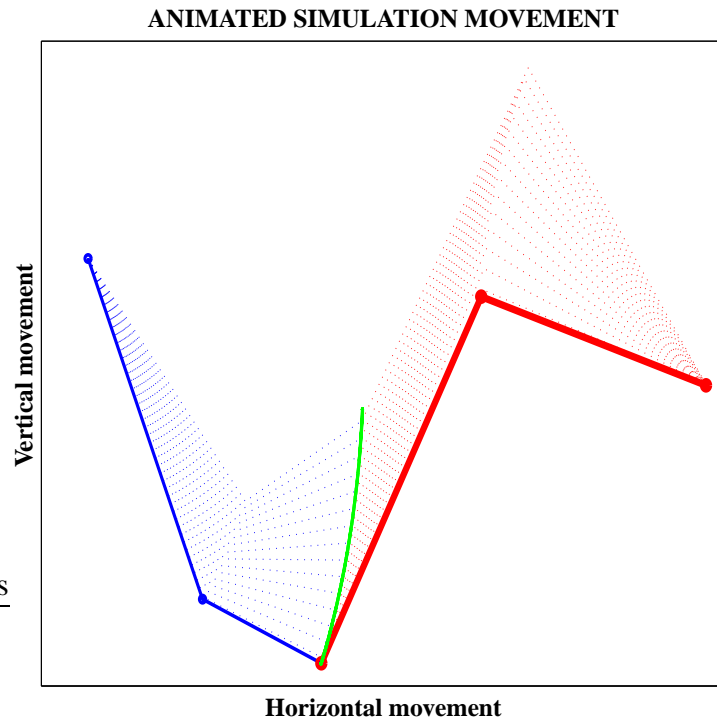


Figure 4.37: A stick figure animation showing the simulation results for the mechanical model arm movement.

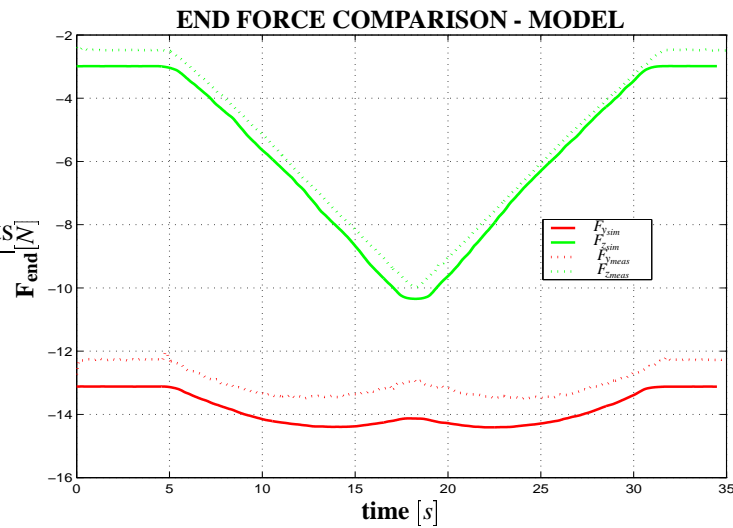


Figure 4.38: The comparison of contact forces between the simulation ($F_{y_{sim}}$ and $F_{z_{sim}}$) and the measurements ($F_{y_{meas}}$ and $F_{z_{meas}}$) made on the mechanical arm.

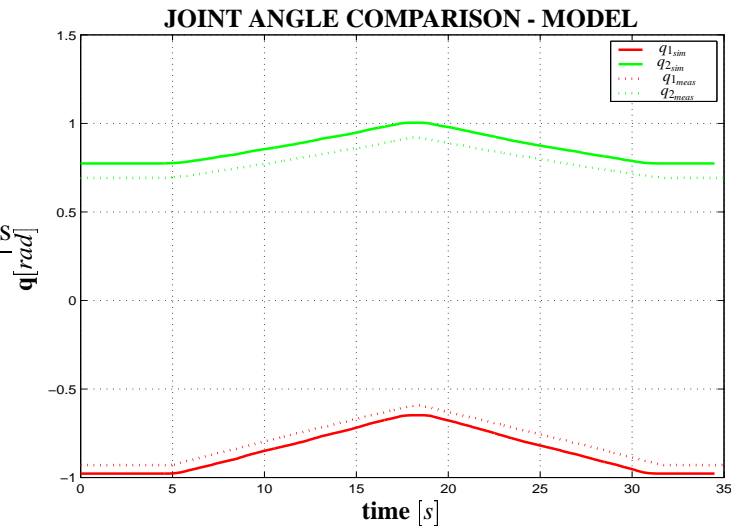


Figure 4.39: The comparison of joint angles between the simulation (q_{1_sim} and q_{2_sim}) and the measurements (q_{1_meas} and q_{2_meas}) made on the mechanical arm.

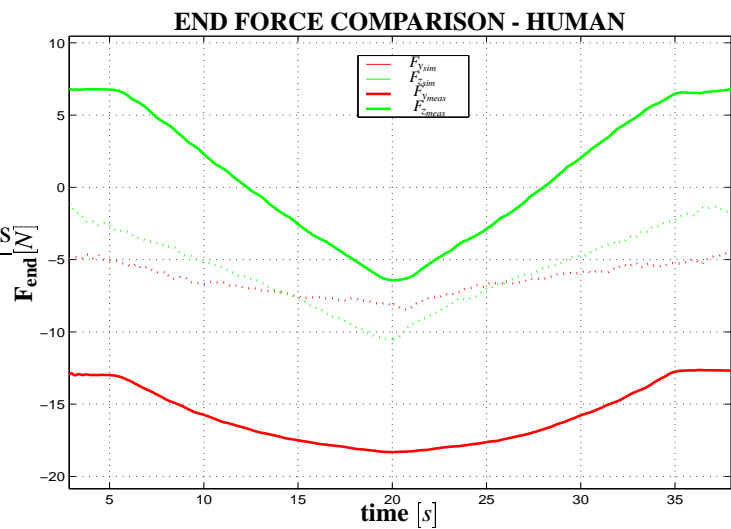


Figure 4.40: The comparison of contact forces between the simulation (F_{y_sim} and F_{z_sim}) and the measurements (F_{y_meas} and F_{z_meas}) as observed on the real human arm.

from table 4.3 were also determined in a way which gave best results. Due to simulation stability reasons the joint damping parameters in \mathbf{K}_D had to be set to a certain value despite the fact that they were discarded throughout the whole course of our study.

When observing the simulation results of the upper extremity the results were not as comparable as those of the mechanical arm (figures 4.40 and 4.41). The

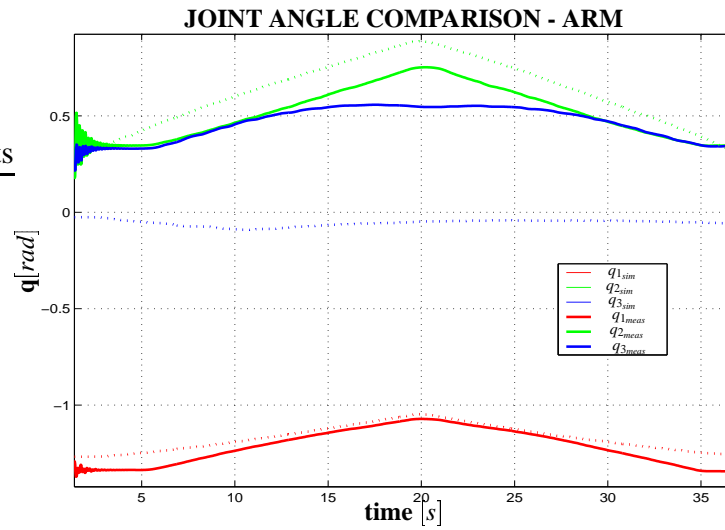


Figure 4.41: *The comparison of joint angles between the simulation (q_{1_sim} and q_{2_sim}) and the measurements (q_{1_meas} and q_{2_meas}) observed on the real human arm.*

largest differences were encountered in the contact forces \mathbf{F}_{end} whereas the angles followed the reference values much better. The results could have been substantially improved by tuning the parameters but this was not done since this was not our primary goal.

Chapter 5

Conclusion

In this work we have tried to present some novel approaches for evaluating joint properties and body segment parameters in the upper extremity. Such evaluation has become increasingly important in the last decade when technological progress made new robotic rehabilitation treatment devices available for more than only research purposes. There has been growing interest in developing such devices, especially due to ageing population bringing various medical indications which increase the demand for upper extremity rehabilitation treatment. The very promising robotic treatment devices are *haptic robots* which allow human-machine interaction by means of force and touch.

Therefore the experimental evaluations presented in this work should be viewed primarily *from the rehabilitation point of view* where they could represent an inherent measurement module while the patient would normally and automatically go through during the exercise process. In many ways these new robotic treatment devices and evaluation methods could serve as an assistance to physiotherapists. On the other hand, the measurements experiments performed in this work could be important in the *field of upper extremity biomechanics*.

In the work we have assumed that measurements such as contact forces and joint angles would be available when dealing with robotic treatment devices. The work is composed of three parts where the first two present two new methods for upper extremity evaluation whereas the third deals with the simulation application which has been developed in order to simulate the executed experiments.

Firstly we tried to determine the nature of *upper extremity joint passive moments* while assuming other biomechanical parameters such as masses and COGs from the literature. The parameters were determined when the shoulder and elbow flexion-extension angles were fixed at ten different angles while the unfixed joint was allowed to slowly move through a wide portion of its range, following the programmed robot trajectory. The method for determining passive moments was derived from the inverse dynamic equation for the assumed planar arm. Com-

paring the obtained passive moments of six young male subjects unequivocally showed that there was a large non-linear adjacent angle dependency.

The second experimental phase focused on *identifying all BSPs* which determine upper extremity motion at low speed. Again, the upper extremity was guided through a specified trajectory while measuring angle data and contact forces. A suitable low velocity trajectory was imposed into all joints, with very small angular deviations. The arm was assumed to be linear within a small angular region. The results were compared to the literature estimates which are based on average population. An optimization based identification procedure was developed, which assumes the upper extremity model of a 3DOF rigid body planar structure in a closed kinematic chain configuration with the robot. The solution is based on fitting the joint torques calculated from contact forces to those predicted by the inverse dynamic model of the linkage. In order to verify the proposed identification procedure the experiment was first performed on a *2DOF mechanical arm* with dimensions similar to those of the actual arm. The obtained results showed good correlation to the literature studies.

Thirdly a simulation of the whole experimental setup was performed with Matlab[®]-Simulink. This gave better insight into the experimental quantities and allowed us to gain much more control over the experiment. The simulation environment allowed an observation of all kinematic data such as joint angles, angular velocities and angular accelerations on one side and dynamic quantities such as joint torques and contact forces on the other. It can be concluded that the results of the simulation gave comparable results to those from the measurement.

5.1 Ideas for future work

Finally it can be concluded that this work undoubtedly presents some new approaches in evaluating the upper extremity internal characteristics. The results may gain a lot of importance in future rehabilitation which will undoubtedly be done with more assistance of robotic devices than is the case today. Apart from this fact this work opens a whole new range of possibilities for future research related to the upper extremity and BSP estimation. Some of the most important ones will be summed up in the following points:

- It would be very interesting to make a comprehensive BSP estimation study presented in this thesis in a study which would include a large test group of subjects. This would give the true quality of the developed method since it could place it into a realistic context with existing parameter estimation methods. Unlike existing BSP estimation methods this study could include a much larger test group due to its simplicity and open new possibilities for estimating BSPs of individuals in the future.

- The downside of the presented BSP estimation method is clearly the fact that segment moments of inertia I_j were not estimated whereas most other studies determined these as well. In our opinion the presented study could also be used in moments of inertia estimation. It would then require a more complicated arm movement trajectory \mathbf{q}_a from figure 3.8 which would impart a certain acceleration diversity.
- A comprehensive study of joint properties, especially passive moments could indicate their relation of various factors such as age, different physical fitness or various neuromuscular disorders. Unlike existing single joint measurement techniques [25,26] which are routinely used in rehabilitation practice nowadays our method suggests that these parameters could be obtained during a certain functional exercise.
- In order to experimentally prove the usefulness of the presented method in rehabilitation practice a study on a number of patients with neurological impairments would need to be done in the future. In this way we could prove the fact that the joint properties change with the progressing of rehabilitation therapy as we have suggested in the thesis. Nevertheless, we need to be aware of the fact that joint properties can be severely affected by spasticity, tremor or other factors accompanying neurological diseases. We speculate that even in these cases our method would enable the quantification of these particular effects which could prove to be very interesting.

List of symbols and abbreviations

\mathbf{F}_{end}	Vector of contact forces and moments
F_y	Horizontal contact force component
F_z	Vertical contact force component
M_x	Contact torque around x axis (perpendicular to the motion plane)
$F_{y\text{meas}}$	Measured horizontal force
$F_{z\text{meas}}$	Measured vertical force
$F_{y\text{sim}}$	Simulated horizontal force
j	Joint or segment index
\mathbf{q}	Joint angle vector
$\dot{\mathbf{q}}$	Joint velocity vector
$\ddot{\mathbf{q}}$	Joint acceleration vector
$\mathbf{q}(\mathbf{0})$	Initial arm joint angle condition vector
$\dot{\mathbf{q}}(\mathbf{0})$	Initial arm joint angular velocity condition
\mathbf{q}_j	Upper extremity joint angle trajectory
$\dot{\mathbf{q}}_j$	Upper extremity joint velocity trajectory
$\ddot{\mathbf{q}}_j$	Upper extremity joint acceleration trajectory
\mathbf{q}_d	Desired upper extremity joint trajectory
\mathbf{q}_r	Required robot joint angle trajectory
q_{rj}	Robot joint angle in joint j
$\dot{\mathbf{q}}_r$	Robot joint velocity trajectory
$\ddot{\mathbf{q}}_r$	Required robot joint acceleration trajectory
a_j	Segment length
$a_{j\text{ref}}$	Segment j reference length
Ra_j	Robot segment j length
m_j	Segment mass
$m_{j\text{ref}}$	Segment j reference mass
l_j	Segment center of gravity (COG) location
$l_{j\text{ref}}$	Segment j reference COG
l_{hand}	Hand center of gravity location
l_{handle}	Rotating handle center of gravity location
m_{fa}	Forearm mass
m_{lo}	Lower orthosis part mass
m_{ua}	Upper arm mass
m_{uo}	Upper orthosis part mass
m_{hand}	Hand mass
m_{handle}	Mass of rotating handle
$\mathbf{B}(\mathbf{q})$	Inertia matrix
b_{jj}	Coefficient in row j and column k of the inertia matrix $B(\mathbf{q})$

$\mathbf{C}(\mathbf{q}, \dot{\mathbf{q}})$	Coriolis matrix
c_{ij}	Coefficients in row i and column j of the Coriolis-centrifugal matrix $C(q, \dot{q})$
$\mathbf{G}(\mathbf{q})$	gravity vector
g_0	Gravity acceleration constant (9.81 m/s ²)
$\tau_{\mathbf{B}}(\ddot{\mathbf{q}})$	Inertial joint torque contribution vector
τ_{bj}	Inertial torque contribution in joint j
$\tau_{\mathbf{C}}(\mathbf{q}\dot{\mathbf{q}})$	Coriolis-centrifugal joint torque vector
τ_{cj}	Coriolis-centrifugal torque contribution in joint j
$\tau_{\mathbf{G}}(\mathbf{q})$	Gravity torque vector
τ_{gj}	Gravity torque contribution in joint j
$\tau_{\mathbf{v}}(\dot{\mathbf{q}}, \mathbf{q}, \mathbf{u})$	Viscous torque vector
τ_{vj}	Viscous torque contribution in joint j
$\tau_{\mathbf{d}}(\text{sgn}(\dot{\mathbf{q}}), \mathbf{q}, \mathbf{u})$	Dissipative torque vector
τ_{dj}	Dissipative torque contribution in joint j
$\tau_{\mathbf{e}}(\mathbf{q}, \mathbf{u})$	Elastic torque vector
τ_{ej}	Elastic torque contribution in joint j
τ_{end}	Joint torques due to contact force
τ_{end_j}	Joint torques due to contact force in joint j
τ_{ve}	The sum of all viscoelastic contributions
τ_j	Generalized joint j torque (the right side of equations 3.25-5.1)
$\tau_{\mathbf{p}}$	Passive moment vector
τ_{pj}	Passive moment in joint j
$\tau_{pj_{ref}}$	Segment j reference passive moment value
$\bar{\tau}_{\mathbf{p}}$	Average passive moment vector
$\tau(\mathbf{u})$	Voluntary muscle torque
\mathbf{u}	Muscle activation vector
τ_{jid}	Identified joint j generalized torque
τ_{pjid}	Identified passive moment in joint j
σ_{max}	Maximum standard deviation
x_{ref}	Reference parameter value
\bar{x}	Average parameter value
x_i	Parameter value in measurement i
\mathbf{m}	Optotrak marker data
\mathbf{L}	Mechanical model load cell data
\mathbf{v}	Robot motor voltage reference
\mathbf{i}	Robot motor current
$\mathbf{K}_{\mathbf{d}}$	Dissipative coefficient matrix
$\mathbf{K}_{\mathbf{e}}$	Elastic coefficient matrix
$\mathbf{K}_{\mathbf{v}}$	Viscous coefficient matrix
$\mathbf{J}^T(\mathbf{q})$	Jacobian matrix transpose
I_j	Transversal (perpendicular to motion plane) inertial tensor of segment j
c_{123}	Denoting $\cos(q_1 + q_2 + q_3)$
s_{123}	Denoting $\sin(q_1 + q_2 + q_3)$
\mathbf{Y}_j	Segment j regressor matrix
π_j	Segment j identification vector
$\pi_{j_{ref}}$	Segment j reference identification vector

$F_{t_i}(\pi_j)$	Optimization function
N	Number of time samples
t_i	A certain time sample
\mathbf{u}_b	Upper optimization boundary
\mathbf{u}_l	Lower optimization boundary
$\mathbf{T}_A(\dots)$	Forward arm kinematics
$\mathbf{T}_R^{-1}(\dots)$	Robot inverse kinematics
$\mathbf{D}(\dots)$	Forward arm dynamics
\mathbf{S}	Contact stiffness matrix
\mathbf{x}_d	Desired contact point trajectory vector
\mathbf{x}	Actual contact point trajectory vector
$\Delta\mathbf{x}$	Error in contact point trajectory vector
$F_{z_{sim}}$	Simulated vertical force
$q_{j_{meas}}$	Measured joint j angle
$q_{j_{sim}}$	Simulated joint j angle

BSP	Body Segment Parameters
CAD	Computer Aided Design
CNS	Central Nervous System
COG	Centre Of Gravity
CT	Computer Tomography
DOF	Degrees Of Freedom
EMG	Electro-Mio-Gram
IR	Infra-Red
MRI	Magnetic Resonance Imaging
PCSA	Psychological Cross Sectional Area

Bibliography

- [1] E. Harless, "The static moments of human limbs," *Treatises of the Math-Phys Class of the Royal Acad Of Sc Of Bavaria*, vol. 8, pp. 257–294, 1860.
- [2] T. Bajd, A. Kralj, and R. Turk, "Standing-up of a healthy subject and a paraplegic patient," *Journal of Biomechanics*, vol. 15, pp. 1–10, 1982.
- [3] T. Karčnik, "Stability in legged locomotion," *Biological Cybernetics*, vol. 90, pp. 51–58, 2004.
- [4] Aristoteles, *De partibus animalum, 340 b.c., translated by D.M. Balme, De partibus animalium I and De generatione animalium I (wit passages from II. 1–3)*, Oxford. Clarendon Press, 1992.
- [5] P. van de Hel, B. Diressen, M. Oderwald, S. Coote, and E. Stokes, "Gentle/s robot mediated therapy for stroke patients in a virtual world makes exercising more enjoyable and effective," *Proceedings of AAATE 2001*, pp. 256–61, 2001.
- [6] M. Ponikvar, *Analiza trajektorij gibanja roke v haptičnem okolju (eng. - An analysis of arm motion trajectories in a haptic environment) - (in Slovene)*. PhD thesis, University of Ljubljana, Faculty of Electrical Engineering, Slovenia, 2003.
- [7] A. Bardorfer, *Haptični vmesnik pri kvantitativnem vrednotenju funkcionalnega stanja gornjih Ekstremitet (eng. - Using a haptic interface with quantitative evaluation of the functional condition in upper extremities) - (in Slovene)*. PhD thesis, University of Ljubljana, Faculty of Electrical Engineering, Slovenia, 2003.
- [8] H. Krebs and N. H. *et al.*, "Robot-aided neuro-rehabilitation," *IEEE Transaction on Rehabilitation Engineering*, vol. 6/1, pp. 75–87, 1998.
- [9] "Reharob project, deliverable 7 - report - analysis of the upper limb motion, impairments, and the motion therapies used and improvements proposed for the impairment rehabilitation," Tech. Rep. IST-1999-13109, 2000.

- [10] D. Popović and T. S. r, *Control of movement for the physically disabled*. Springer Verlag, 2000.
- [11] V. Zatsiorsky, *Kinematics of human motion*. Human Kinetics, 1998.
- [12] T. Iberall, "Human prehension and dexterous robot hands," *The International Journal of Robotics Research*, vol. 16, pp. 285–299, 1989.
- [13] A. U. Venturini, *Kinematika elevacije človeške roke (eng. - Kinematics in the elevation of the human arm) - (in Slovene)*. PhD thesis, University of Ljubljana, Faculty of Computer and Information Science, Slovenia, 1996.
- [14] F. V. der Helm, "Analysis of the kinematic and dynamic behavior of the shoulder mechanism," *Journal of Biomechanics*, vol. 27, pp. 527–550, 1994.
- [15] M. Suzuki, Y. Yamazaki, and K. Matsunami, "Simplified dynamics of planar two-joint arm movements," *Journal of Biomechanics*, vol. 33, pp. 925–931, 2000.
- [16] T. Kodek and M. Munih, "An analysis of static and dynamic joint torques in elbow flexion-extension movements," *Simulation Modelling Practice and Theory*, vol. 11, pp. 297–311, 2003.
- [17] H. Hatze, "A three-dimensional multivariate model of passive human joint torques and articular boundaries," *Clinical Biomechanics*, vol. 12, pp. 128–135, 1997.
- [18] A. Esteki and J. Mansour, "An experimentally based nonlinear viscoelastic model of joint passive moment," *Journal of Biomechanics*, vol. 29, pp. 443–450, 1996.
- [19] A. Engin, "On the damping properties of the shoulder complex," *Journal of Biomechanical Engineering*, vol. 106, pp. 360–363, 1984.
- [20] C. Gielen, J. Houk, S. Marcus, and L. Miller, "Viscoelastic properties of the wrist motor servo in man," *Annals of Biomedical Engineering*, vol. 12, pp. 599–620, 1984.
- [21] V. Zatsiorsky and V. Seluyanov, "The mass and inertia characteristics of the main segments of the human body," *International Biomechanics - Human Kinetic Illinois*, vol. 4B, pp. 1152–1159, 1983.
- [22] H. Hatze, "A mathematical model for the computational determination of parameter values of antropometric segments," *Journal of Biomechanics*, vol. 13, pp. 833–843, 1980.

- [23] C. Wei and R. Jensen, "The application of segment axial density profiles to a human body inertial model," *Journal of Biomechanics*, vol. 28, pp. 103–108, 1995.
- [24] P. Martin, M. Mungiole, M. Marzke, and J. Longhill, "The use of magnetic resonance imaging for measuring segment inertial properties," *Journal of Biomechanics*, vol. 22, pp. 367–376, 1989.
- [25] J. Dewald and R. Beer, "Abnormal joint torque patterns in the paretic upper limb of subjects with hemiparesis," *Muscle Nerve*, vol. 24, pp. 273–283, 2001.
- [26] J. Given, J. Dewald, and W. Rymer, "Joint dependent passive stiffness in paretic and contralateral limbs of spastic patients with hemiparetic stroke," *Journal of Neurology, Neurosurgery and Psychiatry*, vol. 59, pp. 271–279, 1995.
- [27] W. Dempster, "Space requirement of the seated operator," *AMRL Technical Report - Wright-Patterson Air Force Base, Ohio*, pp. 55–159, 1955.
- [28] C. Clauser, J. McConville, and J. Young, "Weight, volume and centre of mass of segments of the human body," Tech. Rep. AMRL-TR-69-70, Wright Patterson Air Force Base, Ohio, 1969.
- [29] J. Napier, "The prehensile movements of the human hand," *The Journal of Bone and Joint Surgery*, vol. 38B/4, pp. 902–913, 1956.
- [30] A. Bicchi, "Hands for dexterous manipulation and robot grasping - a difficult road towards simplicity," *IEEE Transaction on Robotics and Automation*, vol. 16/6, pp. 652–662, 2000.
- [31] M. S. G.J. Gelderblom, G. Cremers, "Rehabilitation robotics state of the art - 2003, (cd-rom)," tech. rep., iRv, Institute for Rehabilitation Research, Hoensbroek, Netherlands.
- [32] I. Murray, *Determining upper limb kinematics and dynamics during everyday tasks*. PhD thesis, CREST Department of Mechanical, Materials and Manufacturing Engineering, University of Newcastle upon Tyne, UK, 1999.
- [33] A. Engin and S. Tumer, "Three-dimensional kinematic modelling of the human shoulder complex - part i, physical model and determination of joint sinus cones," *Journal of Biomechanical Engineering*, vol. 111, pp. 107–112, 1988.

- [34] A. Peyton, "Determination of the moment of inertia of limb segments by a simple method," *Journal of Biomechanics*, vol. 5, pp. 405–410, 1986.
- [35] J. Allum, "The relaxed oscillation technique for the determination of the moment of inertia of limb segments," *Journal of Biomechanics*, vol. 9, pp. 21–55, 1976.
- [36] S. Bouisset and E. Pertuzon, "Experimental determination of the moment of inertia of limb segments," in *Proceedings of the First International Seminar on Biomechanics - Zurich*, pp. 106–109, 1968.
- [37] V. Zatsiorsky, *Kinetics of human motion*. Human Kinetics, 2002.
- [38] L. Siciliano and B. Sciavicco, *Modeling and control of robot manipulators*. The McGraw-Hill Companies, Inc., 1996.
- [39] M. Kawato, "Internal models for motor control and trajectory planning," *Current Opinion in Neurobiology*, vol. 9, pp. 718–727, 1999.
- [40] A. Feldman and M. Levin, "Positional frames of reference in motor control, their origin and use," *Behav. Brain Science*, vol. 18, pp. 723–806, 1995.
- [41] M. Latash and G. Gottlieb, "Reconstruction of joint compliant characteristics during fast and slow movements," *Neuroscience*, vol. 43, pp. 697–712, 1991.
- [42] T. Kodek and M. Muni, "Quantification of shoulder and elbow passive moments in the sagittal plane as a function of adjacent angle fixations," *Journal of Technology and Health Care*, vol. 11, pp. 89–103, 2003.
- [43] G. Wu and Z. Ladin, "Limitations of quasi-static estimation of human joint loading during locomotion," *Medical & Biological Engineering & Computing*, vol. 34, pp. 472–476, 1996.
- [44] E. Hutchinson, P. Riley, and D. Krebs, "A dynamic analysis of the joint forces and torques during rising from a chair," *IEEE Transactions on Rehabilitation Engineering*, vol. 2(2), pp. 49–56, 1994.
- [45] T. Bernard, M. Ayoub, and C. Lin, "Effects of speed of lift on static and inertial moments at the joints," *International Journal of Industrial Ergonomics*, vol. 24, pp. 39–47, 1999.
- [46] Y. Pai and M. Rogers, "Control of body mass transfer as a function of speed of ascent in sit-to-stand," *Medicine and Science in Sports and Exercise*, vol. 22(3), pp. 378–384, 1989.

- [47] J. Hollerbach and T. Flash, "Dynamic interactions between limb segments during planar arm movement," *Biological Cybernetics*, vol. 44, pp. 67–77, 1982.
- [48] M. Suzuki, Y. Yamazaki, N. Mizuno, and K. Matzunami, "Trajectory formation of the center-of-mass of the arm during reaching movements," *Neuroscience*, vol. 76, pp. 597–610, 1997.
- [49] N. Lan, "Analysis of an optimal control model of multi-joint arm movements," *Biological Cybernetics*, vol. 76, pp. 107–117, 1997.
- [50] P. Morasso, "Three dimensional arm trajectories," *Biological Cybernetics*, vol. 48, pp. 187–194, 1983.
- [51] X. Zhang and D. Chaffin, "The effects of speed variation on joint kinematics during multisegment movements," *Human Movement Science*, vol. 18, pp. 741–757, 1999.
- [52] T. Flash, "The control of hand equilibrium trajectories in multi-joint arm movements," *Biological Cybernetics*, vol. 57, pp. 257–274, 1987.
- [53] H. Guomi and M. Kawato, "Equilibrium-point control hypothesis examined by measured arm stiffness during multijoint movement," *Science*, vol. 272, pp. 117–120, 1996.
- [54] R. Riener and T. Edrich, "Identification of passive elastic moments in the lower extremities," *Journal of Biomechanics*, vol. 32, pp. 539–544, 1999.
- [55] Y. Yoon and M. Mansour, "The passive elastic moments at the hip," *Journal of Biomechanics*, vol. 12, pp. 905–910, 1982.
- [56] J. Mansour and M. Audu, "The passive elastic moment at the knee and its influence on human gait," *Journal of Biomechanics*, vol. 5, pp. 369–373, 1986.
- [57] M. Audu and D. Davy, "The influence of muscle model complexity in musculoskeletal motion modeling," *Journal of Biomechanical Engineering*, vol. 107, pp. 147–156, 1985.
- [58] D. Bennett, "Torques generated at the human elbow joint in response to constant position errors imposed during voluntary movements," *Experimental Brain Research*, vol. 95, pp. 488–498, 1993.

- [59] D. Bennett, J. Hollerbach, and I. H. Y. Xu, "Time varying stiffness of human elbow joint during cyclic voluntary movement," *Experimental Brain Research*, vol. 88, pp. 433–442, 1992.
- [60] Y. Xu and J. Hollerbach, "A robust ensemble data method for identification of human joint mechanical properties during movement," *IEEE Transactions on Biomedical Engineering*, vol. 46, pp. 409–419, 1999.
- [61] Y. Xu and J. Hollerbach, "Identification of human joint mechanical properties from single trial data," *IEEE Transactions on Biomedical Engineering*, vol. 45, pp. 1051–1059, 1998.
- [62] A. Acosta, R. Kirsch, and E. Perreault, "A robotic manipulator for the characterization of two-dimensional dynamic stiffness using stochastic displacement perturbations," *Journal of Neuroscience Methods*, vol. 102, pp. 177–186, 2000.
- [63] E. Perreault, R. Kirsch, and P. Crago, "Effects of shoulder stability on end-point stiffness," *IEEE Engineering in Medicine and Biology*, vol. Nov./Dec. 2000, pp. 53–58, 2000.
- [64] M. Pierre and R. Kirsch, "Measuring dynamic characteristics of the human arm in three dimensional space," in *Proceeding of the International Functional Electrical Stimulation Society Conference*, Ljubljana, Slovenia, pp. 78–80, 2002.
- [65] E. Perreault, P. Crago, and R. Kirsch, "Estimation of intrinsic and reflex contributions to muscle dynamics, a modelling study," *IEEE Transactions on Biomedical Engineering*, vol. 47, pp. 1413–1421, 2000.
- [66] A. Engin and S. Chen, "Statistical data base for the biomechanical properties of the human shoulder complex - i, kinematics of the shoulder complex," *Journal of Biomechanical Engineering*, vol. 108, pp. 215–221, 1986.
- [67] A. Engin and S. Tumer, "Three-dimensional kinematic modelling of the human shoulder complex - part ii, mathematical modeling and solution via optimization," *Journal of Biomechanical Engineering*, vol. 111, pp. 113–121, 1988.
- [68] A. Engin and S. Chen, "Statistical data base for the biomechanical properties of the human shoulder complex - ii, passive resistive properties beyond the shoulder complex sinus," *Journal of Biomechanical Engineering*, vol. 108, pp. 222–227, 1986.

- [69] A. Engin, R. Peindl, N. Berme, and I. Kaleps, "Kinematic and force data collection in biomechanics by means of sonic emitters - i, kinematic data collection methodology," *Journal of Biomechanical Engineering*, vol. 106, pp. 204–211, 1984.
- [70] A. Engin, R. Peindl, N. Berme, and I. Kaleps, "Kinematic and force data collection in biomechanics by means of sonic emitters - ii, force data collection and application to the human shoulder complex," *Journal of Biomechanical Engineering*, vol. 106, pp. 212–219, 1984.
- [71] A. Engin and S. Chen, "Kinematic and passive resistive properties of human elbow complex," *Journal of Biomechanical Engineering*, vol. 109, pp. 318–323, 1987.
- [72] H. Veeger, B. Yu, K. An, and R. Rozendal, "Parameters for modeling the upper extremity," *Journal of Biomechanics*, vol. 30, pp. 647–652, 1996.
- [73] R. Jensen and G. Nassas, "The increase in segment principal moments of inertia as a result of growth," *International Series on Biomechanics*, vol. 7a, pp. 301–305, 1987.
- [74] R. Jensen, "Changes in segment inertia proportions between 4 and 20 years," *Journal of Biomechanics*, vol. 6/7, pp. 529–536, 1989.
- [75] G. Borelli, *De motu animalium*. Lugduni Batavorum, {This reference is reproduced from Clauser *et al.* }, 1680.
- [76] W. Braune and O. Fischer, "The centre of gravity of the human body as related to the equipment of the german infantryman," *Treat of the Math -Phys Class fo the Royal Acad Of Sci of Saxony (In German)*, vol. 26, pp. 561–672, 1889.
- [77] N. Bernstein, *On the construction of movements*. Moscow, Medgiz (In Russian), 1947.
- [78] R. Drillis and R. Contini, "Body segment mass properties," Tech. Rep. 1166 03, Technical Report - New York University, 1966.
- [79] R. Chandler, C. Clauser, J. McConville, H. Reynolds, and J. Young, "Investigation of the inertial properties of the human body," Tech. Rep. DOT HS-801-430, Wright-Patterson Air Force Base, Ohio, 1975.
- [80] R. Contini, "Body segment parameters, part ii," *Artificial Limbs*, vol. 16, pp. 1–19, 1972.

- [81] P. de Leva, "Adjustments to zatsiorsky-seluyanov's segment inertia parameters," *Journal of Biomechanics*, vol. 29, pp. 1223–1230, 1995.
- [82] H. Huang and S. Wu, "The elevation of mass densities of the human body in vivo from cf scans, {This reference is reproduced from Martin *et al.*}," *Comput. Biol. Med.*, vol. 23/6, pp. 343–377, 1976.
- [83] M. Mungiole and P. Martin, "Estimating segment inertial properties - comparison of magnetic resonance imaging with existing methods," *Journal of Biomechanics*, vol. 23, pp. 1039–1046, 1990.
- [84] N. Reynolds and S. Walt, "The effect of error in inertial parameter estimation on walking and running kinetic analysis of gait," in *Proceedings of the 7th International Symposium on the 3-D Analysis of Human Movement - Newcastle UK*, pp. 76–79, 2002.
- [85] R. Hinrichs, "Regression equations to predict segmental moments of inertia from anthropometric measurements - an extension of the data of chandler *et al.* (1975)," *Journal of Biomechanics*, vol. 18, pp. 621–624, 1985.
- [86] W. Khalil and E. Dombre, *Modeling identification and control of robots*. Herman Penton Science, 2002.
- [87] C. An, C. Atkeson, and J. Hollerbach, *Model-based control of a robot manipulator*. MIT Press, 1988.
- [88] C. Groetsch, *Inverse problems in mathematical sciences*. Vieweg, 1993.
- [89] G. Golub and C. V. Loan, *Matrix computations*. Johns Hopkins Series in the Mathematical Sciences, 1996.
- [90] C. Lawson and R. Hanson, *Solving least squares problems*. Prentice-Hall, 1974.
- [91] T. Kodek, "Obtaining a model of elbow passive moments in five healthy individuals with data mining," tech. rep., Faculty of electrical Engineering, University of Ljubljana, Slovenia, 2002.
- [92] "Error propagation, <http://lectureonline.cl.msu.edu/mmp/labs/error/e2.htm> (last accessible on 3.6. 2004)," tech. rep.

Appendix A

Error analysis in body segment parameter estimation

- **Elbow joint:** Let us calculate the error of the identified parameter π_2 which arises in elbow identification:

$$g_0 c_{12} m_2 l_2 + \tau_{p2} = \tau_{end2}$$

or in matrix form,

$$\begin{aligned} \mathbf{Y}_2 \boldsymbol{\pi}_2 &= \begin{bmatrix} g_0 c_{12} & 1 \end{bmatrix} \begin{bmatrix} m_2 l_2 & \tau_{p2} \end{bmatrix}^T = \tau_2 \\ F_{t_i}(\boldsymbol{\pi}_2) &= \tau_2 - \mathbf{Y}_2 \boldsymbol{\pi}_2 \xrightarrow{Optim.} \boldsymbol{\pi}_2 = \min_{\boldsymbol{\pi}_2} \sum_{t_i=1}^N F_{t_i}(\boldsymbol{\pi}_2)^2 \\ &\Downarrow \\ \boldsymbol{\pi}_2 &= \min_{\boldsymbol{\pi}_2} \sum_{t_i=1}^N (\tau_2 - \mathbf{Y}_2 \boldsymbol{\pi}_2)^2 = \\ &= \min_{\boldsymbol{\pi}_2} \sum_{t_i=1}^N (-\mathbf{J}^T \mathbf{F}_{end}^T[2] - \mathbf{Y}_2 \boldsymbol{\pi}_2)^2 = \\ &= \min_{\boldsymbol{\pi}_2} \sum_{t_i=1}^N ([-a_2 s_{12}, a_2 c_{12}, 1] [F_y, F_z, M_x]^T - \\ &\quad - [g_0 c_{12}, 1] \boldsymbol{\pi}_2)^2 \end{aligned} \tag{5.1}$$

Because $M_x \approx 0$ we can now simplify the upper terms as $\tau_2 = \tau_{end2} = f_1(a_2, q_1, q_2, F_y, F_z)$ and $\mathbf{Y}_2 \boldsymbol{\pi}_2 = f_2(q_1, q_2)$:

$$\boldsymbol{\pi}_2 = \min_{\boldsymbol{\pi}_2} \sum_{t_i=1}^N (f_1(a_2, q_1, q_2, F_y, F_z) - f_2(q_1, q_2))^2 \tag{5.2}$$

Every one of the independent variables above was a result of measurement and therefore subject to a certain absolute error ($\delta_{a_2}, \delta_{q_1}, \delta_{q_2}, \delta_{F_y}, \delta_{F_z}$). We express the total absolute error of functions f_1 and f_2 as [92]:

$$\begin{aligned}\delta_{f_1} &= f_1 \sqrt{\left(\frac{\delta_{a_2}}{a_2}\right)^2 + \left(\frac{\delta_{q_1}}{q_1}\right)^2 + \left(\frac{\delta_{q_2}}{q_2}\right)^2 + \left(\frac{\delta_{F_y}}{F_y}\right)^2 + \left(\frac{\delta_{F_z}}{F_z}\right)^2} \\ \delta_{f_2} &= f_2 \sqrt{\left(\frac{\delta_{q_1}}{q_1}\right)^2 + \left(\frac{\delta_{q_2}}{q_2}\right)^2}\end{aligned}\quad (5.3)$$

π_2 can now be expressed as:

$$\pi_2 = \min_{\pi_2} \sum_{t_i=1}^N (f_1 \pm \delta_{f_1} - f_2 \mp \delta_{f_2})^2 \quad (5.4)$$

When applying for the sum along all time samples and the square we obtain total error δ_{π_2} as [92]:

$$\delta_{\pi_2} = 2N(\delta_{f_1} + \delta_{f_2}) \quad (5.5)$$

Let's perform the same analysis on the shoulder joint for parameter π_1 .

- *Shoulder joint:*

$$g_0 c_1 m_1 l_1 + g_0 a_1 c_1 m_2 + \tau_{p1} = \tau_{end1} - g_0 c_1 m_2 l_2$$

or in matrix form,

$$\begin{aligned}\mathbf{Y}_1 \boldsymbol{\pi}_1 &= \begin{bmatrix} g_0 c_1 & g_0 a_1 c_1 & 1 \end{bmatrix} \begin{bmatrix} m_1 l_1 & m_2 & \tau_{p1} \end{bmatrix}^T = \boldsymbol{\tau}_1 \\ F_{t_i}(\boldsymbol{\pi}_1) &= \boldsymbol{\tau}_1 - \mathbf{Y}_1 \boldsymbol{\pi}_1 \xrightarrow{Optim.} \boldsymbol{\pi}_1 = \min_{\boldsymbol{\pi}_1} \sum_{t_i=1}^N F_{t_i}(\boldsymbol{\pi}_1)^2 \\ &\Downarrow \\ \boldsymbol{\pi}_1 &= \min_{\boldsymbol{\pi}_1} \sum_{t_i=1}^N (\boldsymbol{\tau}_1 - \mathbf{Y}_1 \boldsymbol{\pi}_1)^2 = \\ &= \min_{\boldsymbol{\pi}_1} \sum_{t_i=1}^N (-\mathbf{J}^T \mathbf{F}_{end}^T [1] - g_0 c_1 m_2 l_2 - \mathbf{Y}_1 \boldsymbol{\pi}_1)^2 = \\ &= \min_{\boldsymbol{\pi}_1} \sum_{t_i=1}^N ([-a_1 s_1 - a_2 s_{12}, a_1 c_1 + a_2 c_{12}, 1] [F_y, F_z, M_x]^T - g_0 c_1 m_2 l_2 - \\ &\quad - [g_0 \cos_1, g_0 a_1 c_1, 1] \boldsymbol{\pi}_1)^2\end{aligned}\quad (5.6)$$

Because $M_x \approx 0$ we can now simplify the upper terms as $\tau_{end1} = f_3(a_1, a_2, q_1, q_2, F_y, F_z)$, $g_0c_1m_2l_2 = f_4(q_1, m_2l_2)$ and $\mathbf{Y}_2\pi_2 = f_5(a_1, q_1, q_2)$:

$$\pi_1 = \min_{\pi_1} \sum_{t_i=1}^N (f_3(a_1, a_2, q_1, q_2, F_y, F_z) - f_4(q_1, m_2l_2) - f_5(a_1, q_1, q_2))^2 \quad (5.7)$$

Every one of the independent variables above was a result of measurement and therefore subject to a certain absolute error ($\delta_{a_2}, \delta_{a_1}, \delta_{q_1}, \delta_{q_2}, \delta_{F_y}, \delta_{F_z}, \delta_{m_2l_2}$). We express the total absolute error of functions f_3 , f_4 and f_5 as [92]:

$$\begin{aligned} \delta_{f_3} &= f_3 \sqrt{\left(\frac{\delta_{a_1}}{a_1}\right)^2 + \left(\frac{\delta_{a_2}}{a_2}\right)^2 + \left(\frac{\delta_{q_1}}{q_1}\right)^2 + \left(\frac{\delta_{q_2}}{q_2}\right)^2 + \left(\frac{\delta_{F_y}}{F_y}\right)^2 + \left(\frac{\delta_{F_z}}{F_z}\right)^2} \\ \delta_{f_4} &= f_4 \sqrt{\left(\frac{\delta_{q_1}}{q_1}\right)^2 + \left(\frac{\delta_{m_2l_2}}{m_2l_2}\right)^2} \\ \delta_{f_5} &= f_5 \sqrt{\left(\frac{\delta_{a_1}}{a_1}\right)^2 + \left(\frac{\delta_{q_1}}{q_1}\right)^2 + \left(\frac{\delta_{q_2}}{q_2}\right)^2} \end{aligned} \quad (5.8)$$

π_2 can now be expressed as:

$$\pi_1 = \min_{\pi_1} \sum_{t_i=1}^N (f_3 \pm \delta_{f_3} - f_4 \mp \delta_{f_4} - f_5 \mp \delta_{f_5})^2 \quad (5.9)$$

When applying for the sum along all N time samples and the square we obtain total error δ_{π_1} as [92]:

$$\delta_{\pi_1} = 2N(\delta_{f_3} + \delta_{f_4} + \delta_{f_5}) \quad (5.10)$$

- **Elbow passive moment** Let us introduce a new variable X , which corresponds to the difference between the measured joint moments $\tau_2 = \tau_{end2}$ and the identified joint moments $\mathbf{Y}_2\pi_2(1) = [g_0c_{12}][m_2l_2]$ along all time samples of the measurement:

$$X = \frac{1}{N} |\tau_2 - \mathbf{Y}_2\pi_2| \quad (5.11)$$

Let us first determine the error in X by considering δ_{f_1} , δ_{f_2} and δ_{π_2} , which

were calculated previously and the fact that $f_1 = \tau_2$:

$$\begin{aligned} X &= f_1(a_2, q_1, q_2, F_y, F_z) - \mathbf{Y}_2\pi_2 = \\ &= f_1 \pm \delta_{f_1} - f_2\pi_2 \mp \delta_{\mathbf{Y}_2\pi_2} \\ &\quad \Downarrow \\ \delta_X &= \delta_{f_1} + \delta_{f_2\pi_2} = \delta_{f_1} + \mathbf{Y}_2\pi_2 \sqrt{\frac{\delta_{\mathbf{Y}_2}}{\mathbf{Y}_2} + \frac{\delta_{\pi_2}}{\pi_2}} \end{aligned}$$

by considering that $\mathbf{Y}_2 = \mathbf{Y}_2(q_1, q_2)$ we get,

$$\delta_{\mathbf{Y}_2} = \mathbf{Y}_2 \sqrt{\left(\frac{\delta_{q_1}}{q_1}\right)^2 + \left(\frac{\delta_{q_2}}{q_2}\right)^2} \quad (5.12)$$

The total error in τ_{p2} is now:

$$\delta_{\tau_{p2}} = 2\delta_X = 2\delta_{f_1} + 2\delta_{\mathbf{Y}_2\pi_2} \quad (5.13)$$

- **Shoulder passive moment** If we introduce a new variable Z , which corresponds to the difference between generalized joint moments $\tau_1 = \tau_{e1} - g_0\cos_1 m_2 l_2$ and the identified moments $\mathbf{Y}_2\pi_2 = [g_0\cos_1, g_0 a_1 \cos_1][m_1 l_1, m_2]^T$ along all time samples of the measurement:

$$Z = \frac{1}{N} |\tau_1 - \mathbf{Y}_1\pi_1| \quad (5.14)$$

Let us first determine the error in Z by considering δ_{f_3} , δ_{f_4} , δ_{f_5} and δ_{π_1} , which were calculated previously and the fact that $f_3 = \tau_{1e}$ and $f_4 = g_0\cos_1 m_2 l_2$:

$$\begin{aligned} Z &= f_3(a_1, a_2, q_1, q_2, F_y, F_z) - f_4(q_1, m_2 l_2) - \mathbf{Y}_1\pi_1 = \\ &= f_3 \pm \delta_{f_3} - f_4 \mp \delta_{f_4} - \mathbf{Y}_1\pi_1 \mp \delta_{\mathbf{Y}_1\pi_1} \\ &\quad \Downarrow \\ \delta_Z &= \delta_{f_3} + \delta_{f_4} + \delta_{\mathbf{Y}_1\pi_1} = \delta_{f_3} + \delta_{f_4} + \mathbf{Y}_1\pi_1 \sqrt{\frac{\delta_{\mathbf{Y}_1}}{\mathbf{Y}_1} + \frac{\delta_{\pi_1}}{\pi_1}} \end{aligned}$$

by considering that $\mathbf{Y}_1 = \mathbf{Y}_1(a_1, q_1, q_2)$ we get,

$$\delta_{\mathbf{Y}_1} = \mathbf{Y}_1 \sqrt{\left(\frac{\delta_{a_1}}{a_1}\right)^2 + \left(\frac{\delta_{q_1}}{q_1}\right)^2 + \left(\frac{\delta_{q_2}}{q_2}\right)^2} \quad (5.15)$$

The total error in τ_{p1} is now:

$$\delta_{\tau_{p1}} = 2\delta_Z = 2\delta_{f_3} + 2\delta_{f_4} + 2\delta_{Y_1\pi_1} \quad (5.16)$$

Appendix B

Quantification of shoulder and elbow passive moments in the sagittal plane as a function of adjacent angle fixations

Timotej Kodek and Marko Munih

Faculty of electrical engineering, University of Ljubljana, Slovenia Laboratory for robotics, Tr žaška 25, 1000 Ljubljana, Slovenia

Tel.: +386 1 4768465; Fax: +386 1 4768239; E-mail: {timotej.kodek,marko.munih}@robo.fe.uni-lj.si

Abstract. The goal of this study was an assessment of the shoulder and elbow joint passive moments in the sagittal plane for six healthy individuals. Either the shoulder or elbow joints were moved at a constant speed, very slowly throughout a large portion of their range by means of an industrial robot. During the whole process the arm was held fully passively, while the end point force data and the shoulder, elbow and wrist angle data were collected. The presented method unequivocally reveals a large passive moment adjacent angle dependency in the central angular range, where most everyday actions are performed. It is expected to prove useful in the future work when examining subjects with neuromuscular disorders. Their passive moments may show a fully different pattern than the ones obtained in this study.

Keywords: Elbow passive moments, shoulder passive moments, dynamic model, upper extremity, static movement, sagittal plane, industrial robot

1. Introduction

The passive moments exerted in the human musculoskeletal system are an internal property of every joint in the upper and lower extremities. They arise mostly from the presence and deformations of structures such as tendons, ligaments, skin, joint capsules, inactive muscles and bones [12,13] composing a particular joint. They could be expressed in terms of elastic and dissipative contributions [12]. Several authors in the past concentrated only on the elastic effects [13,19]. There have been a large number of studies dealing with these properties, out of which the majority were concentrated on lower extremities [16,19,25]. In addition to examining torque-angle properties for one joint, many authors have attempted to construct a model expressing the passive moments as a function of the two adjacent joint angles. Most [12,19] have used a technique proposed by Audu and Davy [2] where this function was taken to be a double exponential curve, indicating a significant torque increase at extreme angles. On the other hand, Hatze [13] proposed a model, consisting of a sum of several individual tissue exponential contributions relating to an observed joint. This relation was further simplified into a hyperbolic one, requiring an identification of a total of 53 elastic and viscous parameters for each degree of freedom in the human elbow joint (i.e. flexion-extension and pronation-supination). It has to be pointed out that all these studies were made without any voluntary muscle action.

There has also been a number of studies concentrating on the arm dynamics in the presence of a voluntary movement, particularly in the elbow joint. Following a study on torques produced in the elbow

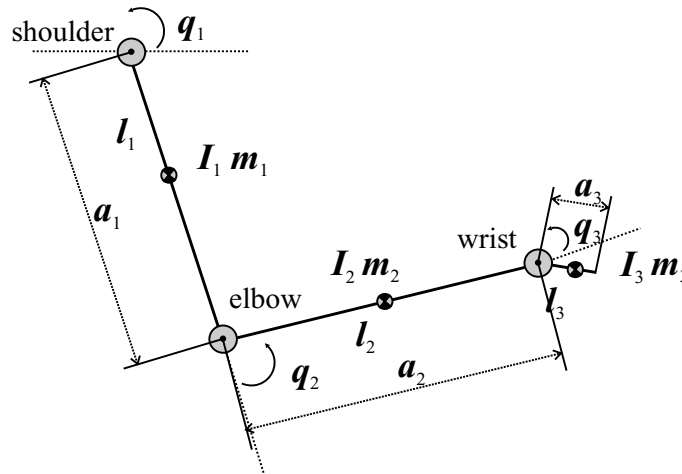


Fig. 1. Geometric definitions for the assumed human arm structure, consisting of three segments.

joint with voluntary movements [3], Bennett and Hollerbach et al. [4] devised an ensemble parametric method for identifying the time-varying compliance of the human elbow joint, using an airjet actuator apparatus. Further studies by Xu and Hollerbach [23,24] on the elbow joint mechanical properties concentrated on estimating elasticity, viscosity and inertial contributions during a voluntary movement, using a similar technique and a two-dimensional device capable of imposing random torque perturbations. In all these studies, the inertia contribution was shown to remain constant despite the varying voluntary muscle action, whereas elasticity and viscosity, both increased and decreased proportionally with the applied muscle force. A number of other studies concentrated on the endpoint stiffness of the human arm mechanism, as a result of all upper limb joint mechanical properties acting in concert [1,17,18].

The studies of Engin et al. concentrated mostly on the shoulder joint. They dealt extensively with kinematics of the human shoulder complex [5–7] and also investigated its passive resistive properties [8, 10,11]. A study of passive resistive properties limited to an area beyond the full elbow extension was also performed [9]. A comprehensive analysis of the kinematic and dynamic behavior of the shoulder mechanism providing a good insight into mechanics of the shoulder mechanism, was presented by Van der Helm [14]. Some parameters acquired in the study of Veeger et al. [22] were also a good lead to our study.

Unlike the work of Xu and Hollerbach [23,24], the study presented here is aimed at separating the effects of passive and active musculoskeletal contributions to the human arm dynamics. This work firstly concentrates on identifying the passive moments (i.e. elasticity, and dissipative effects) of the elbow and shoulder joints being moved one at a time through a large portion of their flexion-extension range in the sagittal plane. This was achieved by imposing slow (i.e. static) angular movements to a particular joint, while keeping the second joint at a fixed angle. The wrist passive moment was also acquired in the process, but was not thoroughly investigated, because the joint was not displaced. The upper extremity was modelled in terms of an inverse dynamics equation for a three segment planar manipulator [20,21].

The aim of the presented study is providing an alternative upper extremity clinical evaluation method which could be used on patients suffering from neuromuscular disorders usually following a stroke. Passive moment patterns obtained from such subjects are expected to show noticeable differences from the healthy ones.

2. Methods

2.1. Mathematical modeling

In this experimental work the human arm was described as a three degree of freedom kinematic and dynamic structure (Fig. 1). The segment lengths are denoted with a_i , their centers of mass with l_i while q_i indicate the positive angle directions with respect to the zero position (dashed line). Positive angle values are denoted with the arrow. The masses and inertias are presented with the m_i and I_i variables. The centers of gravity were expressed as a distal distance from the joint marked with the same index.

As in every other manipulator system, the dynamic behavior, as a relationship between applied driving torques $\tau(u)$, environment forces h and joint motion trajectories \ddot{q}, \dot{q}, q , of mechanical joints can be described as [20]:

$$B(q)\ddot{q} + C(q, \dot{q})(\dot{q}) + G(q) + F_v\dot{q} + F_e q + F_d \text{sgn}(\dot{q}) = \tau(u) - J^T(q)h \quad (1)$$

Here q, \dot{q} and \ddot{q} represent the three component joint angle, angular velocity and angular acceleration vectors. The *moments of inertia* are represented as a $(3 \times 3)B(q)$ matrix, while the second square matrix $C(q, \dot{q})$ expresses the *centrifugal* and *Coriolis* effects on the arm dynamics.

The *gravitational* contribution is expressed with a three element column vector, where every element g_i represents the moment generated at the joint i axis due to the presence of gravity:

$$G(q) = [g_1 \quad g_2 \quad g_3]^T, \quad (2)$$

where

$$g_1 = g_0 \{ [l_1 m_1 + a_1(m_2 + m_3)] c_1 + (l_2 m_2 + a_2 m_3) c_{12} + l_3 m_3 c_{123} \},$$

$$g_2 = g_0 [(l_2 m_2 + a_2 m_3 + a_2 m_3) c_{12} + l_3 m_3 c_{123}],$$

$$g_3 = g_0 l_3 m_3 c_{123}.$$

In this equation the cosines were simply denoted as $c_1 = \cos(q_1)$, $c_{12} = \cos(q_1 + q_2)$ and $c_{123} = \cos(q_1 + q_2 + q_3)$. While the individual segment lengths a_i for a particular person were determined from IR markers used by a 3D positioning system, the masses m_i and gravity centers l_i , were obtained from the literature [15]. The gravitational acceleration g_0 was taken to be 9.81 m/s^2 .

The connection between the hand and the robot handle (see Section 3) creates a closed chain kinematic linkage. Thus, the end effector connection is described as a three dimensional vector with its horizontal and vertical forces (F_y, F_z) and the moment around the axis perpendicular to the plane of motion (M_x) :

$$h = [F_y \quad F_z \quad M_x]^T \quad (3)$$

These forces have to be transformed to the joint level with the Jacobian matrix $J^T(q)$ as seen in the last product of Eq. 1. The joint muscle activity is expressed in terms of the active contribution $\tau(u)$, which is a function of muscle activation u .

The viscous contribution of the system is expressed in terms of $F_v\dot{q}$. $F_d \text{sgn}(\dot{q})$ indicates the *dissipative* torques and is in the literature usually denoted as the static friction torque [20]. Finally, the *passive elastic torque* contributions in a particular joint are expressed with the product $F_e q$, where F_e is a diagonal matrix with the elements expressing the elasticity coefficients of every single joint.

Determining passive moments, as the sum of elastic and dissipative contributions, $F_e q + F_d \text{sgn}(\dot{q})$ was the topic of this study. It has to be emphasized at this point, that $F_e(q)$ behaves non-linearly, where the diagonal elements are a function of all three joint angles. On the other hand, the term $F_d \text{sgn}(\dot{q})$ contributes to the hysteresis observed later in Section 4.

3. The passive and static assumption

All measurement motions preprogrammed into the robot manipulator were slow, with arm joint angular speeds which did not exceed 0.3 rad/s for the elbow and 0.2 rad/s for the shoulder joint movement. The angular accelerations reached values of up to 1.2 rad/s² at points where the motion direction was altered, 0.6 rad/s² where the movement was started and ended and almost zero elsewhere. Because these were all verified to be very low values, the contributions of all dynamic terms in Eq. (1), were negligible compared to the non velocity and acceleration dependent terms:

$$B(q)\ddot{q} \approx 0, \quad C(q, \dot{q})\dot{q} \approx 0, \quad F_v\dot{q} \approx 0 \quad (4)$$

The next observation concerns the term $\tau(u)$ in Eq. (1). Because the subject was instructed before the experiment, to induce no voluntary muscle action whatsoever, a further assumption was made:

$$\tau(u) \approx 0 \quad (5)$$

To verify if this was justified, the EMG of a typical elbow flexion-extension trial was recorded prior to the large batch of experiments, to assess the difference between active contribution of the person and inactivity. The surface electrodes were placed on the four major flexion and extension muscles by a skilled professional (i.e. biceps long and short head, triceps and brachioradialis). It is evident that no EMG activity in those muscles contributing to the movement was present (Fig. 2), confirming Eq. (5).

All these assumptions were accounted for in Eq. (1), modifying now to:

$$F_e q + F_d \text{sgn}(\dot{q}) = -G(q) - J^T(q)h \quad (6)$$

The passive moments represented with the left side of Eq. (6) consist of the elastic contribution $F_e(q)$ and direction dependent dissipative moments $F_d \text{sgn}(\dot{q})$ also known as Coulomb friction [20]. The passive moments can be summed up as a time and angle dependent column vector $\tau_p(q, t)$ or simply τ_p which was the focal point of this study:

$$\tau_p = [\tau_{p1} \quad \tau_{p2} \quad \tau_{p3}]^T \quad (7)$$

4. Measurement

In the performed experiment a positionally controlled anthropomorphic 6-DOF industrial robot (*Yaskawa*[©] *MOTOMANsk6*) was used for imposing a slow linear movement on the human arm in the sagittal plane (Fig. 3). A *JR3*[©] 4 dimensional strain gauge force sensor was mounted on the manipulator end effector and used for force data collection. The maximum force for the specified output was ± 110 N, with an acquisition resolution of 12 bits. A bicycle-like circular rubber coated handle was mounted on top of the sensor in such a way, that rotation around the x axis was freely allowed. The next element in the system was a bus passenger seat, equipped with additional straps as evident from Fig. 3. The plane of motion was perpendicular to the ground and fully aligned with the sagittal plane of the subject. In the first part of the experiment, the subject was asked to keep his muscles relaxed while holding the handle.

The handle was held gently, while still allowing the arm to stay in good contact during the movement. Before starting the real measurements, it was also inspected whether the slight muscle activation due to

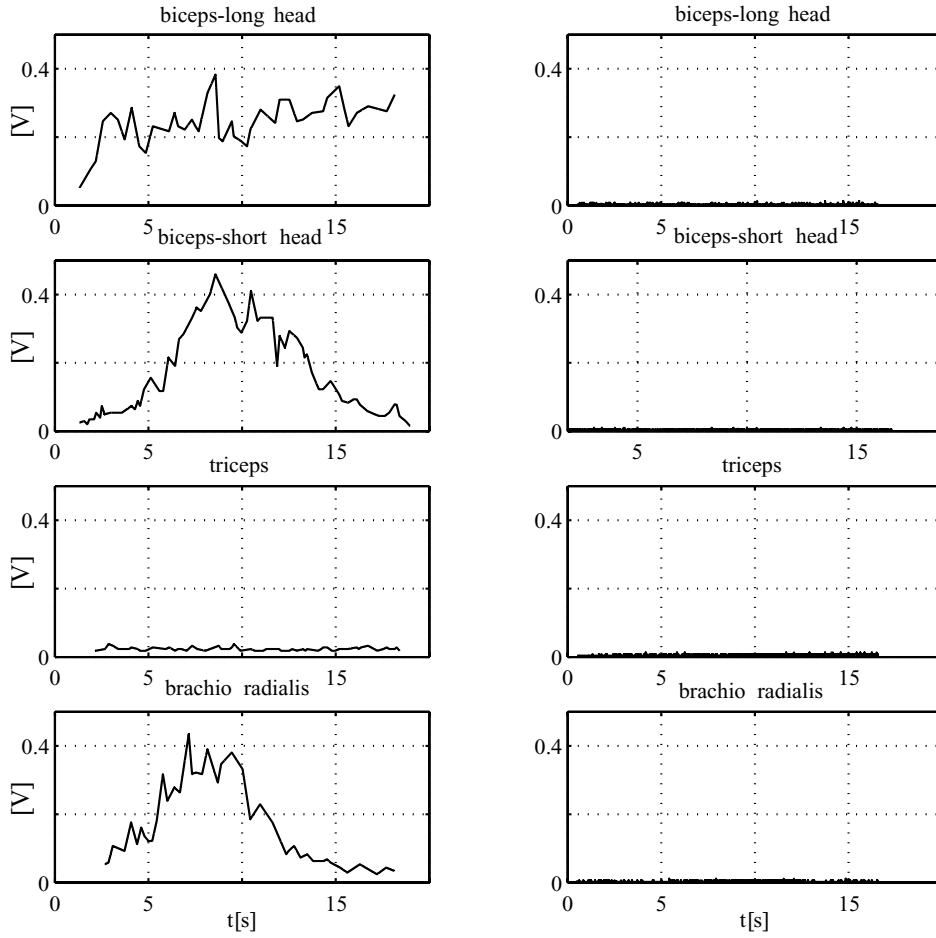


Fig. 2. EMG signals in the voluntary elbow flexion attempt (left column) and a passively held arm such as during the experiment (right column).

gripping had any significant effect on the passive torque identification process. No significant difference was found when comparing this data to the one when the hand was tightly strapped to the handle.

Due to the free handle rotation the hand dynamic parameters were properly adjusted. The mass and all geometric dimensions of the handle were accurately measured before the experiment. The handle mass m_{handle} was then added to the one of the hand m_{hand} , to yield a new third segment mass m_3 , while the center of gravity locations l_{handle} and l_{hand} were also considered in obtaining a new location l_3 :

$$\begin{aligned}
 m_3 &= m_{\text{hand}} + m_{\text{handle}}, \\
 l_3 &= \frac{l_{\text{hand}}m_{\text{hand}} + l_{\text{handle}}m_{\text{handle}}}{m_{\text{handle}} + m_{\text{hand}}}
 \end{aligned} \tag{8}$$

Two main sets of measurements were made:

1. With the shoulder angle fixed at various angles, while the elbow angle was varied smoothly.
2. With the elbow fixed, while the shoulder was moved through a range of angles.

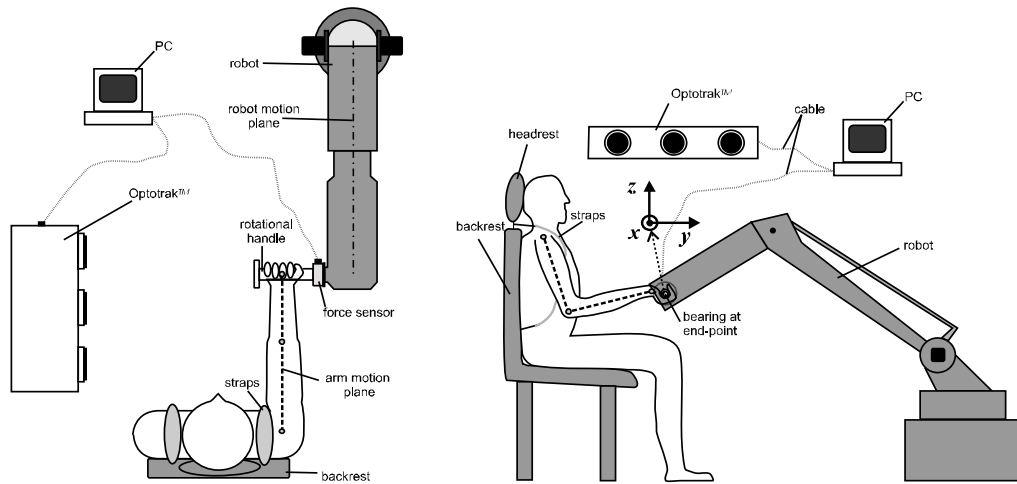


Fig. 3. Experimental setup from above (left) and a side view (right).

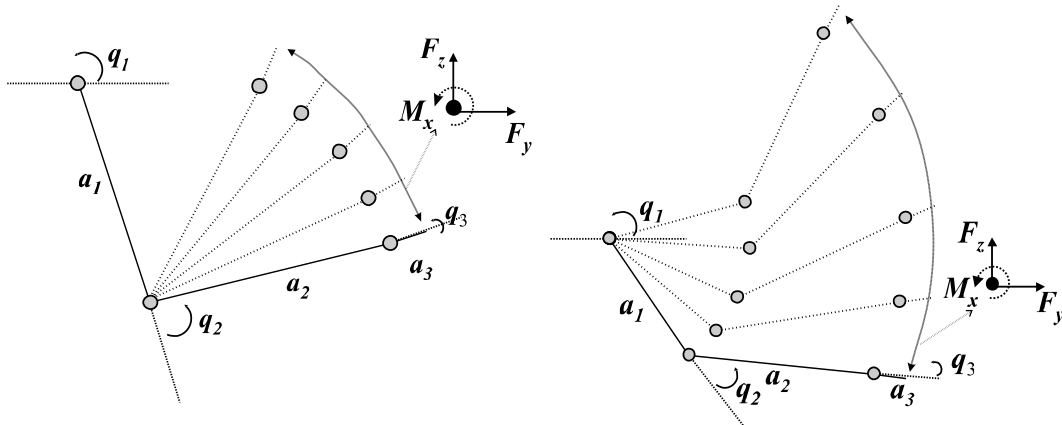


Fig. 4. A typical programmed elbow trajectory (left) at a certain fixed shoulder angle q_1 and shoulder trajectory (right) at a fixed elbow angle q_2 .

In both cases the wrist was not fixed and was allowed to move freely since the deviation from the neutral position was found to be only a few degrees. Before the particular measurements, ten different circular trajectories (not shown here) were programmed into the robot for each subject. The first five measurements concentrated on the elbow angle smooth variation from one boundary angle to the other and backwards, with the shoulder fixed at different angles ($-68^\circ, -40^\circ, +16^\circ, +10^\circ, +36^\circ$). The shoulder angle was kept constant by programming an appropriate trajectory, using no additional fixation mechanisms Fig. 4–left side).

The second set of trials focused on movements of the shoulder joint, with the elbow kept at constant angles ($20^\circ, 30^\circ, 41^\circ, 49^\circ, 59^\circ$). For fixating the elbow angle, an orthosis was used, which allowed angle adjustments from extension to a flexion angle of 85 degrees (Fig. 4–right side).

The mass of the orthosis utilized for shoulder movements was included into the calculation of the $G(q)$ matrix in Eq. (2), which describes the new upper and forearm masses and center of gravity locations as

m_i and l_i :

$$\begin{aligned} m_1 &= m_{ua} + m_{uo}, \quad m_2 = m_{fa} + m_{lo} \\ l_1 &= a_1 - \frac{l_{ua}m_{ua} + l_{uo}m_{uo}}{m_{ua} + m_{uo}} \\ l_2 &= \frac{l_{fa}m_{fa} + l_{fo}m_{fo}}{m_{fa} + m_{fo}} \end{aligned} \quad (9)$$

Here the ua and fa indices refer to the *upper arm* and *forearm*, whereas uo and fo describe the *upper* and *lower orthosis* parts. The orthosis masses and centers of gravity were accurately determined before the experiment.

A 3D tracking system *Optotrak*[©] was used to precisely record the movements during the experiment. The IR markers were attached to the skin above the rotation points of the three arm joints in consideration, to the handle and to robot manipulator joints to allow for later verification and complete reconstruction of the measurement. All calculations mentioned here were performed off-line using Matlab[©]. The *Optotrak*[©] and Force sensor data were both lowpass filtered at 5 Hz using a sixth order Butterworth filter provided by the Matlab[©] Signal Processing toolbox.

Six healthy subjects were tested with body masses ranging from 64 kg to 77 kg. They were all right-handed males aged from 25 to 39 years. None had ever suffered from any kind of neuromuscular disease. All were asked to sit in a chair, lightly grip the robot attached handle and not exert any voluntary muscle action. Before the experiment at least two preliminary movements were made to assure that the programmed trajectory was appropriate and that the subject was comfortable. After defining 10 different trajectories a set of the first ten movements was measured for the elbow and the second ten, for the shoulder joint.

Initially, six twenty-trial sets were made on one particular subject (age 25, weigh 77 kg), with every set performed on a separate day. Every movement was repeated six times, for a total of sixty measurements. Hence, all together six measurements were made for the every movement (i.e. extension to flexion and backwards). All other subjects were only measured twice for every movement.

5. Results

The results section is composed of two parts. First, a detailed overview of data acquired for one intact person is given. Among checking the general trends the purpose of this batch was to assess fidelity and repeatability of the method. The second part includes measurements on six persons to gain insight into data variability among several persons.

It has to be noted that for these measurements the shoulder and elbow were not moved throughout their complete range of motion because of a limitation imposed by the working space of the robot manipulator. Due to that, the exponential nature of the passive moments for intact population, which is more expressed near the articular boundaries, is in these results not always evident. Because of this fact the passive moment values are sometimes of very low value and therefore realistically also a subject to larger errors.

5.1. Passive moment results for one subject

Initially, six measurements of all ten movements were made on one particular subject (age 25, weight 77 kg), with every one performed on a separate day.

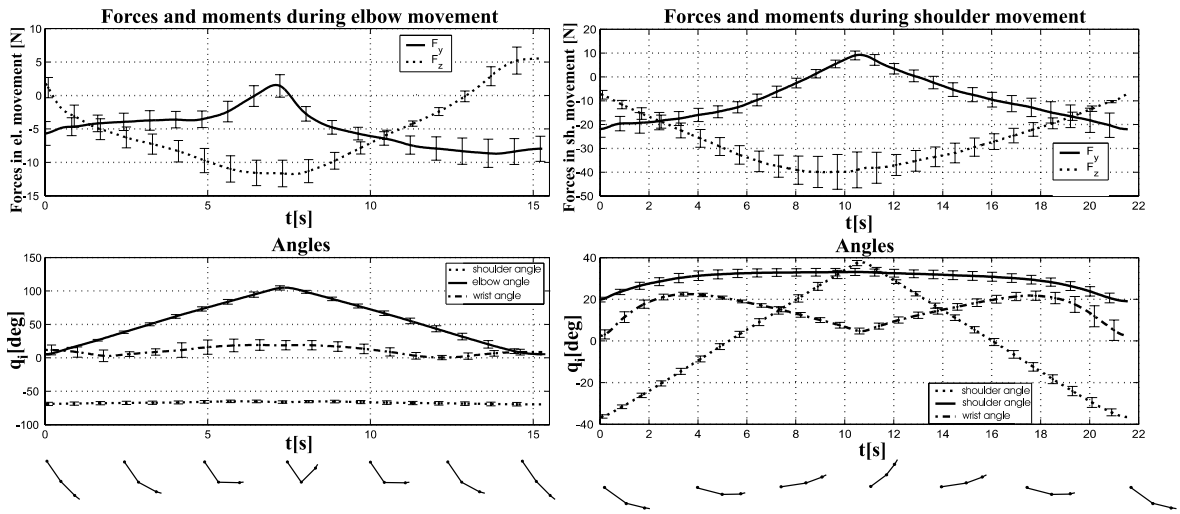


Fig. 5. The average handle force h and joint angle q_i trajectories with their standard deviation error bars in six trials, in an elbow movement while the shoulder was fixed at $q_1 \approx -68^\circ$ (left column) and in a shoulder movement while the elbow was fixed at $q_2 \approx 27^\circ$ (right column). The arm movement is sketched below the figure.

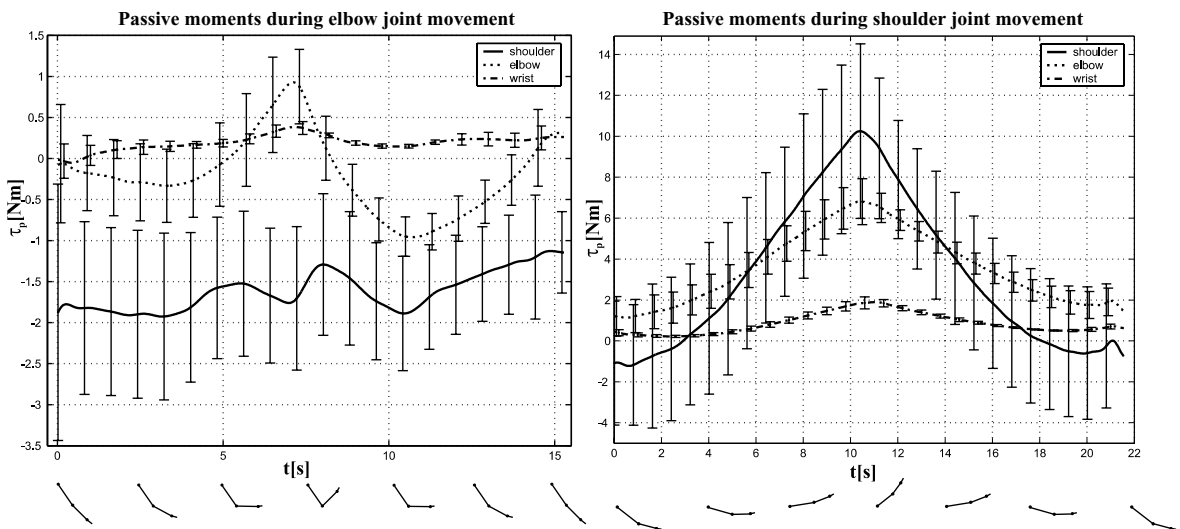


Fig. 6. The average passive moments in all three joints, computed from the data in Fig. 5 (above) with their standard deviation error bars, in an elbow movement while the shoulder was fixed at $q_1 \approx -68^\circ$ (left column) and in a shoulder movement while the elbow was fixed at $q_2 \approx 27^\circ$ (right column). The arm movement is sketched below the figure.

In total six measurements were made for every movement (i.e. extension to flexion and backwards). In Fig. 5 average time courses and six-trial standard deviations of force and kinematic data for one fixed-elbow and one fixed-shoulder configuration, are shown (the other eight configurations are not shown here due to lack of space). Note that the scale in the right column of Fig. 5 is much larger than the one in the left. The force data deviations are also larger in both plots than the ones of kinematic data.

The x axis torque M_x was negligible due to a bearing attached in the mechanism of the handle and is not shown. These averaged data were then applied to the Eq. (6), yielding a vector of average passive

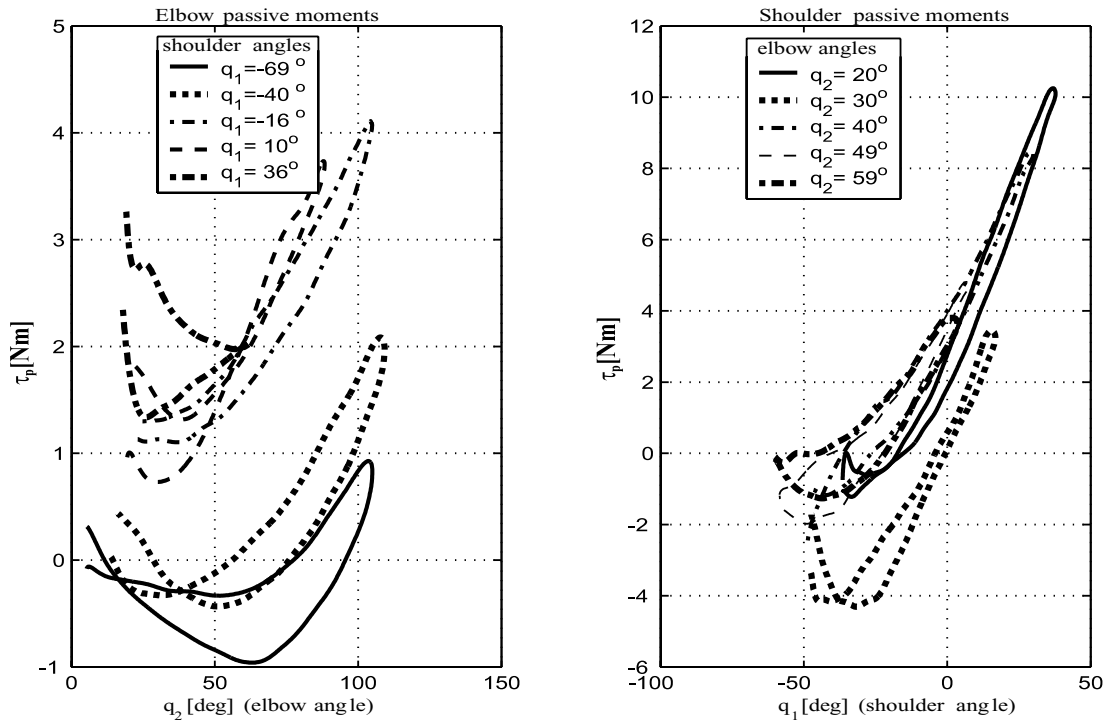


Fig. 7. All five average elbow (left) and shoulder (right) passive moments as a function of both angles for the same person. Every curve represents an average of six measurements.

Table 1

Maximum elbow passive moment standard deviations from average (as seen in the left side of Fig. 7) at five different shoulder fixation angles

	$\sigma_{\max}(q_1 = -69^\circ)$	$\sigma_{\max}(q_1 = -40^\circ)$	$\sigma_{\max}(q_1 = -16^\circ)$	$\sigma_{\max}(q_1 = 10^\circ)$	$\sigma_{\max}(q_1 = 35^\circ)$
elbow passive moment (τ_{p2})	0.7 Nm	1.1 Nm	1.0 Nm	0.4 Nm	1.1 Nm

Table 2

Maximum shoulder passive moment standard deviations from average (as seen in the right side of Fig. 7) at five different shoulder fixation angles

	$\sigma_{\max}(q_2 = 20^\circ)$	$\sigma_{\max}(q_2 = 30^\circ)$	$\sigma_{\max}(q_2 = 40^\circ)$	$\sigma_{\max}(q_2 = 49^\circ)$	$\sigma_{\max}(q_2 = 59^\circ)$
shoulder passive moment (τ_{p1})	4.4 Nm	3.6 Nm	2.7 Nm	3.0 Nm	2.2 Nm

moments $\bar{\tau}_p$ for these two configurations (Fig. 6). Again the scale in the right side of Fig. 6 is much larger.

It is sensible to represent the passive moments in relation to the displaced angle, which can be seen in Fig. 7. The fixation angles of the elbow (q_2) and shoulder (q_1) as measured by the Optotrak system, are also denoted.

Clearly the passive moments of the shoulder are much less influenced by adjacent angle fixation than the ones of the elbow. This comes as a result of a smaller number of passive muscles spanning the elbow joint (7) compared to a much greater number of muscles in the shoulder (15). The maximum standard deviations (σ_{\max}) acquired for every passive moment seen in Fig. 7 can be seen in Tables 1 and 2.

It is obvious that these standard deviations are quite large, contributing to a large relative error at

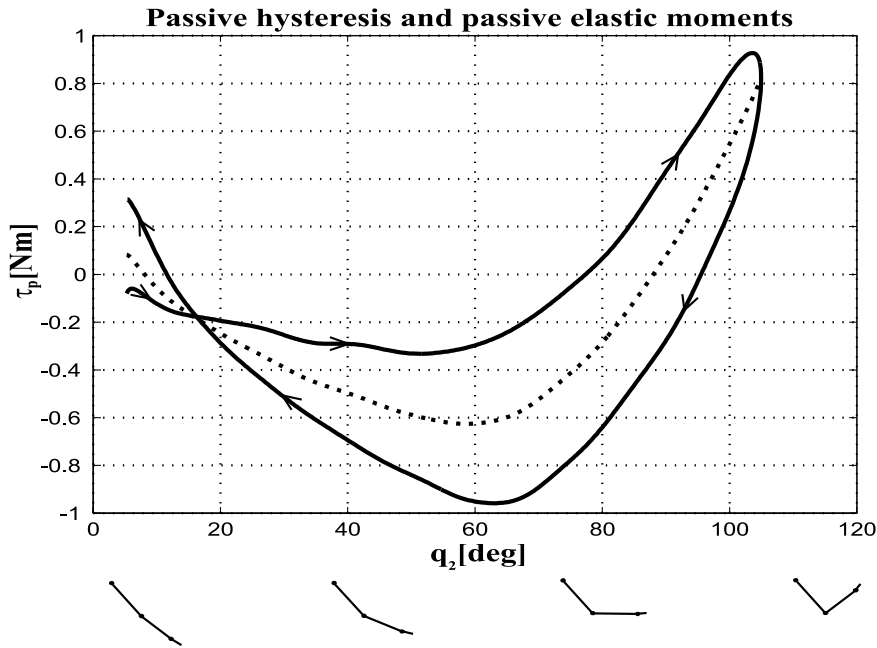


Fig. 8. Elbow passive moment hysteresis (solid line) with the elastic moment (dashed line) and the movement direction (arrow). Below the figure the arm movement scheme is depicted. The shoulder angle was fixed at $q_1 \approx -68^\circ$.

points where passive moment values are around zero. This error is mostly due to a large force standard deviation, which was observed in Fig. 5.

It has to be noted that in Fig. 7, the range of displaced angles was different for every particular movement because of different joint movement ranges at corresponding adjacent angle fixations. In all curves a hysteresis arising due to muscle dissipative effects can clearly be observed [12], where the upper part of the curve always indicates movements from extension to flexion. The hysteresis average is known to be the passive elastic moment, which was the interest of some earlier studies [13,19] and can also be seen from Fig. 8 for a typical elbow trajectory (at shoulder fixation). The passive moment curve patterns show an ascending pattern most of the time, at small angles, however, this is sometimes a descending one resulting in a global minimum.

5.2. Passive moment results for six subjects

The same data analysis was used for all six subjects in the study and all measurements were made under the same conditions. Every movement was measured twice for every subject.

It needs to be emphasized that for practical reasons the shoulder and elbow angles were not fixed completely equally for all subjects. This is mostly due to a fairly complex process of trajectory programming and different arm geometry among subjects. This fact inseparably results also in slightly different passive moments. Similar standard deviations as with one subject were observed. To limit the presentation space here, only two of the ten calculated passive moments for all subjects are shown. To show the variation of results among all six subjects, only traces for two different movements are shown in Fig. 9. It should again be noted that the scale of shoulder passive moments is larger than for elbow passive moments.

Every curve in this plot represents an average of two measurements. Most subjects show a similar pattern, although some show quite obvious differences in the hysteresis size and slope. However, it can

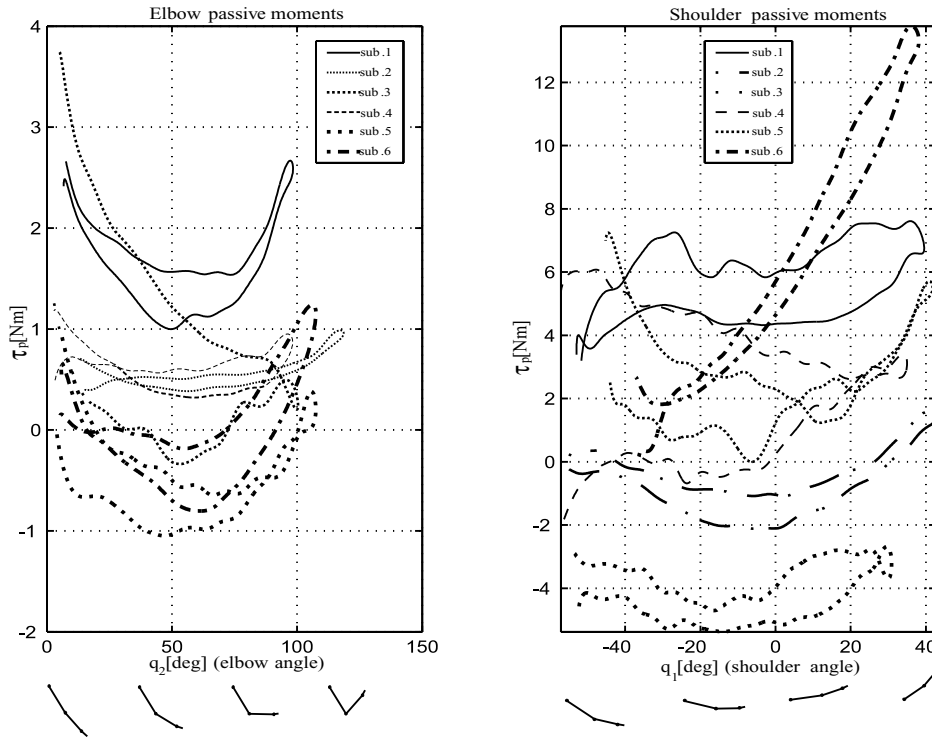


Fig. 9. Obtained passive moments for all six subjects performing two particular movements when the shoulder joint was fixed at $q_1 \approx -63^\circ$ (left) and the elbow joint at $q_2 \approx 27^\circ$ (right). Every point was obtained as an average of two measurements.

be concluded that most curves show a similar pattern.

6. Discussion and conclusion

In this paper a method for estimating arm passive moments is proposed, which according to our knowledge has not been used before. Similar angle-dependent studies have been made before for the lower extremities [19,25], while the upper extremity passive moments were not studied as much. In the measurement process, firstly one healthy individual was studied more in detail as described in Section 3. The repeatability of data obtained from six measurements can be observed in Fig. 5. While the angle data is very repeatable, the force sensor data on the other hand, shows more deviations. This is caused by a difficulty with which a subject is capable of maintaining the arm-robot connection fully equally in two successive trials. These raw data were then applied to Eq. (6), producing a passive moment vector, represented in Fig. 6 as a function of time. From this vector τ_{p2} represents the elbow passive moment and τ_{p1} the shoulder passive moment. Five elbow and five shoulder passive moments were inspected, with adjacent joints being fixed at various angles (Fig. 7). In addressing the repeatability issue, it can be observed that every curve obtained on a separate day, shows a similar pattern. The amplitude variations arise mostly from the errors in the measurement process.

Furthermore, five more healthy subjects were measured in the same way. The force and kinematic data among subjects show larger deviations than for one subject, due to geometrical and dynamical differences (not shown in this paper). This also explains why there is no straightforward correlation in

the passive moments among all subjects (Fig. 9). Just two passive moments are being presented, while the other eight are not shown in order to limit the presentation space. A large amplitude variation among different subjects was observed, especially in the shoulder joint.

It can be seen that the passive moments are strongly influenced by adjacent joint fixation. However, this is much less evident for the shoulder joint, as it is for the elbow (Fig. 7). It is also obvious that the shoulder passive moments are far larger than the ones obtained for the elbow. The reason lies in passive one and two-joint muscles, which span over both joints and are very likely the major contributor to the passive properties. While there are only seven muscles producing elbow joint movements, there are fifteen, which are involved in the shoulder, with a total cross section area far greater than the one of the elbow muscles. Apart from this, the biceps and triceps muscles, which contribute to elbow joint motions are two-joint muscles spanning the whole upper arm and hence influence the passive properties of both the shoulder and the elbow joint.

In all similar works the passive elastic torque was found to resemble a symmetrical double exponential curve with highly positive values at complete extension and negative ones at extreme flexion. Other parts of the curve were found to be almost linear. It needs to be emphasized that the passive moments in this study, contain elastic and dissipative contributions as explained in Eq. (6) and seen in Fig. 8. The calculated average passive moment patterns observed in Figs 7 and 9, sometimes show a descending tendency at low angles. The reasons for this lies in the fact that the gravity contributions $G(q)$ from Eq. (6) have a larger inverse tendency than the environment contributions $J^T(q)h$ in that particular angular region. With the continuing flexion motion, however, the passive moments always show an increasing trend.

It has to be underlined that the flexion-extension movement limits in this study never reached the articular boundaries of either the elbow or the shoulder joint. This occurs due to a limited robot workspace and almost no physical constraining of the arm. Therefore the passive moments were quantified only in the central region of the movement range. The calculated passive moments here are also opposite in sign and show an inverse tendency compared to many other studies because the angle notation is different.

Apart from the relatively large force sensor data deviations (Fig. 5), another source of error is also the term $G(q)$ in Eq. 6 which was calculated by using the segment masses m_i , lengths a_i and centers of gravity l_i , from the literature [15]. Because the segment mass estimation m_i affects only the term $G(q)$ in this equation, the inexact value causes significant errors to the passive moment calculation. A comprehensive analysis on these errors would be very beneficial in the future. On the other hand, segment length and center of gravity location errors do not affect the result greatly. The effect they have on the term $G(q)$ cancels itself with that from the environment contribution term $J^T(q)h$ (Eq. 6). The reason lies in the Jacobian matrix $J^T(q)$ which also depends on l_i and a_i . Hence, the error imposed by a marker misalignment, is not very prominent, resulting in low percentage changes in segment lengths a_i and subsequently centers of gravity l_i .

Owing to the fact that the planar model structure is mathematically far less complex to describe than any other alternative, some studies suggest that the motor control system in the human brain actually uses a simplified version of such a model in determining the inverse dynamics problem [21]. In the model used in this study, the segments are presumed to be rigid, while the joints include pure rotation without any translation. Apart from that, the shoulder complex also includes two translational degrees of freedom. The study of Veeger et al. [22] shows that the flexion-extension rotational center translation of the glenohumeral joint was within just 4 mm of the geometric center, making our assumption reasonably justified.

The study presented here simultaneously determines all three passive moments from the inverse dynamics model by using a robot manipulator. If compared to other studies on passive moments, the

method seems to be elegant from the subject point of view, with less physical constraining of particular arm segments required. The single required constraining mechanism in the process is the elbow orthosis, utilized for all shoulder movement trajectories, whereas all elbow motion trajectories are performed with all arm joints being completely unconstrained. Moreover the methods used for assessing the passive moments in other studies concentrate on masses and other dynamic parameters of the body segment in motion, enabling the determination of passive moments for only one considered joint.

The experimental results shown here were obtained for healthy individuals with an experimental setup using an industrial robot as the main apparatus. We expect that impaired subjects that we would like to measure in the future should show values clearly distinguishable from the results on intact subjects. Such measurements would be useful on patients with neuromuscular disorders, usually following a stroke or some neuromuscular disease. These patients are considered to be good candidates for treatment with new rehabilitation treatment devices such as haptic robots, which allow human machine interaction by means of force and touch. In these environments the methodology shown here would represent a measurement module. Such a method has the power to provide an alternative upper extremity clinical evaluation method, which could provide results instantaneously during the rehabilitation practice itself.

Acknowledgements

The authors would like to thank Prof. Garth R. Johnson from the University of Newcastle for his assistance during the initiation of this work and comments to the manuscript. This work was stimulated by the European Community project GENTLE/S–Quality of life under Framework 5.

Nomenclature

- $B(q)$ =moment of inertia matrix
- $C(q, \dot{q})$ =Coriolis matrix
- $G(q)$ =gravity matrix
- F_y =horizontal force component
- F_z =vertical force component
- F_d =dissipative coefficient matrix
- F_e =elastic coefficient matrix
- F_v =viscous coefficient matrix
- I_i =arm segment inertia
- J^T =Jacobian matrix transpose
- M_x =torque around x axis (perpendicular to the motion plane)
- a_i =segment length
- h =vector of end effector forces and moments
- l_i =segment center of gravity location
- l_{hand} =hand center of gravity location
- l_{handle} =rotating handle center of gravity location
- m_i =segment mass
- m_{fa} =forearm mass
- m_{lo} =lower orthosis part mass
- m_{ua} =upper arm mass

m_{uo} =upper orthosis part mass
 m_{hand} =hand mass
 m_{handle} =mass of rotating handle
 q =joint angle vector
 \dot{q} =joint velocity vector
 \ddot{q} =joint acceleration vector
 τ_p =passive moment vector
 $\tau(u)$ =voluntary muscle torque

References

- [1] A.M. Acosta, R.F. Kirsch and E.J. Perreault, A robotic manipulator for the characterization of two-dimensional dynamic stiffness using stochastic displacement perturbations, *Journal of Neuroscience Methods* **102** (2000), 177–186.
- [2] M.L. Audu and D.T. Davy, The influence of muscle model complexity in musculoskeletal motion modeling, *Journal of Biomechanical Engineering* **107** (1985), 147–156.
- [3] D.J. Bennett, Torques generated at the human elbow joint in response to constant position errors imposed during voluntary movements, *Experimental Brain Research* **95** (1993), 488–498.
- [4] D.J. Bennett, J.M. Hollerbach, Y. Xu and I.W. Hunter, Time varying stiffness of human elbow joint during cyclic voluntary movement, *Experimental Brain Research* **88** (1992), 433–442.
- [5] A.E. Engin and S.M. Chen, Statistical Data Base for the biomechanical properties of the human shoulder complex I: Kinematics of the shoulder complex, *Journal of Biomechanical Engineering* **108** (1986), 215–221.
- [6] A.E. Engin and S.T. Tumer, Three-dimensional kinematic modelling of the human shoulder complex–Part I: Physical model and determination of joint sinus cones, *Journal of Biomechanical Engineering* **111** (1988), 107–112.
- [7] A.E. Engin and S.T. Tumer, Three-dimensional kinematic modelling of the human shoulder complex–Part II: Mathematical modeling and solution via optimization, *Journal of Biomechanical Engineering* **111** (1988), 113–121.
- [8] A.E. Engin and S.M. Chen, Statistical Data Base for the biomechanical properties of the human shoulder complex–II: Passive resistive properties beyond the shoulder complex sinus, *Journal of Biomechanical Engineering* **108** (1986), 222–227.
- [9] A.E. Engin and S.M. Chen, Kinematic and passive resistive properties of human elbow complex, *Journal of Biomechanical Engineering* **109** (1987), 318–323.
- [10] A.E. Engin, R.D. Peindl, N. Berme and I. Kaleps, Kinematic and force data collection in biomechanics by means of sonic emitters– I: Kinematic data collection methodology, *Journal of Biomechanical Engineering* **106** (1984), 204–211.
- [11] A.E. Engin, R.D. Peindl, N. Berme and I. Kaleps, Kinematic and force data collection in biomechanics by means of sonic emitters– II: Force data collection and application to the human shoulder complex, *Journal of Biomechanical Engineering* **106** (1984), 212–219.
- [12] A. Esteki and J.M. Mansour, An experimentally based nonlinear viscoelastic model of joint passive moment, *Journal of Biomechanics* **29** (1996), 443–450.
- [13] H. Hatze, A three-dimensional multivariate model of passive human joint torques and articular boundaries, *Clinical Biomechanics* **12** (1997), 128–135.
- [14] F.C.T. Van der Helm, Analysis of the kinematic and dynamic behavior of the shoulder mechanism, *Journal of Biomechanics* **27** (1994), 527–550.
- [15] P. de Leva, Adjustments to Zatsiorsky-Seluyanov’s segment inertia parameters, *Journal of Biomechanics* **29** (1995), 1223–1230.
- [16] J.M. Mansour and M.L.L. Audu, The passive elastic moment at the knee and its influence on human gait, *Journal of Biomechanics* **5** (1996), 369–373.
- [17] E.J. Perreault, P.E. Crago and R.F. Kirsch, Estimation of intrinsic and reflex contributions to muscle dynamics: A modelling study, *IEEE transactions on biomedical engineering* **47** (2000), 1413–1421.
- [18] E.J. Perreault, R.F. Kirsch and P.E. Crago, Effects of shoulder stability on endpoint stiffness, *IEEE engineering in medicine and biology* (November/December 2000), 53–58.
- [19] R. Riener and T. Edrich, Identification of passive elastic moments in the lower extremities, *Journal of Biomechanics* **32** (1999), 539–544.
- [20] L. Siciliano and B. Sciacivco, *Modeling and control of robot manipulators*, The McGraw-Hill Companies, Inc, 1996.
- [21] M. Suzuki, Y. Yamazaki and K. Matsunami, Simplified dynamics of planar two-joint arm movements, *Journal of biomechanics* **33** (2000), 925–931.

- [22] H.E.J. Veeger, B. Yu, K. An and R.H. Rozendal, Parameters for modeling the upper extremity, *Journal of Biomechanics* **30** (2000), 647–652.
- [23] Y. Xu and J.M. Hollerbach, A robust ensemble data method for identification of human joint mechanical properties during movement, *IEEE transactions on biomedical engineering* **46** (2000), 409–419.
- [24] Y. Xu and J.M. Hollerbach, Identification of human joint mechanical properties from single trial data, *IEEE transactions on biomedical engineering* **45** (1998), 1051–1059.
- [25] Y.S. Yoon and M. Mansour, The passive elastic moments at the hip, *Journal of Biomechanics* **12** (1982), 905–910.

Appendix C

An identification technique for evaluating static body segment parameters in the upper extremity

Timotej Kodek, Marko Munih University of Ljubljana, Faculty of Electrical Engineering
Laboratory of Robotics and Biomedical Engineering
Tržaška 25, 1000 Ljubljana, Slovenia
E-mail: tim@robo.fe.uni-lj.si

Abstract—In this paper we present a method for identifying the static biomechanical parameters of all three upper extremity body segments. The experiment is based on coupling the human arm with an industrial robot which is then used for imposing a specified sagittal plane trajectory. Joint angles and forces in the contact point are collected during this process. An optimization based identification procedure was developed, which assumes the upper extremity model of a 3 Degree of Freedom (3DOF) rigid body planar structure in a closed kinematic chain configuration with the robot. The solution is based on fitting the joint torques calculated from contact forces to those predicted by the inverse dynamic model of the linkage. In order to verify the developed identification procedure the experiment was first performed on a 2DOF mechanical arm with dimensions similar to those of the actual arm. This mechanical model was designed using CAD software that provides an accurate assessment of all necessary dynamic parameters. A suitable low velocity trajectory was imposed into all joints, with very small angular deviations. The outcome of the identification is an estimate of masses and center of gravity (COG) coordinates for the lower arm and palm segments, their products for the upper arm and the passive moments around the measured angle of all joints in the sagittal plane. Finally, the results obtained for the human arm are compared to the literature estimates which are based on average population.

I. INTRODUCTION

In many of today's biomechanical studies there is a need for estimating static and dynamic body segment parameters such as masses, centers of gravity (COG) and inertial moments. These parameters are often required for modelling purposes as well as in studies which evaluate certain performances in fields such as rehabilitation engineering or kinesiological studies. Due to obvious difficulties in determining these data for a particular person directly, authors usually refer to studies from literature which state the desired parameters in the form of regression curves as a function of easily measurable quantities of such as body masses and body heights. The oldest such studies were made *in vitro* on cadavers and only dealt with a relatively small test group. The importance of such studies is indicated by the fact that the oldest one was already made in 1860 by Harless [17]. Among the still commonly cited *in vitro* studies are the pioneering works of Dempster (1955) [4] and Clauser (1969) [3]. The former analyzed 8 male cadavers with an average age of 68.5 years while the latter focused on a group of 13 male cadavers with an average age of 49.3 years. Today most such studies are non-invasive, performed *in vivo* and include much larger test groups. Among these one

of the best known was made by Russian scientists Zatsiorsky and Seluyanov [2] who used the γ ray absorption method for measuring average segment densities on a large group of 100 healthy young Caucasian male subjects. A slight modification of this method, performed by DeLeva [1], is often used in many present day biomechanical studies.

With technological progress made in the last decades some other non-invasive methods have also become available. The most significant ones are Computer Tomography (CT) and Magnetic Resonance Imaging (MRI), which both give detailed information concerning the distribution of internal structures such as tissues and bones in body segments. By assuming the mean tissue density values and accounting for the measured spacial distributions, it is then possible to calculate the values of various body segment parameters. Several attempts in this direction have already been made [13]–[16]. Out of these only the study of Wei and Jensen [15] was performed on a larger group consisting of 50 individuals. Others, however, do not give a comprehensive analysis on a very large test group of individuals, but it must be said that both methods offer good prospects for future research.

Considering all these studies a question of estimated regression curve accuracies arises since body segment properties among various people may differ quite significantly due to factors such as different body structure, age or sex. For example the average age of subjects involved in the study made by Zatsiorsky [2] was approximately 24 years, whereas many of today's studies requiring body segment parameters focus on older individuals who have in the past suffered from certain neuromuscular disorders. Hinrichs [8] stated: "The use of indirect estimates of body segment masses, centers of mass and moments of inertia is arguably one of the biggest sources of error in biomechanics research."

Because of the addressed problem this study proposes an alternative *in vivo* technique for determining values of static body segment parameters in the upper extremity by utilizing an optimization curve fitting technique. In the experiment, parameters were firstly estimated on a mechanical arm to obtain the accuracy level of the procedure. Afterwards the same process was performed on one healthy individual and the obtained data compared to studies from the literature.

The motivation for the presented study also comes as a result of new rehabilitation devices such as haptic robots [18], where this method could enable an on-line parameter estimation technique used for subsequent evaluations during

rehabilitation practice.

II. METHODS

The experiment is based on moving the upper extremity along a specified trajectory with an industrial robot (Fig. 1). During this process joint angle data was collected by means of an IR marker based motion tracking system (*Optotrak*[®]) as well as forces and moments in the contact point (*JR*³[®] force sensor). Collection frequencies in both cases were 50 Hz.

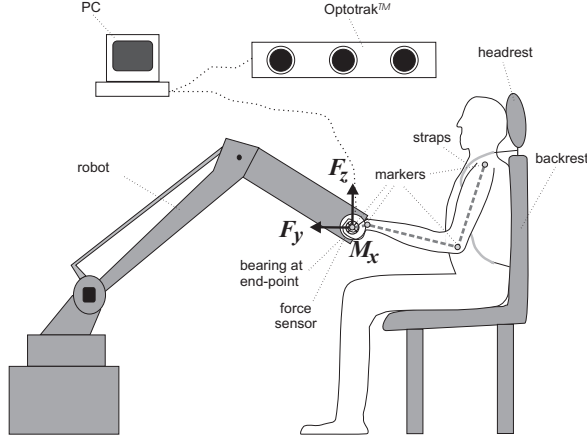


Fig. 1. A side view of the experimental setup. The subject is seated on a strap equipped passenger type seat which minimizes trunk movements. Three IR markers were attached above joint rotation centers as recommended in [1]. The contact forces and moments $F_e = [F_y, F_z, M_x]^T$ were measured with a 4D *JR*³ strain gauge force sensor. Due to a bearing at the robot attached handle, the torque value M_x was minimal.

The human arm description was simplified to the level of a 3DOF rigid body planar structure in the sagittal plane with the following notation (Fig. 2).

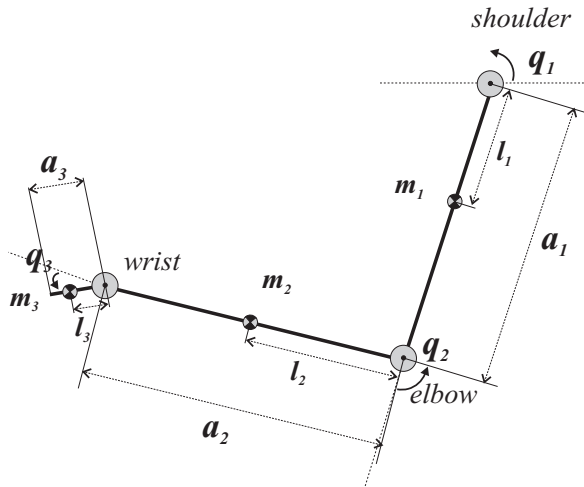


Fig. 2. Geometric definitions for the assumed human arm structure, consisting of three rigid body segments. The segment lengths are denoted with a_j , their COGs with l_j while q_j indicates joint angle directions with respect to the zero position (dashed line). The segment masses are presented with m_j .

The inverse dynamics is described as a relationship between applied muscle produced torques $\tau(u)$, environment forces F_e

and the joint motion trajectory \ddot{q} , \dot{q} , q of mechanical joints as in [5]:

$$B(q)\ddot{q} + C(q, \dot{q})\dot{q} + G(q) + \tau_{vel}(q, \dot{q}, u) = \tau(u) - \tau_e. \quad (1)$$

The angular velocity and acceleration data was obtained from joint angles with numerical derivation. Every one of the terms in Eq. 1 represent a three-dimensional torque vector with the shoulder as first, elbow as second and wrist as the third coordinate. $B(q)\ddot{q}$ represents *inertial contributions* and $C(q, \dot{q})\dot{q}$ the *centrifugal* and *Coriolis* effects on the arm dynamics. The viscoelastic moments τ_{vel} arise in every joint as a consequence of various structures (*e.g.* tendons, ligaments, muscles). They are a nonlinear function of adjacent joint angles and muscle activations u [7], [9]–[12]. On the right side of Eq. 1 there are active muscle contributions $\tau(u)$ and torques caused by the environment τ_e .

Let us assume that our experimental analysis was done *quasi-statically* and without any significant voluntary muscle activation u . This allows the following assumptions:

$$B(q)\ddot{q} \approx 0, \quad C(q, \dot{q})\dot{q} \approx 0, \quad \tau(u) \approx 0 \quad (2)$$

Accounting for all these, the simplified version of Eq. 1 can now be written as:

$$G(q) + \tau_p(q) = -\tau_e = -J^T(q)F_e \quad (3)$$

Gravity contributions $G(q)$ can be expressed as:

$$\begin{aligned} \tau_{g1} &= g_0 \{ [l_1 m_1 + a_1 (m_2 + m_3)] c_{11} + (l_2 m_2 + a_2 m_3) c_{12} + \\ &\quad + l_3 m_3 c_{123} \}, \\ \tau_{g2} &= g_0 [(l_2 m_2 + a_2 m_3) c_{12} + l_3 m_3 c_{123}], \\ \tau_{g3} &= g_0 l_3 m_3 c_{123}. \end{aligned} \quad (4)$$

The following notation is used: $c_{11} = \cos(q_1)$, $c_{12} = \cos(q_1 + q_2)$, $c_{123} = \cos(q_1 + q_2 + q_3)$ and $s_{11} = \sin(q_1)$, $s_{12} = \sin(q_1 + q_2)$, $s_{123} = \sin(q_1 + q_2 + q_3)$. g_0 denotes the gravity constant.

In Eq. 3, τ_{vel} has been replaced with passive moments $\tau_p(q)$ which are no longer velocity and muscle activation dependent but rather a nonlinear function of only the adjacent joint angles. They include elastic and direction dependent dissipative components, consisting mostly of passive muscles surrounding joints [11], [12]. The environment contribution τ_e are obtained by premultiplying the contact force vector $F_e = [F_y, F_z, M_x]^T$ with a jacobian matrix $J^T(q)F_e$ [5].

Parameter identification

Because angular deviations were small in all measurements ($\Delta|q_i| < 12^\circ$) we assumed that τ_p nonlinearities were small in this region. We can now express Eq. 3 as a linear relationship [6]:

$$Y_j \pi_j = \tau_j, \quad \text{at time } t_i \quad (5)$$

Y_j represents the regression vector, π_j the corresponding vector of identification parameters for segment j and τ_j all other terms which are not related to the identified variables in π_j .

Let us now describe the system in Eq. 5 with three consecutive linear equations, describing the inverse dynamics of every particular joint at time t_i :

- *Wrist joint:*

$$g_0 \cos_{123} m_3 l_3 + \tau_{p3} = \tau_{e3}$$

or in matrix form,

$$Y_3 \pi_3 = \begin{bmatrix} g_0 \cos_{123}, & 1 \end{bmatrix} \begin{bmatrix} m_3 l_3, & \tau_{p3} \end{bmatrix}^T = \tau_3 \quad (6)$$

Accounting for $m_3 l_3$ obtained from π_3 the elbow equation can be expressed.

- *Elbow joint:*

$$g_0 \cos_{12} m_2 l_2 + g_0 a_2 \cos_{12} m_3 + \tau_{p2} = \tau_{e2} - g_0 \cos_{12} m_3 l_3$$

or in matrix form,

$$Y_2 \pi_2 = \begin{bmatrix} g_0 \cos_{12}, & g_0 a_2 \cos_{12}, & 1 \end{bmatrix} \begin{bmatrix} m_2 l_2, & m_3, & \tau_{p2} \end{bmatrix}^T = \tau_2 \quad (7)$$

Accounting for $m_3 l_3$, $m_2 l_2$ and m_3 from π_3 and π_2 we can write the third equation (Eq. 8).

- *Shoulder joint:*

$$g_0 \cos_1 m_1 l_1 + g_0 a_1 \cos_1 m_2 + \tau_{p1} = \tau_{e1} - g_0 (a_1 \cos_1 + a_2 \cos_{12}) m_3 - g_0 \cos_{12} m_2 l_2 - g_0 \cos_{123} m_3 l_3$$

or in matrix form,

$$Y_1 \pi_1 = \begin{bmatrix} g_0 \cos_1, & g_0 a_1 \cos_1, & 1 \end{bmatrix} \begin{bmatrix} m_1 l_1, & m_2, & \tau_{p1} \end{bmatrix}^T = \tau_1 \quad (8)$$

From all three joint equations it can be deduced that the identification vectors π_j were chosen as $\pi_3 = [m_3 l_3, \tau_{p3}]^T$, $\pi_2 = [m_2 l_2, m_3, \tau_{p2}]^T$ and $\pi_1 = [m_1 l_1, m_2, \tau_{p1}]^T$. By considering Eq. 7 and Eq. 8, for every π_j at N time instants t_i , a linearly dependent problem is formed since a_2 and a_1 are constants. Therefore the problem of identifying vectors π_j was described as an optimization problem, which minimizes the difference between both sides of equation 5. At t_i , this difference can be expressed as the following function:

$$F_{t_i}(\pi_j) = \tau_j - Y_j \pi_j \quad (9)$$

The algorithm calculates π_j with a *constrained nonlinear least squares optimization* for all time samples $1 \leq t_i \leq N$ using the MatlabTM `lsqnonlin` function which solves the following minimization [19]:

$$\min_{\pi_j} \sum_{t_i=1}^N F_{t_i}(\pi_j)^2 \quad \text{such that} \quad l_b \leq \pi_j \leq u_b \quad (10)$$

The constraints l_b and u_b were chosen suitably for every particular identification vector.

Algorithm verification

To verify the accuracy of the described algorithm a preliminary experiment was made using a 2DOF mechanical arm. It was designed with CAD software which can calculate all dynamic parameters from geometry data. The segment lengths of the model were chosen comparably to the ones of the human arm as well as the segment masses (Fig. 3). To simulate joint passive moments, screw-adjustable rubber brakes were attached at every joint. These brakes produced

a desirable Coulomb friction force by pressing on stainless steel disks from both sides. The friction force was directly measured with a load cell mounted at a 45 degree angle which enabled the computation of brake-produced passive moments at every instant. The mechanical arm was coupled with the

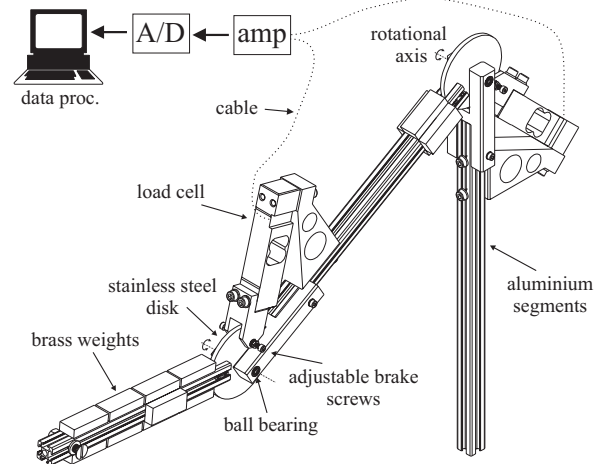


Fig. 3. The 2DOF mechanical model used for algorithm verification. Two HBM type PW2FC3 one dimensional aluminium strain gage load cells were used for measuring mechanical friction. To obtain masses comparable to the human arm, brass weights were properly attached to the aluminium segments. The load cell signals were amplified, digitalized and processed together with contact forces and Optotrak[®] motion data.

robot using a bearing attached screw while motion trajectories and contact forces were measured in the same way as with a human subject.

The identification procedure used, was the same as the one described previously, the only difference being the number of identification parameters. Since the model only consisted of two segments, only two identification vectors π_j had to be determined consisting of a total number of five identification parameters: ($\pi_2 = [m_2 l_2, \tau_{p2}]^T$ and $\pi_1 = [m_1 l_1, m_2, \tau_{p1}]^T$)

The best optimization results were obtained when the upper and lower optimization bounds (u_b and l_b in Eq. 10) for passive moments τ_{p_j} were initially set to values around zero producing $\pi_2 = [m_2 l_2, 0]^T$ and $\pi_1 = [m_1 l_1, m_2, 0]^T$. Let us now denote the identified passive moments with $\tau_{p_{jid}}$ which were obtained by observing the absolute difference between the joint torque trajectory τ_j and the corresponding identified trajectory $\tau_{jid} = Y_j \pi_j$ (Fig. 4 -left) as:

$$\tau_{p_{jid}} = \frac{1}{N} \sum_{t_i=1}^N |\tau_j(t_i) - \tau_{jid}(t_i)| \quad (11)$$

The imposed trajectory in this study was a flexion-extension movement as seen in Fig. 5. The curve fitting optimization problem described in Eq. 10 was performed throughout the whole τ_j trajectory. The friction components in τ_j can be observed as the difference between the measured and identified trajectories in Fig. 4 (left) and can be compared to the measured Coulomb friction torques on the right side of Fig. 4.

The same procedure was also used when determining passive moments in the human arm joints.

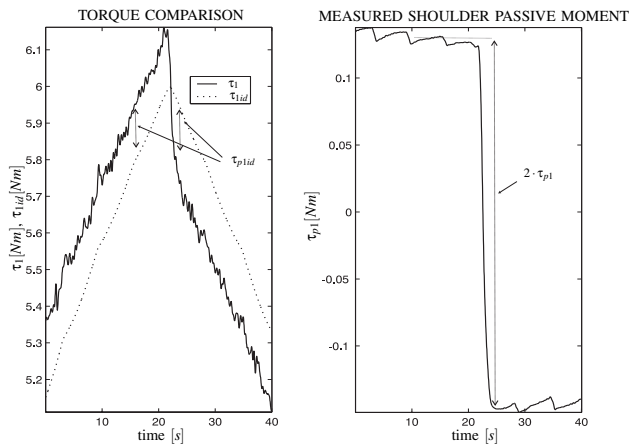


Fig. 4. τ_1 in the mechanical model computed as an average of 10 measurements (solid line - left) in comparison with the identified trajectory $\tau_{1, id} = Y_1 \pi_1$ (dotted line - left) along the whole time course of the mechanical arm motion. The arrow denotes how the passive moments $\tau_{p1, id}$ were obtained in the identification process. The right figure shows the measured brake-produced passive moments τ_{p1} and should roughly equal the difference between both trajectories in the left figure.

III. RESULTS

The motion trajectories imposed into the joints of the mechanical model and human arm were slow with velocities not exceeding 0.03 rad/s and an angular range of at most 12 degrees. It was verified beforehand that at such low velocities the dynamic terms from Eq. 1 had no significant effect on the arm dynamics (Fig. 5). Apart from that a preliminary EMG measurement of the significant arm flexion extension muscles (*i.e.* *biceps long head*, *biceps short head*, *triceps*, *brachioradialis*) was performed to prove that the muscle activation $\tau(u)$ had no significant effect on the contact force. 10 equal measurements were performed for further analysis on the left arm of one particular healthy individual.

Fig. 6 gives an insight into the contact force trajectories and the identified joint torques $\tau_{j, id}$ which were fitted to the measured torques τ_j for the mechanical model in both joints. The numerical results are represented separately for the mechanical arm in table I and for the human arm in table II. They were obtained using MATLABTM. In the mechanical arm the value of x_{ref} denotes the CAD obtained parameters values, while in the human arm this variable denotes literature estimates [1]. The identified parameter values are represented with \bar{x} as average values from 10 measurements. The 10 measurement standard deviations (σ_x) and differences in relative form $\left(\frac{x_{ref} - \bar{x}}{\bar{x}}\right)$ are also given in both tables.

IV. DISCUSSION

The proposed identification method enables a simultaneous computation of all presented static upper extremity biomechanical parameters in one single trial. It is friendly from the subject's point of view as it does not require any special fixation mechanisms and can be performed quickly.

The accuracy of the method can be deduced from the results obtained on the mechanical arm experiment (Table I). The highest error rate of 36.4% can be observed for parameter τ_{p1} ,

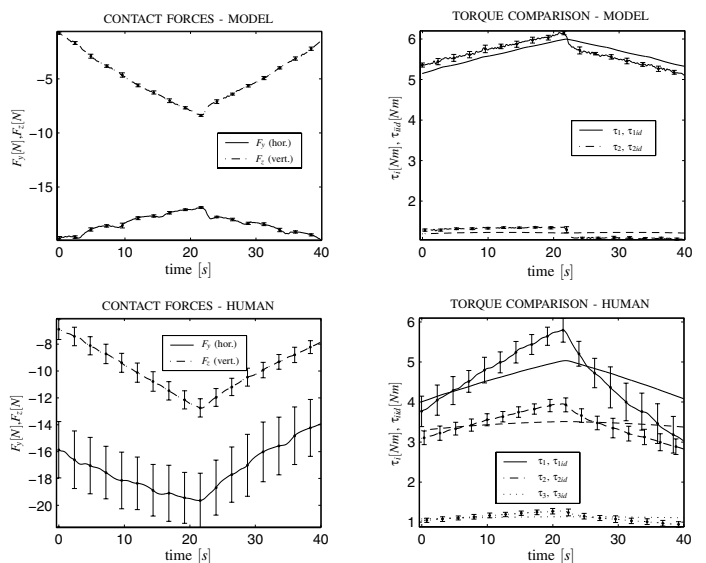


Fig. 6. Average horizontal (F_v) and vertical (F_h) contact forces with measurement standard deviations shown for the mechanical model (top - left) and the human arm (bottom - left). The right column gives a comparison between the average torques τ_i with their standard deviations in comparison to the corresponding identified torques $\tau_{i, id}$ for the mechanical model (top - right) and the human arm (bottom - right).

which seems relatively high. We attribute that mostly due to a non-ideal mechanical model. It is likely that the mechanical model passive properties are not only brake produced but arise also from small mechanical jitter and non-smooth point to point robot motion. Some non-smooth motion effects can be observed from load cell readings (Fig. 4 - right) and contact forces (Fig. 6 - left) as a low-frequency periodical perturbation. On the other hand, jitter could also be observed from the Optotrak[©] markers attached in the shoulder and wrist joints of the model. Errors in other parameters could be attributed to similar reasons and amount to as high as -9.1% in l_2 . Since this parameter value was obtained as $l_2 = \frac{m_2 l_2}{m_2}$ it includes errors in both parameters $m_2 l_2$ and m_2 .

The human arm parameter errors were given in relation to literature estimates which can not be viewed as an accurate source since the errors there are of unpredictable nature. Among the reasons contributing to errors in the human arm parameter estimates we speculate that the most important ones arise as a consequence of the rigid body and axial rotation assumptions (Fig. 2). Unlike in our assumption the real human arm is not composed of rigid bodies and has more DOF than just one single rotation in the joints. The other important error source can be attributed to inaccuracies in the measurement of joint angles and contact forces. These can be seen from larger standard deviations in Fig. 6. While joint angle errors can be explained by an inaccurate marker fixation, contact force errors come as a result of worse repeatability of human arm trajectories in comparison to the model. While errors in $m_3 l_3$ and consequently l_3 are relatively high, all others are very comparable to the literature. The reason for a high error in parameter $m_3 l_3$ is also the fact that the motion range of the wrist joint was relatively small (1.8°). Passive moment

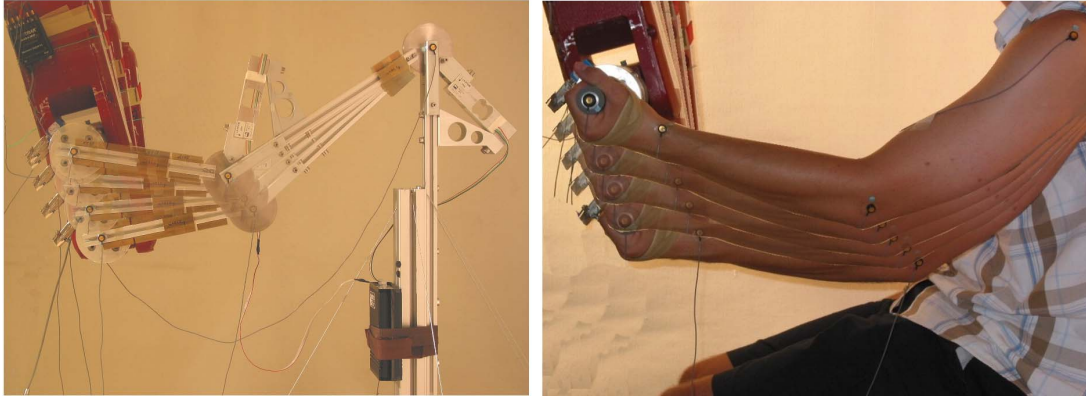


Fig. 5. Two composite images showing the complete courses of the mechanical arm trajectory with shoulder and elbow angular ranges of 11.4° and 11.5° respectively (left). The trajectory of the human arm (right) during the measurement with shoulder, elbow and wrist angular ranges of 12°, 3.4° and 1.8° respectively.

TABLE I
SIGNIFICANT PARAMETERS OBTAINED FOR THE MECHANICAL ARM.

parameter	x_{ref}	\bar{x}	σ_x	$\frac{x-\bar{x}_{ref}}{x_{ref}} [\%]$
$m_2 l_2 [kgm]$	0.130	0.126	0.001	-3.2
$m_2 [kg]$	1.160	1.204	0.001	3.8
$l_2 [m]$	0.115	0.105	0.001	-9.1
$m_1 l_1 [kgm]$	0.260	0.264	0.001	1.5
$\tau_{p2} [Nm]$	0.091	0.121	0.008	34.1
$\tau_{p1} [Nm]$	0.134	0.182	0.020	36.4

TABLE II
SIGNIFICANT PARAMETERS OBTAINED FOR THE HUMAN ARM.

parameter	x_{ref}	\bar{x}	σ_x	$\frac{x_{ref}-\bar{x}}{\bar{x}} [\%]$
$m_3 l_3 [kgm]$	0.061	0.117	0.007	92.1
$m_3 [kg]$	0.753	0.787	0.021	4.6
$l_3 [m]$	0.081	0.148	0.005	63.4
$m_2 l_2 [kgm]$	0.150	0.152	0.012	9.0
$m_2 [kg]$	1.264	1.148	0.043	-9.1
$l_2 [m]$	0.119	0.132	0.010	11.1
$m_1 l_1 [kgm]$	0.394	0.322	0.035	-18.2
$\tau_{p3} [Nm]$	/	0.074	0.007	/
$\tau_{p2} [Nm]$	/	0.228	0.022	/
$\tau_{p1} [Nm]$	/	0.453	0.083	/

references were not given in table II since they could not be reliably obtained from previous studies. Their values severely depend on the anatomical structure of the upper extremity which is very subject-dependent.

When comparing this method to existing studies [1] we can see that the general trend of the obtained parameter estimates is comparable to the parameters obtained with regression curves. It needs to be emphasized that our aim in this paper was to show that an evaluation of body segment parameters is possible with a method described in this work. A statistical analysis on a larger group of individuals therefore remains the focal point of future research.

ACKNOWLEDGMENT

This work was stimulated by the European Community project GENTLE/S - Quality of life under Framework 5 and the Ministry of education, science and sports of the republic of Slovenia.

REFERENCES

- [1] P. de Leva 1995. Adjustments to Zatsiorsky-Seluyanov's segment inertia parameters, *Journal of Biomechanics* 29, 1223-1230.
- [2] V. Zatsiorsky, V. Seluyanov 1983. The Mass and Inertia Characteristics of the Main Segments of the Human Body, *International Biomechanics* vol. 4B, Human Kinetic, Illinois, 1152-1159.

- [3] CE Clauser, JT Mac Conville, JW Young 1969. Weight, volume and center of mass of segments of human body, Wright Patterson Air Force Base: Aerospace Medical Research Laboratory.
- [4] WT Dempster, RT Gaughran 1969. Properties of body segments based on size and weight, Wright Patterson Air Force Base: Wright Air Development Center.
- [5] L. Siciliano, B. Sciavicco 1996. Modeling and control of robot manipulators, The McGraw-Hill Companies, Inc.
- [6] C.H. An, C.G. Atkeson, J.M. Hollerbach 1988. Model-Based Control of a Robot Manipulator, MIT Press.
- [7] T. Kodek, M. Muih, 2003. Quantification of shoulder and elbow passive moments in the sagittal plane as a function of adjacent angle fixations, *Journal of Technology and HealthCare* 11 89–103.
- [8] Hinrichs R.N. 1985. Regression Equations to Predict Segmental Moments of Inertia from Anthropometric Measurements: An Extension of the Data of Chandler et al. (1975). *Journal of Biomechanics*, 18, 621-624.
- [9] H. Hatze, 1997. A three-dimensional multivariate model of passive human joint torques and articular boundaries, *Clinical Biomechanics* 12, 128-135.
- [10] A. Esteki, J.M. Mansour, 1996. An experimentally based nonlinear viscoelastic model of joint passive moment, *Journal of Biomechanics* 29, 443-450.
- [11] R. Riener, T. Edrich, 1999. Identification of passive elastic moments in the lower extremities, *Journal of Biomechanics* 32, 539-544.
- [12] J.M. Mansour, M.L. Audu, 1986. The passive elastic moment at the knee and its influence on human gait, *Journal of Biomechanics* 5, 369-373.
- [13] P.E. Martin, M. Mungiole, M.W. Marzke, J.M. Longhill 1989. The use of magnetic resonance imaging for measuring segment inertial properties, *Journal of Biomechanics*, 22, 367-376.
- [14] M. Mungiole, P.E. Martin, 1990. Estimating segment inertial properties: Comparison of magnetic resonance imaging with existing methods, *Journal of Biomechanics*, 23, 1039-1046.
- [15] C. Wei, R.K. Jensen, 1995. The application of segment axial density profiles to a human body inertial model, *Journal of Biomechanics*, 28, 103-108.
- [16] N. J. Reynolds, S.E. Walt, 2002. The effect of error in inertial parameter estimation on walking and running kinetic analysis of gait, *Proceedings of the 7th International Symposium on the 3-D Analysis of Human Movement* 76-79.
- [17] Harless E., 1860. The Static Moments of Human Limbs. *Treatises of the Math-Phys Class of the Royal Acad Of Sc Of Bavaria*, 8, 257-294.
- [18] P.K.M. van de Hel and B.J.F. Diresen and M.P. Oderwald and S. Coote and E. Stokes, 2001. Gentle/S: Robot Mediated Therapy for Stroke Patients in a Virtual World Makes Exercising More Enjoyable and Effective, *proceedings of AAATE 2001*, 256-61.
- [19] Lawson C.L. and Hanson R.J., 1974. *Solving Least Squares Problems*, Prentice-Hall, pp 161.

Appendix D



ELSEVIER

Available at
WWW.MATHEMATICSWEB.ORG
POWERED BY SCIENCE @ DIRECT®

Simulation Modelling Practice and Theory 11 (2003) 297–311

**SIMULATION
MODELLING**
PRACTICE AND THEORY

www.elsevier.com/locate/simpat

An analysis of static and dynamic joint torques in elbow flexion-extension movements

Timotej Kodek ^{*}, Marko Munih

*Faculty of Electrical Engineering, University of Ljubljana, Slovenia Laboratory for Robotics,
Tržaška 25, 1000 Ljubljana, Slovenia*

Received 11 February 2002; received in revised form 29 April 2003; accepted 14 May 2003

Abstract

The goal of this study was to quantify shoulder, elbow and wrist dynamic and static torques in the elbow flexion-extension movements. The movements were supervised and produced by using an industrial robot manipulator that was capable of imposing a programmed arc trajectory at various velocities in the sagittal plane of the seated human subject. The muscles of the right arm being measured, were kept passive at all times of the experiment, to allow smooth guidance of the arm along a desired path.

These programmed trajectories allowed a very good motion repeatability, which is not possible in normal unconstrained movements. All four velocity and acceleration profiles were taken into account and applied to matrices describing the different dynamic components in the upper extremity motion. A range of velocities which correspond to everyday movements was tested.

The results reveal that the gravitational torque contributions have a prominent effect on the arm dynamics at low elbow velocities ($\dot{q} \approx 0.25$ rad/s). At these speeds the velocity and acceleration dependent terms can justifiably be discarded. However, at higher motion velocities ($\dot{q} \approx 1$ rad/s) the inertial and Coriolis-centrifugal contributions become non-negligible. Their effect is furthermore increased with speed and accompanied accelerations.

© 2003 Elsevier B.V. All rights reserved.

Keywords: Dynamic contributions; Static contributions; Inertial effect; Coriolis-centrifugal effect; Gravity; Human movement

^{*} Corresponding author. Tel.: +386-1-4768465; fax: +386-1-4768239.

E-mail addresses: timotej.kodek@robo.fe.uni-lj.si (T. Kodek), marko.munih@robo.fe.uni-lj.si (M. Munih).

Nomenclature

$B(q)$	moment of inertia matrix
$C(q, \dot{q})$	Coriolis matrix
$G(q)$	gravity vector
F_y	horizontal force component
F_z	vertical force component
F_d	dissipative coefficient matrix
F_e	elastic coefficient matrix
F_v	viscous coefficient matrix
I_i	arm segment inertia
$J^T(q)$	Jacobian matrix transpose
M_x	torque around x axis (perpendicular to the motion plane)
a_i	segment length
b_{ij}	coefficients of the inertial matrix $B(q)$
c_{ij}	coefficients of the Coriolis-centrifugal matrix $C(q, \dot{q})$
v_i	robot end effector velocity
h	vector of end effector forces and moments
l_i	segment center of gravity (COG) location
l_{hand}	hand center of gravity location
l_{handle}	rotating handle center of gravity location
m_i	segment mass
m_{fa}	forearm mass
m_{lo}	lower orthosis part mass
m_{ua}	upper arm mass
m_{uo}	upper orthosis part mass
m_{hand}	hand mass
m_{handle}	mass of rotating handle
q	joint angle vector
\dot{q}	joint velocity vector
\ddot{q}	joint acceleration vector
τ_B	inertial joint torque vector
τ_{bi}	inertial torque contribution in joint i
τ_C	Coriolis-centrifugal joint torque vector
τ_{ci}	Coriolis-centrifugal torque contribution in joint i
τ_G	gravity torque vector
τ_{gi}	gravity torque contribution in joint i
τ_p	passive moment vector
$\tau(u)$	voluntary muscle torque

1. Introduction

In movements of the human body there are many factors contributing to dynamic behavior of limbs which could be divided into two categories: (1) Firstly there are the static contributions which are present at all times such as the gravitational contributions and those arising from the specific biomechanical properties of the muscles, tendons, ligaments, and skin comprising a body segment. The latter are usually referred to as joint passive moments [1,2] and are only a function of joint angles. (2) On the other hand the dynamic contributions are in effect only when motion is in progress. The acceleration is linked to inertial contributions, while the Coriolis-centrifugal effects and viscosity relate to the joint speed of motion. Viscosity, like passive moments is an internal property of all joints in the human body whose effects are proportional to the angular speed of motion in a particular joint [3,4].

There has been a number of studies attempting to quantify the dynamic effects in human body motion, which were mostly concentrated on trajectories of the whole human body. Some studies have dealt with human locomotion [5], whereas in many other studies the dynamic effects in human rising was observed [6,7]. In the latter two studies the subject was asked to rise from a chair at various speeds at which the dynamic contributions were scrutinized, whereas the study of Pai et al. analyzed the dynamic effects of different body weight during the body rising action [8]. The dynamic effect that body motion has on the upper extremity was not studied to such an extent. Hollerbach and Flash studied the generation of various joint dynamic torques using the inverse dynamics Newton–Euler formulation in an experiment involving arm movements in the horizontal plane while holding a simple passive two degree of freedom manipulandum [9].

In the upper extremity dynamic studies there has been much work concentrated on studying angles and angular velocities, especially in the elbow and shoulder joints. The studies of Suzuki et al. and Lan have concentrated on normal reaching movements [10,11], whereas the study of Morasso studied a wide spectrum of every-day movements [12]. From all these measurements it is clearly evident that the arm joint angular velocity profiles are bell shaped. In fact the study of Zhang et al. [15] proved that the joint angle vs. time profiles, derived from point to point reaching movements can be directly scalable among different subjects independent of the motion speed. From this finding it can be deduced that the same applies also for the bell shaped velocity profiles. On the basis of the equilibrium point trajectory hypothesis, Flash derived a method for determining the magnitude of force exerted in the arm during reaching movements in the horizontal plane [13]. Similar conclusions and experimental methods can also be observed in the later work of Guomi and Kawato [14].

The study shown here is instigating the dynamic effects in the human shoulder, elbow and wrist joints in angle trajectories where the elbow is displaced through a wide range of its motion. Due to the experimental setup, where the arm is physically linked to the robot through a handle, and the robot follows the default trapezoidal velocity kinematic trajectory, the arm is also exposed to a trapezoidal joint velocity profile. Trajectories with multiple points are programmed into the robot controller in advance, meaning that the same arm trajectory can be replicated as many times as

desired. This technique with all the conditions being well defined is distinguishing this work from other studies in the field.

To get various dynamic situations during the measurement, the elbow of one subject was moved at four different speeds while following the same arc trajectories. During these actions the inertial and Coriolis-centrifugal dynamic contributions were observed and at the same time compared with the static gravity contributions.

2. Methods

2.1. Mathematical modelling

In this experimental work the human arm was described as a three degree of freedom kinematic and dynamic structure (Fig. 1).

The segment lengths are denoted with a_i , their centers of gravity (COG) with l_i while q_i indicates the positive angle directions with respect to the zero position (*dashed line*). The segment masses and inertias are presented with the m_i and I_i variables. The COG locations l_i are expressed as a distal distance from the joint marked with the same index. As in every other manipulator system, the dynamic behavior, as a relationship between applied driving torques $\tau(u)$, environment forces h and joint motion trajectories \ddot{q} , \dot{q} , q of mechanical joints can be described as [16]:

$$B(q)\ddot{q} + C(q, \dot{q})\dot{q} + G(q) + F_v\dot{q} + F_cq + F_d \operatorname{sgn}(\dot{q}) = \tau(u) - J^T(q)h. \tag{1}$$

Here q , \dot{q} and \ddot{q} represent the joint angle, angular velocity and angular acceleration vectors, which are functions of time, but were for simplicity reasons denoted with q instead of $q(t)$. They can be expressed as column vectors with indices 1, 2 and 3 referring to the shoulder, elbow and wrist respectively:

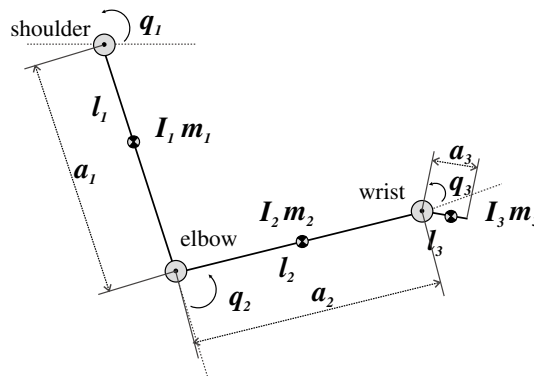


Fig. 1. Geometric definitions for the assumed human arm structure, consisting of three segments.

$$\begin{aligned}
 q &= [q_1 \quad q_2 \quad q_3]^T, \\
 \dot{q} &= [\dot{q}_1 \quad \dot{q}_2 \quad \dot{q}_3]^T, \\
 \ddot{q} &= [\ddot{q}_1 \quad \ddot{q}_2 \quad \ddot{q}_3]^T.
 \end{aligned}
 \tag{2}$$

The *moments of inertia* are represented as a (3×3) $B(q)$ matrix. The diagonal elements of the matrix represent the moment of inertia at joint i axis, while the other two joints are fixed, whereas the non-diagonal ones account for the acceleration effect of joint i on joint j . For a 3-DOF planar manipulator the inertial matrix elements were derived as follows:

$$B(q) = \begin{bmatrix} b_{11} & b_{12} & b_{13} \\ b_{21} & b_{22} & b_{23} \\ b_{31} & b_{32} & b_{33} \end{bmatrix},
 \tag{3}$$

$$\begin{aligned}
 b_{11} &= I_1 + I_2 + I_3 + l_1^2 m_1 + (a_1^2 + l_2^2) m_2 + (a_1^2 + a_2^2 + l_2^2) m_3 \\
 &\quad + 2a_1(l_2 m_2 + a_2 m_3) c_2 + 2l_3 m_3(a_2 c_3 + a_1 c_{23}), \\
 b_{12} &= I_2 + I_3 + l_2^2 m_2 + (a_2^2 + l_3^2) m_3 + a_1(l_2 m_2 + a_2 m_3) c_2 \\
 &\quad + 2a_2 l_3 m_3 c_3 + a_1 l_3 m_3 c_{23}, \\
 b_{13} &= I_3 + l_3^2 m_3 + a_2 l_3 m_3 c_3 + a_1 l_3 m_3 c_{23}, \\
 b_{21} &= I_2 + I_3 + l_2^2 m_2 + (a_2^2 + l_3^2) m_3 + a_1(l_2 m_2 + a_2 m_3) c_2 \\
 &\quad + 2a_2 l_3 m_3 c_3 + a_1 l_3 m_3 c_{23}, \\
 b_{22} &= I_2 + I_3 + l_2^2 m_2 + (a_2^2 + l_3^2) m_3 + 2a_2 l_3 m_3 c_3, \\
 b_{23} &= I_3 + l_3^2 m_3 + a_2 l_3 m_3 c_3, \\
 b_{31} &= I_3 + l_3^2 m_3 + a_2 l_3 m_3 c_3 + a_1 l_3 m_3 c_{23}, \\
 b_{32} &= I_3 + l_3^2 m_3 + a_2 l_3 m_3 c_3, \\
 b_{33} &= I_3 + l_3^2 m_3.
 \end{aligned}
 \tag{4}$$

Multiplying this matrix with the joint accelerations \ddot{q} yields a vector of inertial contributions in all three joints $\tau_B = B(q)\ddot{q}$:

$$\tau_B = [\tau_{b1} \quad \tau_{b2} \quad \tau_{b3}]^T.
 \tag{5}$$

The second matrix, $C(q, \dot{q})$ is identifying the *centrifugal* effects in its diagonal coefficients, while non-diagonal ones account for the *Coriolis* effect induced on joint i by the velocity of joint j . For the given configuration the elements were specified as

$$C(q, \dot{q}) = \begin{bmatrix} c_{11} & c_{12} & c_{13} \\ c_{21} & c_{22} & c_{23} \\ c_{31} & c_{32} & c_{33} \end{bmatrix},
 \tag{6}$$

$$\begin{aligned}
 c_{11} &= -\{a_1[(l_2m_2 + a_2m_3)s_2 + l_3m_3s_{23}]\dot{q}_2 + l_3m_3(a_2s_3 + a_1s_{23})\dot{q}_3\}, \\
 c_{12} &= 0.5\{-2a_1[(l_2m_2 + a_2m_3)s_2 + l_3m_3s_{23}](\dot{q}_1 + \dot{q}_2) - 2l_3m_3(a_2s_3 + a_1s_{23})\dot{q}_3\}, \\
 c_{13} &= -l_3m_3(a_2s_3 + a_1s_{23})\dot{q}_{123}, \\
 c_{21} &= a_1[(l_2m_2 + a_2m_3)s_2 + l_3m_3s_{23}]\dot{q}_1 - a_2l_3m_3s_3\dot{q}_3, \\
 c_{22} &= -a_2l_3m_3s_3\dot{q}_3, \\
 c_{23} &= -a_2l_3m_3s_3\dot{q}_{123}, \\
 c_{31} &= l_3m_3[(a_2s_3 + a_1s_{23})\dot{q}_1 + a_2s_3\dot{q}_2], \\
 c_{32} &= a_2l_3m_3s_3(\dot{q}_1 + \dot{q}_2), \\
 c_{33} &= 0
 \end{aligned} \tag{7}$$

which after applying the velocity vector \dot{q} defines the joint torque dynamic contributions $\tau_C = C(q, \dot{q})\dot{q}$:

$$\tau_C = [\tau_{c1} \quad \tau_{c2} \quad \tau_{c3}]^T. \tag{8}$$

The *gravitational* contribution is expressed with a three element column vector. Every element of the τ_G vector represents the moment generated at the joint i axis as a result of the segment gravity:

$$G(q) = [\tau_{g1} \quad \tau_{g2} \quad \tau_{g3}]^T, \tag{9}$$

where

$$\begin{aligned}
 \tau_{g1} &= g_0\{[l_1m_1 + a_1(m_2 + m_3)]c_1 + (l_2m_2 + a_2m_3)c_{12} + l_3m_3c_{123}\}, \\
 \tau_{g2} &= g_0[(l_2m_2 + a_2m_3)c_{12} + l_3m_3c_{123}], \\
 \tau_{g3} &= g_0l_3m_3c_{123}.
 \end{aligned} \tag{10}$$

In these equations the following abbreviations were used: $c_1 = \cos(q_1)$, $c_{12} = \cos(q_1 + q_2)$, $c_{123} = \cos(q_1 + q_2 + q_3)$ and $s_1 = \sin(q_1)$, $s_{12} = \sin(q_1 + q_2)$, $s_{123} = \sin(q_1 + q_2 + q_3)$. While the individual segment lengths a_i were determined before a particular measurement from IR markers used by a 3D positioning system, the masses m_i , transversal segment inertial values around the COGs I_i and COG locations l_i , were obtained from the literature [17]. The gravitational acceleration g_0 was taken to be 9.81 m/s². The values used are given in Table 1.

The connection between the human hand and the robot handle (see Section 2) creates a closed chain kinematic linkage. Thus, the end effector connection is described as a three dimensional vector with its horizontal and vertical forces (F_x, F_z) and the moment around the axis perpendicular to the plane of motion (M_y) (2):

$$h = [F_x \quad F_z \quad M_y]^T. \tag{11}$$

It should be noted that h is also a function of time. These forces have to be transformed to the joint space with the Jacobian matrix $J^T(q)$ as seen in Eq. (1).

The viscous contribution of the system is expressed with the term $F_v\dot{q}$. F_v is a 3 × 3 diagonal matrix of viscosity coefficients. $F_d \operatorname{sgn}(\dot{q})$ indicates the dissipative torques

Table 1

The values of parameters m_i , l_i and I_i as estimated from the literature [17] and segment lengths a_i as measured during the experiment

m_1 [kg]	2.09
m_2 [kg]	1.25
m_3 [kg]	0.75
l_1 [m]	0.19
l_2 [m]	0.12
l_3 [m]	0.08
I_1 [kg m ²]	0.005
I_2 [kg m ²]	0.001
I_3 [kg m ²]	0.006
m_3 [kg]	0.75
a_1 [m]	0.32
a_2 [m]	0.25
a_3 [m]	0.09

with F_d being a 3×3 diagonal matrix. In the literature this product is usually denoted as the static friction torque [16]. Finally, the passive elastic torque contributions in a particular joint are expressed with the product $F_e q$, where F_e is a 3×3 diagonal matrix with the elements expressing the elasticity coefficients of every single joint.

The next observation concerns the term $\tau(u)$ in Eq. (1). The joint muscle activity is expressed in terms of the active contribution $\tau(u)$, which is in general, a function of muscle activation u . Because the subject was instructed, before the experiment, to induce no voluntary muscle action, an assumption was made:

$$\tau(u) \approx 0. \quad (12)$$

To verify if this was justified, the EMG of a typical elbow flexion-extension was recorded prior to the large batch of experiments, to access the difference between active contribution of the person and inactivity. The surface electrodes were placed on the four major flexion and extension muscles by a skilled professional (i.e. *biceps* long and short head, *triceps* and *brachioradialis*). It was evident that no EMG activity in those muscles contributing to the movement was present. Due to lack of space this is not shown in this presentation.

2.2. Measurement

In the current experiment a positionally controlled anthropomorphic 6-DOF industrial robot (*Yaskawa*[®] *MOTOMAN sk6*) was used for imposing a linear movement trajectory into the human arm in the sagittal plane (Fig. 2). A bicycle-like circular, rubber coated aluminium handle was mounted on top of the sensor in such a way, that rotation around the y axis was freely allowed. The next element in the system was a bus passenger seat, equipped with additional straps as evident from Fig. 2. The plane of motion was perpendicular to the ground and fully aligned with the sagittal plane of the subject. The subject was asked to keep his muscles relaxed at all times, while resting the arm on the handle.

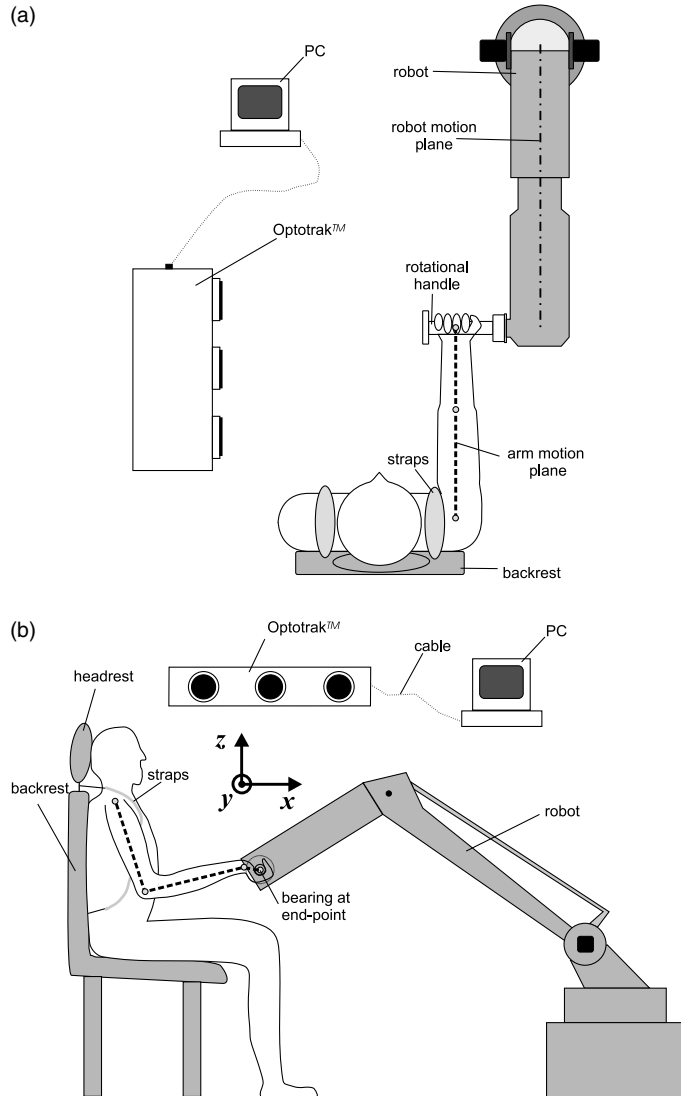


Fig. 2. Experimental setup from above (a) and a side view (b).

The handle was held gently, while still allowing the arm to stay in good contact during the movement. Due to the free handle rotation, the hand dynamic parameters were properly adjusted by considering the mass and all geometric dimensions of the handle which were accurately measured before the experiment. The handle mass m_{handle} was then added to the one of the hand m_{hand} , to yield a new third segment mass m_3 , while the COG locations l_{handle} and l_{hand} were also considered in obtaining a new location l_3 :

$$m_3 = m_{\text{hand}} + m_{\text{handle}},$$

$$l_3 = \frac{l_{\text{hand}}m_{\text{hand}} + l_{\text{handle}}m_{\text{handle}}}{m_{\text{handle}} + m_{\text{hand}}}. \quad (13)$$

In all measurements the elbow angle was moved linearly through a large portion of its motion range, while the shoulder was fixed at approximately -68° . The wrist was allowed to move freely, since the deviation from the neutral position ($q_3 = 0$) was found to be very small. All together four sets of measurements at various robot end effector velocities were made ($v_1 = 0.375$ m/s, $v_2 = 0.25$ m/s, $v_3 = 0.125$ m/s and $v_4 = 0.1$ m/s) resulting in elbow angular velocities of approximately $|\dot{q}_{21}| \approx 1$ rad/s, $|\dot{q}_{22}| \approx 0.65$ rad/s, $|\dot{q}_{23}| \approx 0.3$ rad/s and $|\dot{q}_{24}| \approx 0.25$ rad/s respectively.

The shoulder angle was kept constant by programming an appropriate arc trajectory for the subject, using no additional fixation mechanisms (Fig. 3).

The 3D tracking system *Optotrak*[®] was used to record precisely the movements of the arm during the experiment. The IR markers were attached to the skin above the rotation points of the three arm joints in consideration, to the handle and also to robot manipulator joints to allow for later verification and complete reconstruction of the measurement. The marker data was sampled at a frequency of 50 Hz, which is enough for recording human joint movements that are well within 10 Hz. All data processing was performed off-line using Matlab[®]. To remove the noise contribution, the *Optotrak*[®] sensor data was low-pass filtered at 8 Hz using a sixth order Butterworth filter provided by the Matlab[®] Signal Processing toolbox.

One healthy right-handed male who never suffered from any kind of neuromuscular disease was tested in the process (mass 77 kg, age 25) after an institutional approval. He was asked to sit in a chair, lightly grip the robot attached handle with his right arm and not exert any voluntary muscle action. Before the experiment at

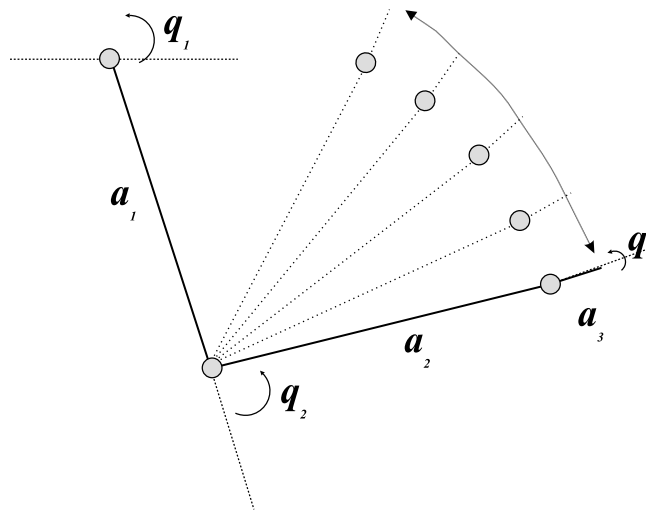


Fig. 3. The programmed elbow trajectory.

least two preliminary tests movements were made to assure that the programmed trajectory was appropriate and that the subject was comfortable. Every trial was performed under the same environmental conditions. After all these conditions were met, every one of the four different velocity trajectories was measured twice in a row. The measurement process was started with the lowest programmed speed in the first trial and later increased for every subsequent trial.

3. Results

First the repeatability of all three angle, velocity and acceleration trajectories for a typical elbow movement was analyzed. The repeatability issue indicates the capability of the apparatus and human arm to recreate the same trajectory at different times, under equal environmental conditions. For this reason six equal movement trials were recorded at the slowest trajectory with a constant elbow angular velocity of: $|\dot{q}_{21}| \approx 0.25$ rad/s (Fig. 4).

The angle standard deviations lie within ± 0.05 rad for the shoulder, ± 0.1 rad for the elbow and ± 0.2 rad for the wrist joint. When programming this trajectory it was

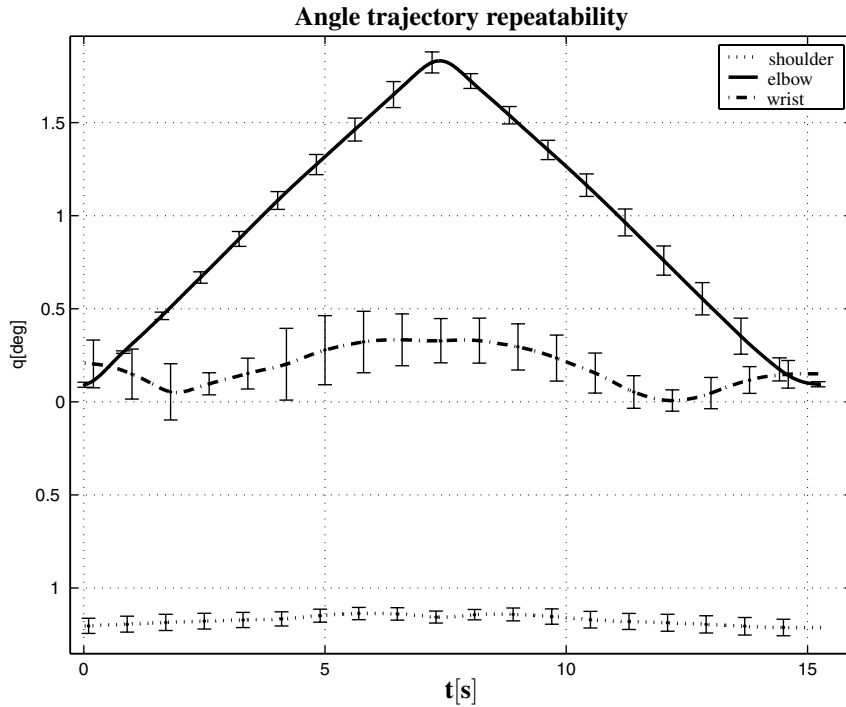


Fig. 4. Average angle trajectories with their maximum and minimum standard deviations in six consecutive same trajectory movements, where the elbow was displaced at the lowest angular velocity ($|\dot{q}_{21}| = 0.25$ rad/s).

desired to keep the shoulder and wrist angles as constant as possible. But positioning the arm fully equally at every trial was very difficult, which lead to some deviations that could be observed. The robot speed for all arm velocities was well within the operational robot speed range meaning that a similar conclusion can be deduced for all three remaining higher angular velocities ($|\dot{q}_{22}| \approx 0.3$ rad/s, $|\dot{q}_{23}| \approx 0.65$ rad/s, $|\dot{q}_{24}| \approx 1$ rad/s).

The kinematic data obtained from the four different-speed elbow joint trajectories need to be observed. The velocities were obtained by applying a simple first order difference equation to the low-pass filtered angle data, whereas accelerations were produced with the same procedure implemented on velocity trajectories (Fig. 5).

These data were used to determine particular dynamic components that contribute to human arm motion (Fig. 6). Because of a different scaling it should be noted that in both plots (Figs. 5 and 6) every row corresponds to a different velocity, the slowest being presented in the first row. With the increase of velocity the acceleration dependent inertial contribution $B(q)\ddot{q}$ and the velocity dependent Coriolis-centrifugal contribution $C(q, \dot{q})\dot{q}$ start to have a significant influence on the total joint torques (Fig. 6).

Please note that only the dynamic components change with speed, while the static gravity contribution is not a function of velocities and accelerations and therefore remains relatively constant with respect to a given angle. At low speeds the dynamic

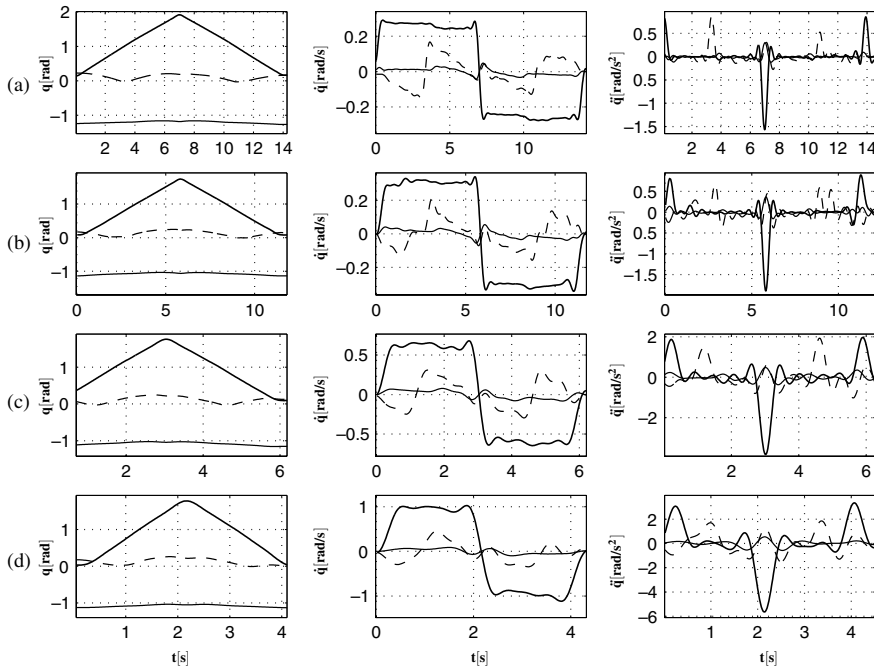


Fig. 5. Angle, velocity and acceleration profiles in all four trials when the maximum elbow angular velocities were $|\dot{q}_{21}| \approx 0.25$ rad/s (a), $|\dot{q}_{22}| \approx 0.3$ rad/s (b), $|\dot{q}_{23}| \approx 0.65$ rad/s (c) and $|\dot{q}_{24}| \approx 1$ rad/s (d) for the shoulder (thick solid), elbow (thin solid) and wrist (thin dashed) respectively.

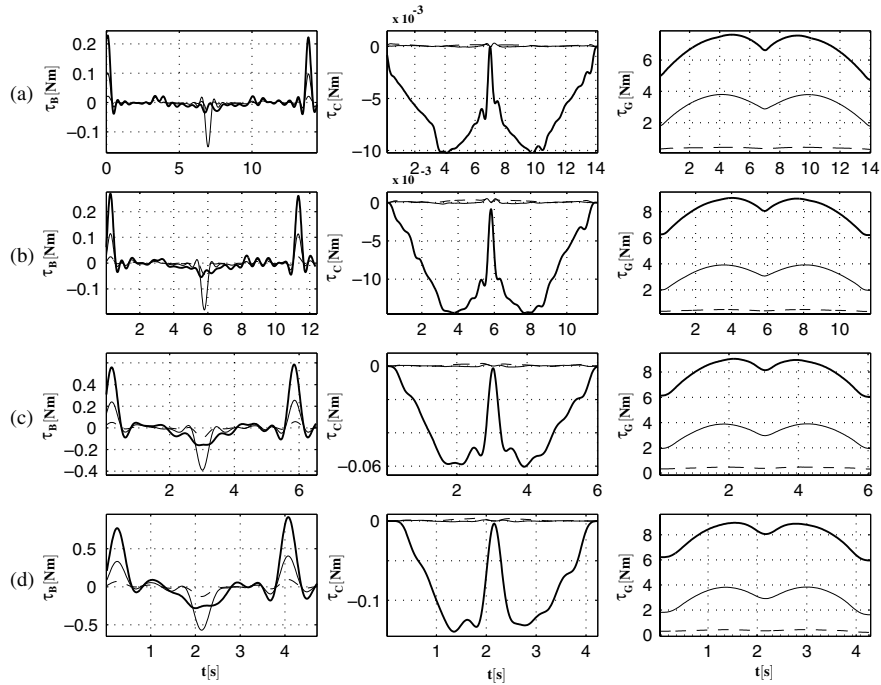


Fig. 6. The inertial, Coriolis and gravity contributions at $|\dot{q}_{21}| \approx 0.25$ rad/s (a), $|\dot{q}_{22}| \approx 0.3$ rad/s (b), $|\dot{q}_{23}| \approx 0.65$ rad/s (c) and $|\dot{q}_{24}| \approx 1$ rad/s (d) for the shoulder (thick solid), elbow (thin solid) and wrist (thin dashed) respectively.

contribution to motion is nearly negligible and is noticeable only at times of motion direction alterations. This effect becomes larger and can also be observed elsewhere with an increase in speed (Fig. 6).

4. Discussion and conclusion

In this paper, different dynamic and static contributions to human arm dynamics are investigated and quantified. Because the computed values of the inertial, Coriolis-centrifugal and gravity contributions directly depend on the obtained kinematic data, the repeatability of different trial angle readings is very important and had to be verified (Fig. 4). The velocity profiles generated with the robot manipulator were trapezoidal, which is in contrast with every-day action, bell-shaped velocity trajectories [10–12,15] (Fig. 5). After obtaining angular velocities and accelerations of particular joints all the kinematic data were applied to Eqs. (4), (7) and (10) respectively. As an outcome, the contributions of the two dynamic and one static term are shown separately (Fig. 6).

In this study only trajectories of the elbow joint were inspected. In ideal conditions the shoulder and wrist should not have any dynamic contributions to motion

but since the velocities and accelerations were non-zero (Fig. 5) this also implies non-zero dynamic contributions. The reason for using the robot manipulator for performing the described motions was that trajectories could be precisely recreated at any time while also allowing for a later complete recreation of the experiment. Nevertheless, the angle trajectories show a slightly smoother flexion-extension transition at higher velocities, which can be attributed to an increased error in positioning of the robot at higher speeds. Considering the fact that the robot movement velocities were well below the maximum possible values, the robot dynamic effects can be neglected.

It needs to be pointed out that the two dynamic contributions, which were the subject of this study (Fig. 6), are not the only dynamic components contributing to upper extremity motion. The viscosity torques $F_v\dot{q}$ from Eq. (1) also have a speed dependent effect on total torques and were not investigated in detail. The identification of $F_v\dot{q}$ exceeds the scope of this presentation and remains the topic for further investigations. The same applies for the sum of elastic and dissipative contributions $F_cq + F_d\text{sgn}(\dot{q})$, which have a considerable angle dependent effect. The viscosity and elastic contributions to motion in the upper extremity were pointed out in some other studies [1–3,18,21].

At low velocities the dynamic contributions to motion (Fig. 6(a)) are almost zero. As found, practically all studies (e.g. [1,2]) dealing with low velocity segment motions discard the dynamic contributions resulting in a substantial model simplification. Applying this fact and the fact that there are no active muscle contributions τ in the inverse dynamics upper extremity model presented in Eq. (1) leads to a very simple model representation:

$$G(q) + F_cq + F_d\text{sgn}(\dot{q}) = -J^T(q)h. \quad (14)$$

This means that the arm dynamics at low velocities is only influenced by the sum of gravitational effects $G(q)$ and passive moments which include elastic muscle and tissue contributions (F_cq) and velocity dependent dissipative effects to motion ($F_d\text{sgn}(\dot{q})$). Deducing from Fig. 6 we think it could be said that such joint velocities should not exceed 0.3 rad/s. At higher speeds the dynamic effects become considerable and are in proportion with the increase in angular velocities and accelerations. The inertial contribution vectors (Fig. 6—column 1) show the highest values at points of movement direction alterations whereas the Coriolis-centrifugal contributions (Fig. 5—column 2) play a much more significant role in the elbow joint than in the adjacent joints. This arises from the elbow angular velocities \dot{q} (Fig. 5—column 2) being much larger than the velocities of other two joints.

Because the computation of the inertial and Coriolis-centrifugal contributions are directly dependent on the derived velocities and accelerations, the method used for this derivation plays a significant role. The differentiation method utilized here is straightforward, using a low-pass Butterworth filter with an 8 Hz bandwidth frequency and a first order numerical derivative. It also needs to be emphasized that the bandwidth frequency significantly influences the results, especially the acceleration computations. The bandwidth was chosen after examining the amplitude spectrum of the angle, velocity and acceleration profiles.

The maximal elbow velocity trajectory $|\dot{q}_{24}| \approx 1$ rad/s from this study is comparable to everyday normal arm movements such as eating or reaching [10–14]. According to the results presented in Fig. 6 the contribution of dynamic terms $B(q)\ddot{q}$ and $C(q, \dot{q})\dot{q}$, in the fast movements is already considerable but still far smaller in comparison with the static gravity contribution. Although the velocity profiles in this study are not bell-shaped the computed contributions still give a reliable insight into torques during every-day actions.

Owing to the fact that the planar model structure is mathematically far less complex to describe than any other alternative, some studies suggest that the motor control system in the human brain actually uses a simplified version of such a model in determining the inverse dynamics problem [19]. In the model used in this study, the segments are presumed to be rigid, while the joints include pure rotation without any translation, which by itself is already a source of error. Apart from that, the shoulder complex also includes two translational degrees of freedom. The study of Veeger et al. [20] shows that the flexion-extension rotational center translation of the glenohumeral joint was within just 4 mm of the geometric center, making our presumption reasonably justified.

A very important issue that we have to be aware of are also anthropometric parameters from the literature [17] (Table 1) used for calculating the $B(q)$, $C(q, \dot{q})$ and $G(q)$ matrices. Masses (m_i), inertial moments (I_i) and COGs (l_i) were obtained by means of regressive equations based on body mass and height. Discrepancies in the estimation of these parameters directly influence coefficients of matrices $B(q)$, $C(q, \dot{q})$ and $G(q)$ as derived in Eqs. (4), (7) and (10). From these equations it can be observed that erroneous estimates of the anthropometric parameters (m_i , l_i , I_i) directly affect the results. However the COG (l_i) quadratically influences the inertial moments (Eq. (4)) just like the segment length a_i . Since the segment lengths were directly measured they can be considered a much more reliable quantity and are presumably not a major error source. It is quite impossible to estimate exactly the errors due to wrong parameter estimates from a literature study [17] which analyzed a population of 100 young male subjects. A further analysis dealing with the impact of parameter estimation errors on calculated torques could result in higher accuracy in the future.

Acknowledgement

This work was stimulated by the European Community project GENTLE/S—Quality of life under Framework 5.

References

- [1] H. Hatze, A three-dimensional multivariate model of passive human joint torques and articular boundaries, *Clinical Biomechanics* 12 (1997) 128–135.
- [2] A. Esteki, J.M. Mansour, An experimentally based nonlinear viscoelastic model of joint passive moment, *Journal of Biomechanics* 29 (1996) 443–450.

- [3] A.E. Engin, On the damping properties of the shoulder complex, *Journal of Biomechanical Engineering* 106 (1984) 360–363.
- [4] C.C.A.M. Gielen, J.C. Houk, S.L. Marcus, L.E. Miller, Viscoelastic properties of the wrist motor servo in man, *Annals of Biomedical Engineering* 12 (1984) 599–620.
- [5] G. Wu, Z. Ladin, Limitations of quasi-static estimation of human joint loading during locomotion, *Medical and Biological Engineering and Computing* 34 (1996) 472–476.
- [6] T.M. Bernard, M.M. Ayoub, C.J. Lin, Effects of speed of lift on static and inertial moments at the joints, *International Journal of Industrial Ergonomics* 24 (1999) 39–47.
- [7] E.B. Hutchinson, P.O. Riley, D.E. Krebs, A dynamic analysis of the joint forces and torques during rising from a chair, *IEEE Transactions on Rehabilitation Engineering* 2 (2) (1994) 49–56.
- [8] Y. Pai, M.W. Rogers, Control of body mass transfer as a function of speed of ascent in sit-to-stand, *Medicine and Science in Sports and Exercise* 22 (3) (1989) 378–384.
- [9] J.M. Hollerbach, T. Flash, Dynamic interactions between limb segments during planar arm movement, *Biological Cybernetics* 44 (1982) 67–77.
- [10] N. Lan, Analysis of an optimal control model of multi-joint arm movements, *Biological Cybernetics* 76 (1997) 107–117.
- [11] M. Suzuki, Y. Yamazaki, N. Mizuno, K. Matsumami, Trajectory formation of the center-of-mass of the arm during reaching movements, *Neuroscience* 76 (1997) 597–610.
- [12] P. Morasso, Three dimensional arm trajectories, *Biological Cybernetics* 48 (1983) 187–194.
- [13] T. Flash, The control of hand equilibrium trajectories in multi-joint arm movements, *Biological Cybernetics* 57 (1987) 257–274.
- [14] H. Guomi, M. Kawato, Equilibrium-point control hypothesis examined by measured arm stiffness during multijoint movement, *Science* 272 (1996) 117–120.
- [15] X. Zhang, D.B. Chaffin, The effects of speed variation on joint kinematics during multisegment movements, *Human Movement Science* 18 (1999) 741–757.
- [16] L. Siciliano, B. Sciavicco, *Modeling and control of robot manipulators*, The McGraw-Hill Companies, New York, 1996.
- [17] P. de Leva, Adjustments to Zatsiorsky–Seluyanov’s segment inertia parameters, *Journal of Biomechanics* 29 (1995) 1223–1230.
- [18] A.E. Engin, S.M. Chen, Kinematic and passive resistive properties of human elbow complexon, *Journal of Biomechanical Engineering* 109 (1987) 318–323.
- [19] M. Suzuki, Y. Yamazaki, K. Matsunami, Simplified dynamics of planar two-joint arm movements, *Journal of Biomechanics* 33 (2000) 925–931.
- [20] H.E.J. Veeger, B. Yu, K. An, R.H. Rozendal, Parameters for modeling the upper extremity, *Journal of Biomechanics* 30 (1996) 647–652.
- [21] T. Kodek, M. Munih, Quantification of shoulder and elbow passive moments in the sagittal plane as a function of adjacent angle fixations, *Journal of Technology and Health Care* 11 (2003) 89–103.

Izjava

Izjavljam, da sem doktorsko delo in disertacijo izdelal samostojno pod mentorstvom prof. dr. Marka Muniha. Izkazano pomoč drugih sodelavcev sem v celoti navedel v zahvali. Že objavljeni dosežki drugih avtorjev so navedeni v okviru bibliografije.

Timotej Kodek

Ljubljana, 20. september 2004